Chem Soc Rev

Advanced Supramolecular Design for Direct Ink Writing of Soft Materials

Journal:	*Chemical Society Reviews*
Manuscript ID	CS-REV-12-2022-001011.R1
Article Type:	Review Article
Date Submitted by the Author:	13-Jan-2023
Complete List of Authors:	Tang, Miao; Dartmouth College, Chemistry Zhong, Zhuoran; Dartmouth College, Chemistry Ke, Chenfeng; Dartmouth College, Chemistry

SCHOLARONE™
Manuscripts

Advanced Supramolecular Design for Direct Ink Writing of Soft Materials

Miao Tang,[a] Zhuoran Zhong,[a] Chenfeng Ke[*a]

[a] Department of Chemistry, Dartmouth College, 41 College Street, Hanover, 03755 NH, United States

Email: chenfeng.ke@dartmouth.edu

Abstract:

The exciting advancements in 3D-printing of soft materials are changing the landscape of materials development and fabrication. Among various 3D-printers that are designed for soft materials fabrication, the direct ink writing (DIW) system is particularly attractive for chemists and materials scientists due to the mild fabrication conditions, compatibility with a wide range of organic and inorganic materials, and the ease of multi-materials 3D-printing. Inks for DIW need to possess suitable viscoelastic properties to allow for smooth extrusion and be self-supportive after printing, but molecularly facilitating 3D printability to functional materials remains nontrivial. While supramolecular binding motifs have been increasingly used for 3D-printing, these inks are largely optimized empirically for DIW. Hence, this review aims to establish a clear connection between the molecular understanding of the supramolecularly bound motifs and their viscoelastic properties at bulk. Herein, extrudable (but not self-supportive) and 3D-printable (self-supportive) polymeric materials that utilize noncovalent interactions, including hydrogen bonding, host-guest inclusion, metal-ligand coordination, micro-crystallization, and van der Waals interaction, have been discussed in detail. In particular, the rheological distinctions between extrudable and 3D-printable inks have been discussed from a supramolecular design perspective. Examples shown in this review also highlight the exciting macroscale functions amplified from the molecular design. Challenges associated with the hierarchical control and characterizations of supramolecularly designed DIW inks are also outlined. The perspective of utilizing supramolecular binding motifs in soft materials DIW printing has been discussed. This review serves to connect researchers across disciplines to develop innovative solutions that connect top-down 3D-printing and bottom-up supramolecular design to accelerate the development to 3D-print soft materials for a sustainable future.
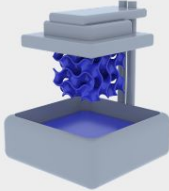
1. Introduction

Additive manufacturing (AM),[1-4] often referred to as 3D-printing, is changing the landscape of manufacturing through (i) the fabrication of complex and customized architectures and (ii) the integration of multiple materials that were unattainable previously. The rapid development of AM demands tailor-designed materials with suitable mechanical properties.[5] Compared to laser sintering-based AM techniques for producing metals and ceramics,[6] soft materials 3D-printing utilizes very different AM platforms for the fabrication of plastics,[7] hydrogels,[8] elastomers,[4, 9] and bio-inks.[10] For example, fused deposition modeling (FDM)-based 3D-printers extrude thermoplastic filaments.[11] They have occupied most of the hobbyist market for low-cost 3D-printing.[12] Vat-polymerization-based 3D-printers including stereolithography (SLA),[13] digital light processing (DLP),[14] two-photon polymerization lithography,[15] and computed axial lithography[16-18] (CAL or volumetric 3D-printing) have shown impressive capabilities in producing complex architectures sizing from micrometer to sub-meter. Direct-ink-writing (DIW) is widely used to create architectured functional materials and bio-compatible constructs.[19] DIW 3D-printers extrude viscoelastic paste[20] from the nozzle onto (ir)regularly shaped substrates at ambient temperature.[21] These features make DIW particularly powerful for multi-materials 3D-printing,[22] fabricating soft materials that exhibit stimuli-responsiveness.[23, 24]

Over the past decade, the advancement of materials design has greatly accelerated soft materials 3D-printing.[25] For example, De Simone *et al.* introduced an oxygen-permeable membrane to allow for fast photo-polymerization in vat-polymerization-based 3D-printers, increasing the printing speed significantly.[26] Dynamic covalent chemistry has been introduced to FDM filaments, generating products with better isotropic performance.[27-29] A variety of polymer designs have been introduced for DIW, producing a plethora of new materials with stimuli-responsiveness,[30, 31] outstanding mechanical properties,[32] biocompatibility,[33, 34] and optical/electronic properties.[35, 36]

DIW and vat-polymerization-based 3D-printers are widely used for soft materials AM (Fig. 1), and they have their advantages and limitations.[37, 38] For example, vat-polymerization-based 3D-printers offer fast production speed and sub-100-μm printing resolution.[39] However, a large volume of printing resin is required,[40] and multi-material 3D-printing remains a significant challenge (Fig. 1, *right*).[41] Meanwhile, DIW is compatible with a wide range of materials and crosslinking methods, but it is difficult to fabricate architectures with large overhanging structures like gyroids.[42] The resolution of DIW 3D-printing is largely determined by the dimensions of the printing nozzles.[1] While nozzles as fine as 100-500 nm have been reported for patterning[43] and DIW,[44, 45] most DIW 3D-printing practices are performed using printing nozzles of 100 μm to 1 mm (Table 1). From a materials development perspective, the rheological requirements for vat-polymerization and DIW 3D-printers are nearly the opposite.[46] Vat-polymerization-

based 3D-printers require low-viscosity photo-resins for fast production, but DIW demands thick viscoelastic pastes for smooth extrusion and shape retention. The crosslinking methods used in these systems, however, are similar (e.g., photo-crosslinking) with interchangeable chemical designs.[47, 48] While this review discusses the supramolecular design of soft materials for DIW, we also want to draw design connections to vat-based 3D-printing systems. Sometimes, if a functional material does not meet the rheological requirements for DIW, it may be considered for vat-3D-printing with some modifications.[48]

direct ink writing	VS	vat photopolymerization
high viscosity	*viscosity*	low viscosity
shear-thinning and self-healing	*fluids*	Newtonian liquid desired
multiple crosslinking methods	*polymerization*	largely photo-crosslinking
ambient condition	*operation environment*	ambient condition (UV irradiation)
tip-determined	*resolution*	optical display-controlled
slow	*speed*	fast
multi-material integration	*integration*	mostly one material
bio-inks, hydrogels, organogels, elastomers	*material systems*	thermosets, elastomers, hydrogels

Fig. 1 Comparisons between DIW and vat-polymerization-based 3D-printers.

A typical DIW system (Fig. 2a) contains ink-loading barrels (often syringes), extrusion heads, a motorized printing arm or printing platform, and pneumatic pressure or mechanical dispensers. During DIW, inks are dispensed onto the substrate guided by computer-aided design. Under the ambient temperature and humidity, the viscosity of the ink is decreased to allow for smooth extrusion, and the viscosity is then recovered to self-stand. The mild deposition requirement is compatible with various solvents and deposition nozzles, allowing for multi-materials 3D-printing.[49-51] Furthermore, DIW allows for reactive mixing-and-printing,[52] coaxial printing,[53] photo-/acoustic-assisted fabrication,[54, 55] magnetically guided printing,[56] gel-in-gel printing,[57-59] liquid-in-liquid printing,[60] and temperature-varied 3D-printing.[61, 62] This wide compatibility and tunability of DIW has encouraged new chemical designs, such as integrations with frontal polymerization,[63] sonochemistry,[54, 64, 65] mechanochemistry,[66-68] and supramolecular chemistry.[20, 25, 69]
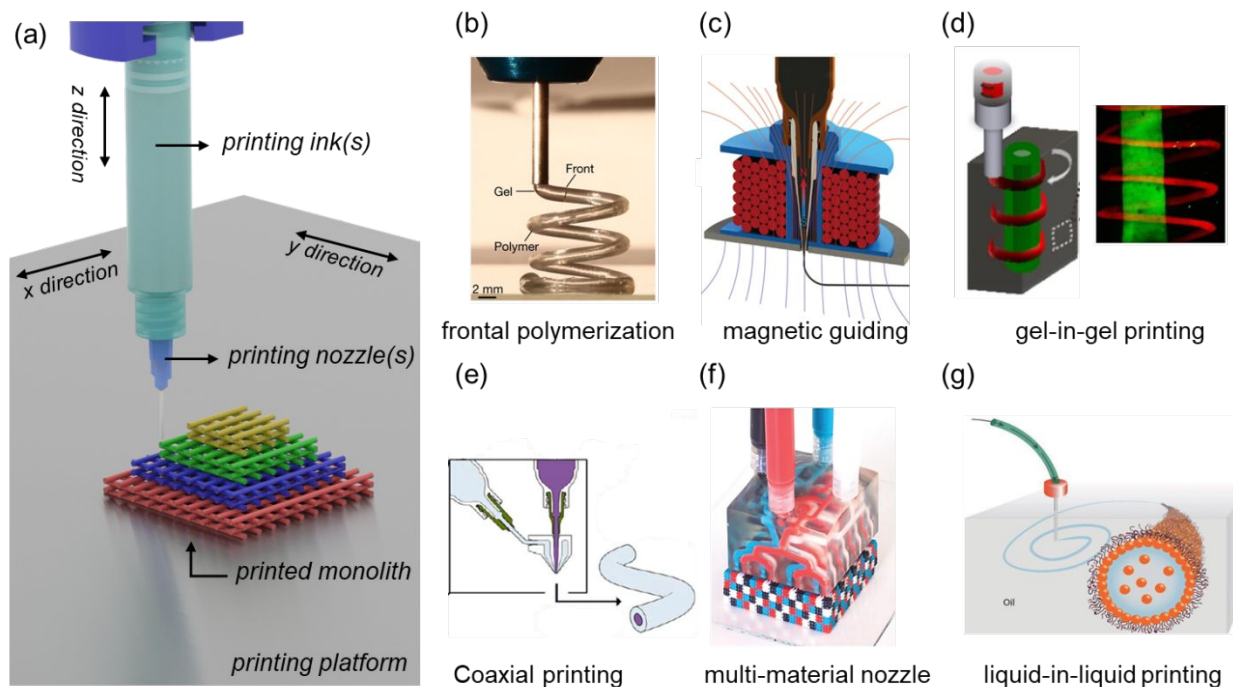
Fig. 2 (a) A typical setup of a DIW 3D-printer. (b) An image of a frontal polymerization 3D-printing. Reproduced with permission from reference 63. Copyright 2018 Springer Nature. (c) An image of a magnetic-guiding DIW. Reproduced with permission from reference 56. Copyright 2018 Springer Nature. (d) Images of a gel-in-gel 3D-printing. Reproduced with permission from reference 59. Copyright 2017 Springer Nature. (e) Images of a coaxial 3D-printing. Reproduced with permission from reference 53. Copyright 2019 IOP Publishing. (f) An image of a multi-nozzle multi-material 3D-printing. Reproduced with permission from reference 51. Copyright 2019 Springer Nature. (g) An image of a liquid-in-liquid 3D-printing. Reproduced with permission from reference 60. Copyright 2018 John Wiley & Sons, Inc.

Inks for DIW need to be shear-thinned during the extrusion and self-healed after the deposition. While adding colloidal particles to inks for DIW has been demonstrated effective in tailoring their rheological properties, they have been discussed in other reviews.[70-72] The interactions in these systems are complicated without clearly demonstrated binding models, and they are not discussed in this review. Hydrogels formed by naturally occurring biopolymers such as alginate, chitosan, collagen, and gelatin meet these requirements for DIW.[73] The hydrogen-bonding networks formed within these hydrogels are disrupted during the extrusion and rapidly reformed after dispensing.[20, 25] Following this principle, other supramolecular gels or pastes (Fig. 3), including hydrogen-bonded polymers,[74] host-guest networks,[75] metal-ligand coordination polymers,[76] electrostatic polymer networks,[77] and mechanically interlocked systems (e.g., polyrotaxanes),[78] have been successfully introduced as DIW inks (see Table 1). These 3D-printing materials demonstrated exciting stimuli-responsive features and shape-morphing capabilities.[1, 23] These advancements also raise

new challenges and opportunities. Unlike traditional solution-phase supramolecular assemblies, 3D-printable supramolecular systems are formulated in highly concentrated and viscous environments. At the molecular level, the van der Waals interactions among the supramolecular binding motifs and solvents are no longer negligible, different from traditional binding studies carried out in dilute solutions (only accounting for strong noncovalent interactions).[79, 80] Therefore, *how can we understand, assemble, characterize, and fabricate these molecular components in a controlled manner across the nano-to-macroscale?* In addition, the extrusion process of DIW has a strong non-equilibrium character. *How can we understand and take advantage of the non-equilibrium character of DIW in materials design?* In this review, we will walk through the fundamental design principles across the length scale, discuss the designs and tools in these supramolecular systems, and showcase the properties of these 3D-printing materials. We hope the general strategies and case studies presented in this review will inspire researchers to unfold the answers to those questions and accelerate materials development with better mechanical performance and biocompatibility for high-speed and high-resolution DIW.
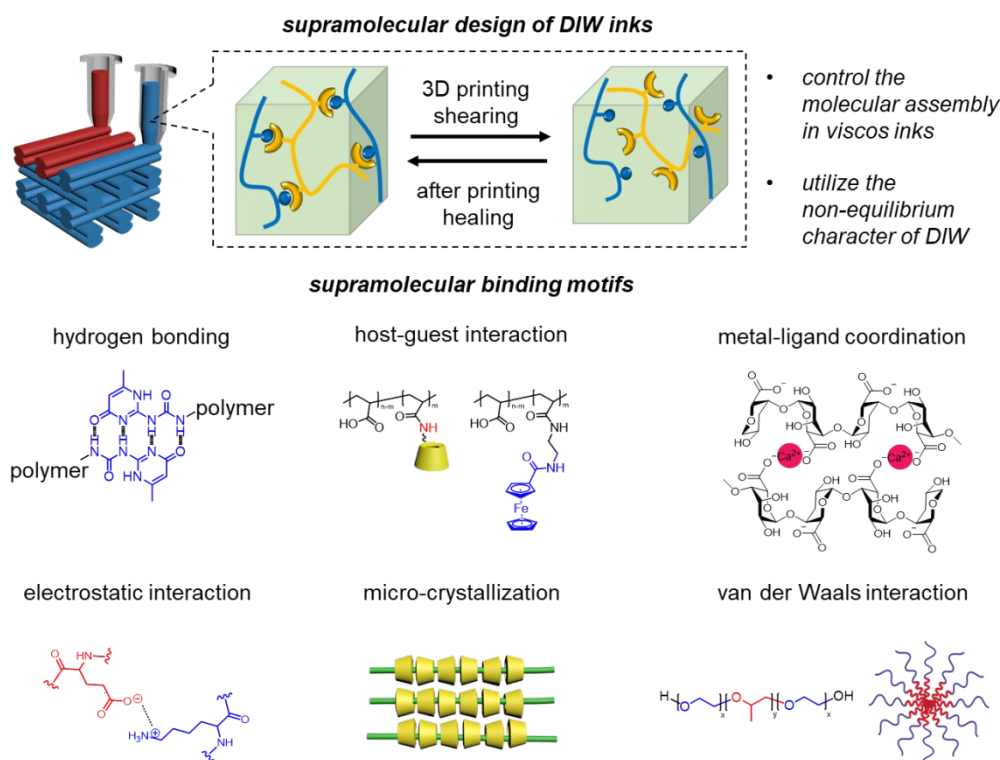

Fig. 3 Supramolecular binding motifs for the design of DIW inks.

2. Tools and design considerations for DIW inks

When supramolecular inks are developed for DIW, their rheological behaviors are critical to evaluate the 3D-printability. In addition, the molecular arrangements in these 3D-printed materials are also critical to

establish the structure-property relationship. To investigate the nano-to-macroscale features of 3D-printing materials and the corresponding crosslinked monoliths, a series of tools have been employed to investigate the hierarchical assemblies of these supramolecular materials.

Tools for molecular interactions. Supramolecular chemists have employed various tools to study noncovalent interactions at the molecular level. For example, nuclear magnetic resonance (NMR) titrations[79] and isothermal titration calorimetry (ITC)[81] are often employed to measure the binding affinities (K_a), binding enthalpy (ΔH), and entropy (ΔS) between the supramolecular binding motifs in solution. Photospectrocopic measurements such as infrared (IR), Raman, and ultraviolet-visible (UV-Vis) spectroscopies are also used to study the supramolecular assemblies.[82] When supramolecular binding motifs are embedded or grafted on polymer backbones, their multivalent and cooperative binding events[83] are also studied.[84-87]However, weak interactions such as van der Waals interactions are often neglected in these studies. In highly concentrated 3D-printing inks, weak interactions cumulatively contribute to the overall self-assembly and are no longer negligible. Currently, methods to quantitatively assess supramolecular binding events in highly viscous gels are still missing.
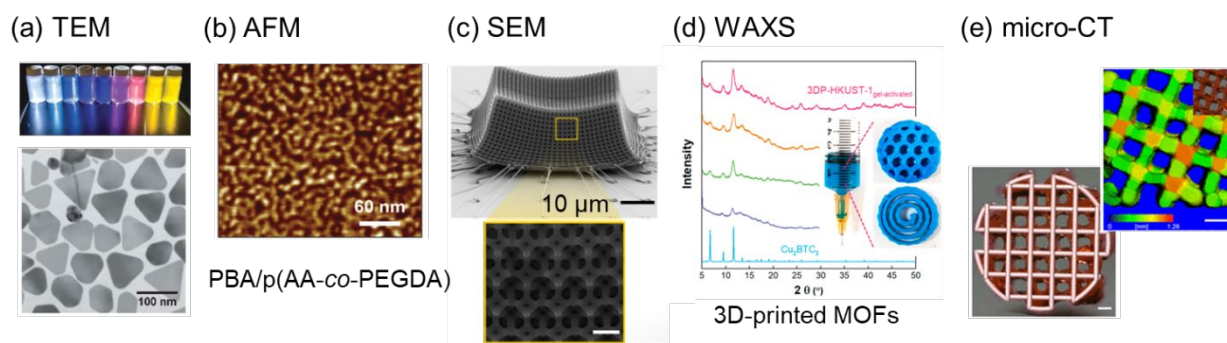
Fig. 4 (a) A TEM image of silver nanoprisms embedded in an F127 hydrogel. Reproduced with permission from reference 88. Copyright 2017 John Wiley & Sons, Inc. (b) Phase separation of a PBA/P(AA-*co*-PEGDA) assembly observed under AFM. Soft PBA block is shown in dark color. Reproduced with permission from reference 89. Copyright 2022 John Wiley & Sons, Inc. (c) SEM images of a 3D-printed carbon monolith. Reproduced with permission from reference 90. Copyright 2021 Springer Nature. (d) WAXS profiles of 3D-printable MOF gels. Reproduced with permission from reference 91. Copyright 2019 American Chemical Society. (e) Micro-CT images of 3D-printed bioinks comprised of tyramine hyaluronan. The CAD design is superpositioned on the sample shown on the left. Reproduced with permission from reference 92. Copyright 2019 American Chemical Society.

Tools for hierarchical assemblies. The morphology of supramolecular assemblies in DIW inks and printed monoliths are studied via different microscopies. Transmission electron microscopy (TEM), atomic

force microscopy (AFM), and scanning electron microscopy (SEM) are often employed to capture the assembled morphologies at different length scales. For example, TEM is used to characterize nanoparticles and nanoporous structures in 3D-printed samples. Liu and Johnson *et al.* introduced silver nanoprisms into F127-based hydrogels to fabricate plasmonic constructs,[88] with the silver nanoprisms of 15–79 nm shown in the TEM images (Fig. 4a). AFM provides height, phase, and stiffness information of the material at the nanometer scale. Boyer *et al*. designed a poly(*n*-butyl acrylate) (PBA)-based macromolecular chain-transfer agent for the construction of 3D-printed objects via DLP (Fig. 4b).[89] In the presence of acrylic acid (AA) and polyethylene glycol diacrylate (PEG-Ac$_2$), polymerization-induced self-assembly led to phase separation as observed in AFM studies (Fig. 4b). At a larger scale, SEM is powerful in revealing the micrometer sized features, including the monolith size and line width of the 3D-printed constructs (Fig. 4c).[90]

The short- and long-range orders of supramolecular assemblies are studied using various X-ray scattering diffractions. Wide-angle X-ray scattering (WAXS) is often used to study the structural information of crystalline domains in (semi-)crystalline materials (Fig. 4d), including 3D-printed metal-organic frameworks (MOFs)[91] and covalent organic frameworks (COFs).[93] Small-angle X-ray scattering (SAXS) analysis provides structural information of assembled structures at 1–100 nm scale. Angelini *et al*. 3D-printed silicone structures in light mineral oil via self-assembled micro-organogels, which comprise a polystyrene-*b*-poly(ethylene/propylene) (PS-*b*-PE/PP) diblock copolymer and a PS-*b*-PE/PP-*b*-PS triblock copolymer in light mineral oil.[94] The assembled structures at different diblock to triblock copolymer ratios were revealed by SAXS. Beyond the range of SAXS, X-ray-computed tomography (XCT) is used to study the 3D-printed objects.[92] The experimentally generated 3D features are compared with the CAD design to investigate the shape fidelity of the printing outcomes (Fig. 4e).

Rheological studies for 3D-printability. Rheological studies are particularly powerful in revealing DIW inks' deformation and flow behavior under stress and their recovery after stress removal.[70, 95] Four rheological sweeps are often measured for DIW inks. They are oscillation strain sweep, angular frequency sweep, shear rate sweep, and step-strain sweep (Fig. 5),[25] where the viscosity and moduli change against oscillation strain, angular frequency, shear rate, and step-strain are studied. In these measurements, the elastic modulus (G' in Pa) represents the solid-like behavior of the ink, and the loss modulus (G'' in Pa) represents the viscous feature of the ink.[96] A typical 3D-printable ink possesses both good shear-thinning and self-healing behaviors (Fig. 5), allowing it to flow under pressure ($G'' > G'$, Fig. 5a) and rapidly recover after extrusion ($G' > G''$, Fig. 5d). The viscoelastic properties of a DIW ink measured in the four rheological sweeps not only determine its 3D-printability, but also represent the sum of supramolecular interactions at the molecular level. Here, we offer our viewpoint to interpret these rheological data from a supramolecular design perspective.

In an oscillation strain sweep (Fig. 5a), two regions are worth attention– the plateau region and the yield point (G' = G''). The plateau region informs the extent of an applied strain, indicating that the supramolecular network remains the same degree of supramolecular (or physical) crosslinking. Beyond the plateau region, the supramolecularly crosslinked network starts to dissociate and becomes extensively dissociated at the yield point. For example, the yield points of inks with colloidal rheological modifiers such as clay and salt particles are usually found at the low strain range ($\leq$ 10% strain) due to the weak colloid-colloid interactions.[97] Inks connected via micro-crystalline domains show a yield point at the medium strain range (10–20% strain).[78] High yield points are often found in those inks with spatially well-dispersed supramolecular crosslinks, which require a large strain (> 20% strain) to dissociate them extensively.[98]
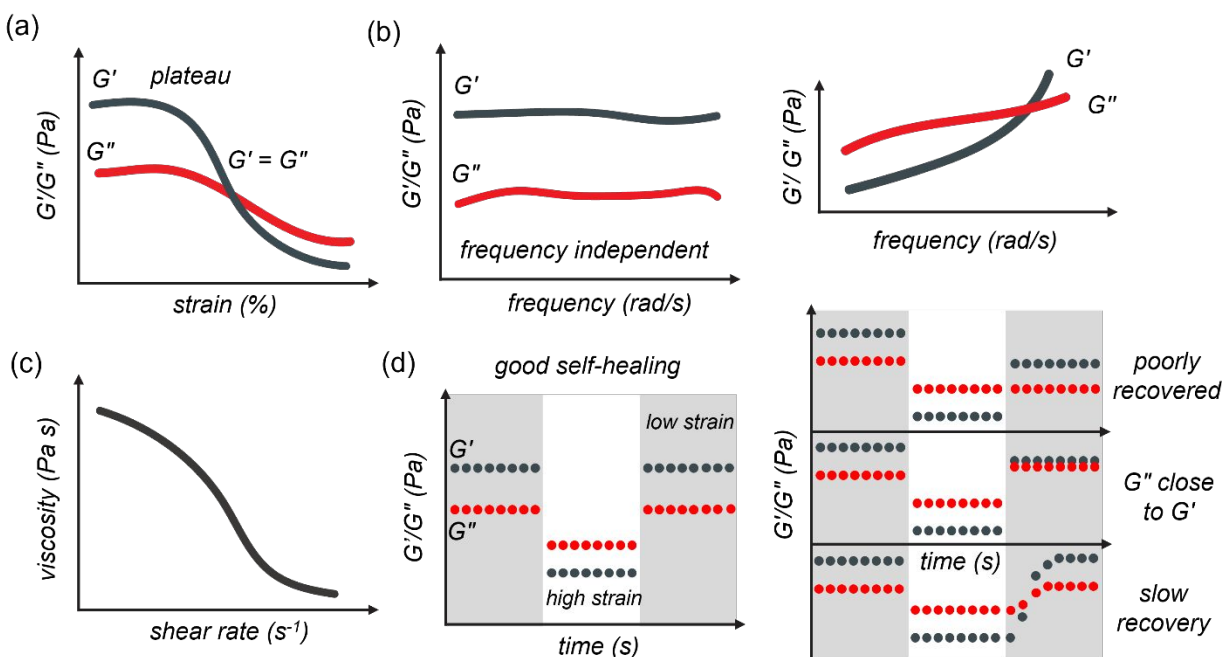
Fig. 5 Representative rheological investigations of DIW inks. (a) A shear-thinning ink studied in an oscillation strain sweep. (b) Angular frequency sweeps of a DIW ink (*left*) and an extrudable ink (*right*). (c) The shear-thinning feature in a shear rate sweep. (d) Supramolecular networks showing good self-healing features (*left*) and limited self-healing capabilities (*right*) in step-strain sweeps.

Angular frequency sweeps are usually performed at a low strain (Fig. 5b), where the oscillation sweep determines the strain in the plateau region. Good DIW inks usually show no frequency dependence, and G' > G'' are consistently measured in a wide frequency range. In comparison, extrudable but not 3D-printable supramolecular gels often show strong frequency dependence, where G'' > G' are measured at the low-frequency range and G' > G'' are measured in the high-frequency range (Fig. 5b, *right*). In these gels, the

binding affinities or densities of the binding motifs are usually low. Hence, their effective supramolecular crosslinking densities are limited. Therefore, they exhibit liquid-like behaviors at low frequencies. At increased frequencies, the applied strains gradually match the on-off binding kinetics of these supramolecular binding events,[99] thus increasing the effective crosslinking densities at these transient states, resulting in the elastic and loss moduli cross-over.[100] Having stronger supramolecular binding motifs in a gel is usually beneficial to strengthen the network, shown as higher elastic moduli in angular frequency sweeps.[20, 25]

Shear rate and step-strain sweeps are two measurements that are particularly important for the 3D-printing practice (Fig. 5c-d). The viscosities of inks at different shear rates are correlated with their extrusion flow rates during DIW.[95, 101] Step-strain sweep informs the extent of ink's self-healing after the extrusion.[8, 59, 102-104] These investigations provide researchers with suitable parameters for DIW—for example, the pneumatic pressure applied to the ink and the corresponding printing speed.

What renders a good DIW ink? From the rheology standpoint, the ink needs to possess good shear-thinning properties, as shown in the oscillation-strain and shear rate sweeps, as well as good self-healing properties after the removal of the shear force, as shown in the step-strain sweep. The self-healing feature of the ink determines whether this ink is extrudable or 3D-printable. Some inks with low-to-moderate elastic moduli have been printed as 2D patterns on a supporting substrate. The claim of their 3D-printability is debatable, and they are not considered as DIW inks in this review. At the molecular level, the formation of the polymeric network needs to meet the rheological requirements for successful DIW. Three factors contribute to the viscoelasticity: the individual binding strength of a supramolecular binding pair, the supramolecular crosslinking density, and the network's topology. We will discuss these factors in the next section.

3. Extrudable supramolecular networks

Supramolecular interactions are weaker than covalent bonds, but they are highly dynamic, which enables the construction of supramolecular polymers with stimuli-responsiveness.[105, 106] Many supramolecular gels or pastes can be extruded from syringe nozzles.[107, 108] During the extrusion, the mechanical shear force disrupts the supramolecular interactions and reduces the gel's viscosity. After the extrusion, if these supramolecular interactions are re-established quickly to allow the gels to recover and self-support their structures, they are considered 3D-printable gels for DIW. On the other hand, if supramolecular gels do not self-stand after extrusion, they are only extrudable. This section will discuss extrudable supramolecular networks from a DIW ink design perspective.

Hydrogen-bonded supramolecular polymers. Hydrogen bonding interactions have been widely used to construct supramolecular polymers and networks.[109] Examples include small-molecular-weight gelators, natural polymers, and synthetic polymers with hydrogen-bonding moieties. For instance, Wang *et al.* discovered that a natural anthraquinone derivative rhein self-assembled in water to form a stable hydrogel between pH 8.0 and 9.4 (Fig. 6a).[110] The rhein hydrogel (17.6 mM) showed an elastic moduli G' ~700 Pa at 0.1% strain and ~100 Pa at 35% strain. Although good self-healing was shown in the step-strain sweep, the low elastic modulus G' made this gel too weak to be self-supportive. In another example, Stupp *et al.* reported a quinquethiophene-oligopeptide hydrogelator, which assembled into a gel slowly (hours to days).[111] The slow gelation kinetics make this hydrogel unsuitable for DIW.
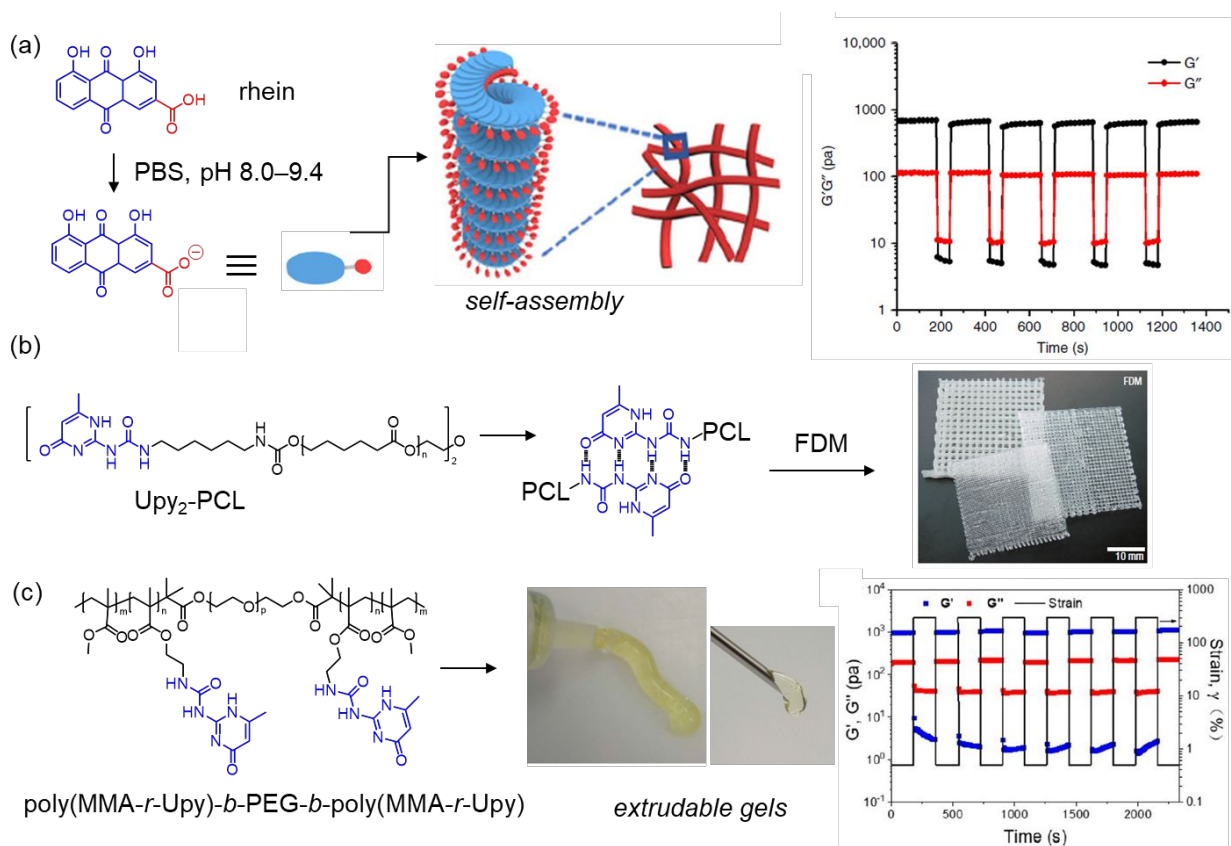
Fig. 6 (a) A small-molecular-weight gelator rhein and its assembled hydrogel. The step-strain sweep is shown on the right. Reproduced with permission from reference 110. Copyright 2019 Springer Nature. (b) A Upy-based supramolecular polymer with a self-complementary hydrogen bonding pattern was 3d-printed into meshes via FDM. Reproduced with permission from reference 112. Copyright 2005 Springer Nature. (c) An extrudable hydrogel formed by a triblock copolymer poly(MMA-*r*-Upy)-*b*-PEG-*b*-poly(MMA-*r*-Upy) and its step-strain sweep. Reproduced with permission from reference 113. Copyright 2022 MDPI.

Other than small-molecular-weight gelators, supramolecular polymers with hydrogen bonding motifs are also potential candidates for 3D-printing. In 2005, Meijer *et al.* introduced ureido-pyrimidinone (UPy) moieties into poly(caprolactone) (PCL-UPy$_2$, Fig. 6b).[112] The strong quadruple hydrogen bonds allowed the assembly between PCL-UPy$_2$ to form a strong and elastic material, which was 3D-printed into lattices using FDM (Fig. 6b). When Upy groups are introduced as the polymers side chains, their strong hydrogen bonding interactions also enabled the formation of hydrogels. Yang *et al.* synthesized a triblock copolymer containing a central PEO (20 kDa) block and two poly(methylmethacrylate) (PMMA) blocks, in which the UPy moieties were randomly incorporated to the PMMA block (Fig. 6c).[113] A hydrogel was formed by dissolving 10 wt% of the copolymer, which exhibited good shear-thinning and self-healing properties (Fig. 6c). However, its elastic modulus G' ~10^3 Pa made it an extrudable hydrogel yet hardly self-supporting.
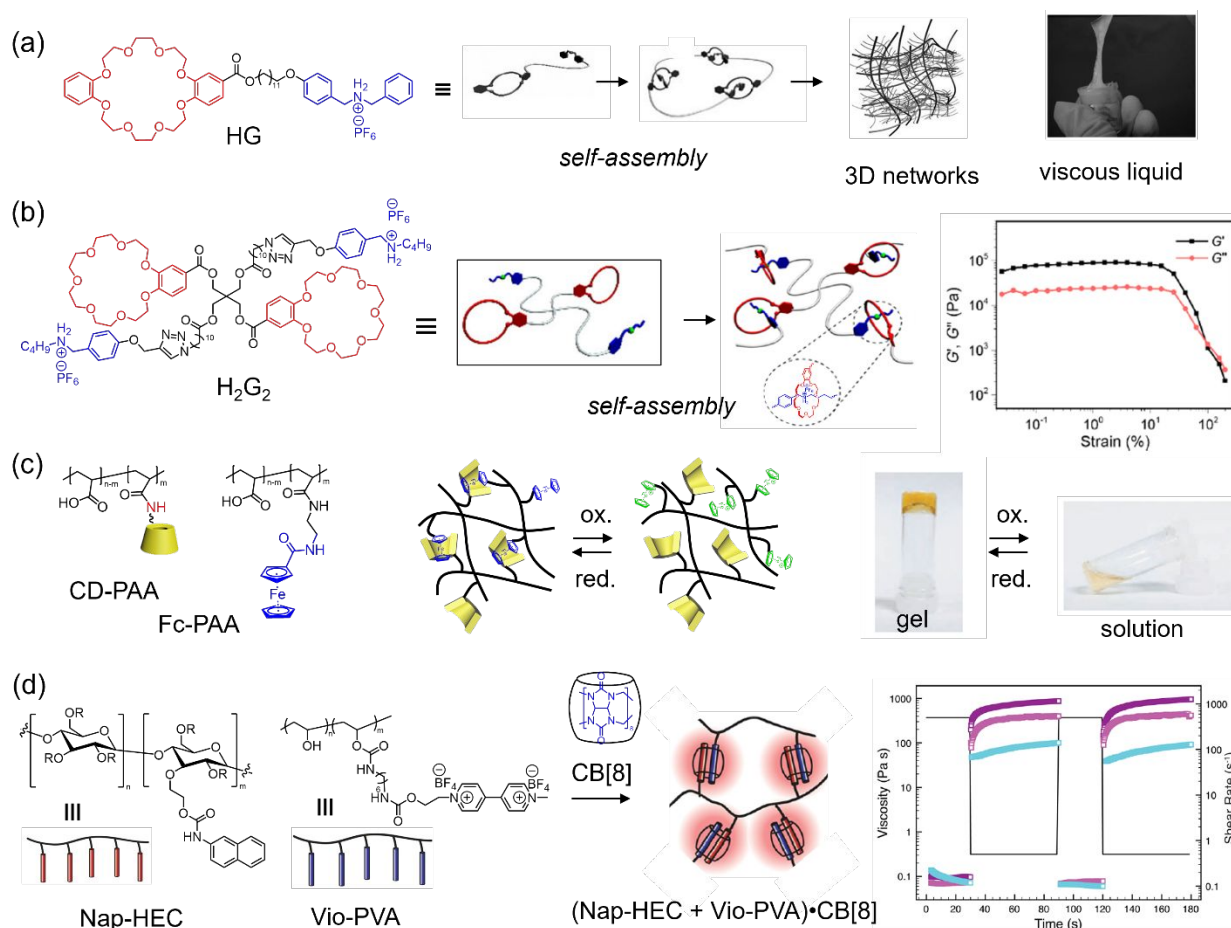

Fig. 7 (a) A dibenzo[24]crown-8-dibenzylammonium conjugate (HG) self-assembled into a supramolecularly crosslinked network as a viscous liquid. Reproduced with permission from reference 114. Copyright 2011 John Wiley & Sons, Inc. (b) A tetra-arm host-guest gelator (H$_2$G$_2$) containing two benzo[21]crown-7 and two dialkylammonium motifs. This gelator self-assembled to form a viscoelastic

organogel in MeCN. The stress-strain sweep is shown on the right. Reproduced with permission from reference 115. Copyright 2018 American Chemical Society. (c) A redox-active hydrogel formed by mixing CD-PAA and Fc-PAA. Reproduced with permission from reference 116. Copyright 2011 Springer Nature. (d) A supramolecularly crosslinked hydrogel formed by co-including naphthyl and viologen moieties in CB[8]. The step-rate sweep data is shown on the right. Reproduced with permission from reference 117. Copyright 2012 American Chemical Society.

Host-guest complex-based supramolecular polymers. Small molecular assemblies and polymers grafted with host-guest binding motifs have been introduced to form supramolecular polymer networks.[118] For example, dibenzo[24]crown-8 forms inclusion complexes with secondary ammonium guests, and the host-guest complexes have been introduced as building blocks to form supramolecular networks. Huang *et al.* synthesized a dibenzo[24]crown-8 and dibenzylammonium HG conjugate,[114] forming linear supramolecular polymers in dilute MeCN solutions (Fig. 7a). The supramolecular polymer aggregates as 3D fibrous networks at higher concentrations, affording a viscous organogel at 1.0 M. By further increasing the concentration of the conjugate to above 1.5 M, elastic and transparent films were formed by casting. Although this organogel is unlikely to meet the rheological requirements for DIW (low modulus and non-self-supportive), the design could be further optimized toward this goal by reinforcing the supramolecular fiber-fiber interactions. Instead of utilizing the monovalent HG conjugate, Yan *et al.* designed a tetra-arm molecule (H_2G_2) containing two benzo[21]crown-7 and two dialkylammonium motifs.[115] This H_2G_2 self-assembled into a supramolecularly crosslinked network to afford a stable organogel (Fig. 7b). The stable MeCN-gel (21 wt% of H_2G_2 in MeCN) possessed an elastic modulus of 5×10^4 Pa with good shear-thinning properties, exhibiting temperature and pH-responsive sol-gel transitions. The self-healing behavior of the gel was not examined, but this example demonstrates the supramolecular design in altering the viscoelasticity.

Cyclodextrins (CDs) bind hydrophobic guests in water due to the hydrophobic effect.[119] When CDs and their corresponding guests are attached to polymer backbones, the side-chain host-guest complexations crosslink the polymers and facilitate a sol-gel transition.[120] Harada *et al.* grafted β-CD and ferrocene (Fc) moieties to polyacrylic acid (CD-PAA and Fc-PAA, M_n = 250 kDa, DP ~3,500), with grafting ratios of 4% and 3%, respectively (Fig. 7c).[116] When CD-PAA and Fc-PAA (1 wt% each) were mixed, a redox-active hydrogel (G' ~150 Pa) was formed. When Fc moieties were oxidized, a gel-sol transition was observed. Although this host-guest hydrogel does not meet the rheological requirements for DIW, it provides a proof of principle for the design of DIW-compatible host-guest hydrogels (see Section 4 for representative examples).

Cucurbit[n]urils (CB[n]s) bind with guests via ion-dipole interactions.[121, 122] The larger cavity of CB[8] allows the formation of ternary inclusion complexes, in which two identical guests (e.g., tryptophan) or charge-transfer complex (viologen and naphthalene) are included inside CB[8]'s cavity.[123-125] For example, Sherman *et al.* synthesized a naphtyl-grafted hydroxyethyl-cellulose (Nap-HEC) and a viologen-grafted polyvinyl alcohol (Vio-PVA).[117] In the presence of CB[8], a series of supramoleculary crosslinked hydrogels were formed (Fig. 7d). At a concentration of 1.8 wt%, a hydrogel with an elastic modulus of ~ 500 Pa was formed. Step-rate sweep showed that the hydrogel was shear-thinned and took 5–10 seconds to recover (Fig. 7d). The hydrogel showed sol-gel transitions in response to competing guests and/or oxidation/reduction. Although this hydrogel was not optimized for DIW, it is expected that this hydrogel with a higher concentration of supramolecular entities is likely to be compatible with DIW. Sherman group showed two identical guests, phenylalanine and tryptophan, also enabled the formation of supramolecular hydrogels when they were grafted to a poly(vinylbenzyl)trimethylammonium chloride) polymer.[126] Phenylalanine and tryptophan assembled with CB[8] to form 2:1 complexes, and shear-thinning hydrogels were obtained. The elastic moduli of the hydrogels were found to be highly frequency dependent, and they are not 3D-printable as suggested by the angular frequency sweeps.
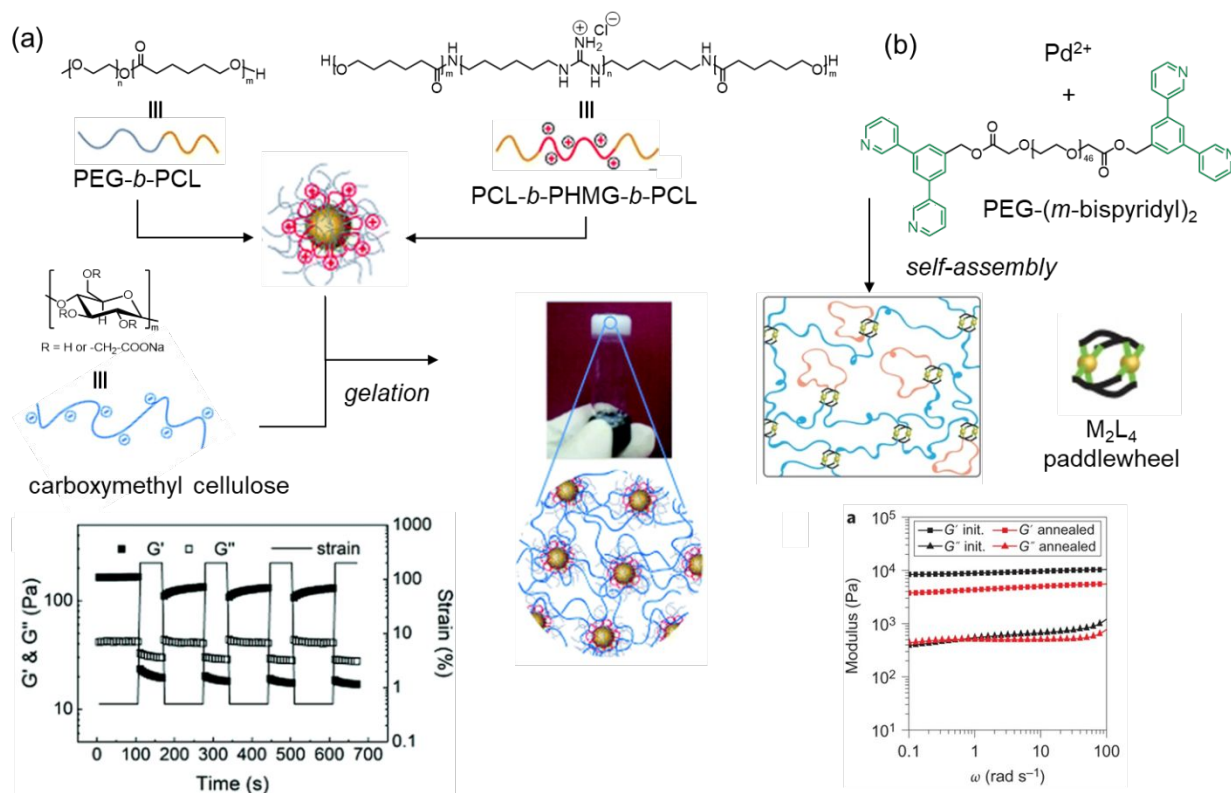
Fig. 8 (a) An electrostatic hydrogel formed via the assembly of PEG-*b*-PCL, PCL-*b*-PHMG-*b*-PCL, and sodium carboxymethyl cellulose. The strain-step sweep is shown at the bottom. Reproduced with

permission from reference 127. Copyright 2020 The Royal Society of Chemistry. (b) A PEG-based polymer network crosslinked via M_2L_4 paddlewheel metal coordination cages. The frequency sweep is shown at the bottom. Reproduced with permission from reference 128. Copyright 2015 Springer Nature.

Ionic interactions and coordination bonds. Supramolecular network formation by polycations and polyanions are highly dependent on the dielectric constant of solvents.[129] Zhu *et al*. designed a shear-thinning electrostatic hydrogel via the ionic interactions between two polyelectrolytes (Fig. 8a).[127] Two block copolymers PEG-*b*-PCL (M_n = 9.1 kDa) and polycaprolactone-*b*-(poly(hexamethylene guanidine) hydrochloride)-*b*-polycaprolactone (PCL-*b*-PHMG-*b*-PCL, M_n = 2.7 kDa) were synthesized via ring-opening polymerizations. In water, PEG-*b*-PCL and polycationic PCL-*b*-PHMG-*b*-PCL assembled as micelles with positively charged corona. When polyanionic sodium carboxymethyl cellulose (1 wt%) was introduced to the micellar solution, an electrostatically crosslinked hydrogel was obtained with G' ~200 Pa measured at a low strain. This hydrogel showed good shear-thinning and self-healing properties, but it is too weak to be self-supportive (Fig. 8a, *bottom*).

Metal-ligand coordinations are strong and highly directional. Metallogels with coordination polymer networks have been well-studied.[130, 131] For example, Johnson *et al.* developed a supramolecular polymer network using metal-coordination cages as supramolecular crosslinkers (Fig. 8b).[128] Telechelic PEG with *meta*-bispyridyl (PEG-*m*-bispyridyl) end groups assembled with Pd^{2+} to form a M_2L_4 paddlewheel-cage crosslinked network. This gel showed frequency independence in the angular frequency sweep and no shear-thinning, suggesting that the coordination cage-connected network is much less dynamic for DIW. Hence, the bonding association and dissociation kinetics need to be carefully examined when considering metal-ligand coordinations.

Microcrytallization-enabled gelation. In semi-crystalline polymers such as PE,[132] PP,[133] and PLA,[134] segments of polymers are packed in an ordered manner to form crystalline domains, leaving the rest amorphous. The formation of the crystalline domains drives the assembly of the polymers in solution. For example, Manners *et al.* synthesized a variety of polyferrocenylsilane block copolymers and assembled 2D and 3D superstructures via crystallization-driven self-assembly.[135-137] At higher concentrations, polymers with self-assembled crystalline domains form viscoelastic gels.[138] The formation and disruption of these crystalline domains facilitate the shear-thinning and self-healing features to the gels, making them potentially suitable for DIW. Since the crystallization is largely kinetically controlled, the formation and recovery of larger crystalline domains generally takes a long time since the adjustment of each polymer segment with long-range order is kinetically slow. Hence, employing smaller crystalline domains for DIW ink design is highly desired. Before extrusion, micro-crystalline domains serve as supramolecular

crosslinkages to increase the ink's elastic modulus. Upon shearing, they are disrupted to reduce the viscosity of the ink. After the extrusion, the fast recrystallization of these polymers allows for rapid self-healing.[78]

It is well documented that α-CDs with PEG (400–5000 Da) form crystalline precipitates in water via a two-step process (Fig. 9a).[139, 140] The first α-CD threads onto the PEG and assists the threading of subsequent α-CDs via CD-CD hydrogen bonding interactions.[141] The formed rigid polypseudorotaxanes pack hexagonally and crystallize in water. Tonelli *et al.* proposed that these polypseudorotaxanes are stacked in parallel based on the WAXS diffraction pattern (Fig. 9b, *left*).[142, 143] This proposed model was widely referenced, implying that all polypseudorotaxanes need to possess the same number of α-CDs for crystallization. We have corrected the stacking model and unit cell parameters by obtaining single crystal structures of PEG_{600}-$(OH)_2/6(\alpha$-CD$)$ and $[(EG)_4/2(\alpha$-CD$)_n]$ (Fig. 9c).[144] In these X-ray structures, the polypseudorotaxanes are stacked hexagonally in an offset unparalleled manner (Fig. 9b, *right*), which allows for the crystallization of polypseudorotaxanes with ill-matched α-CDs.[144]
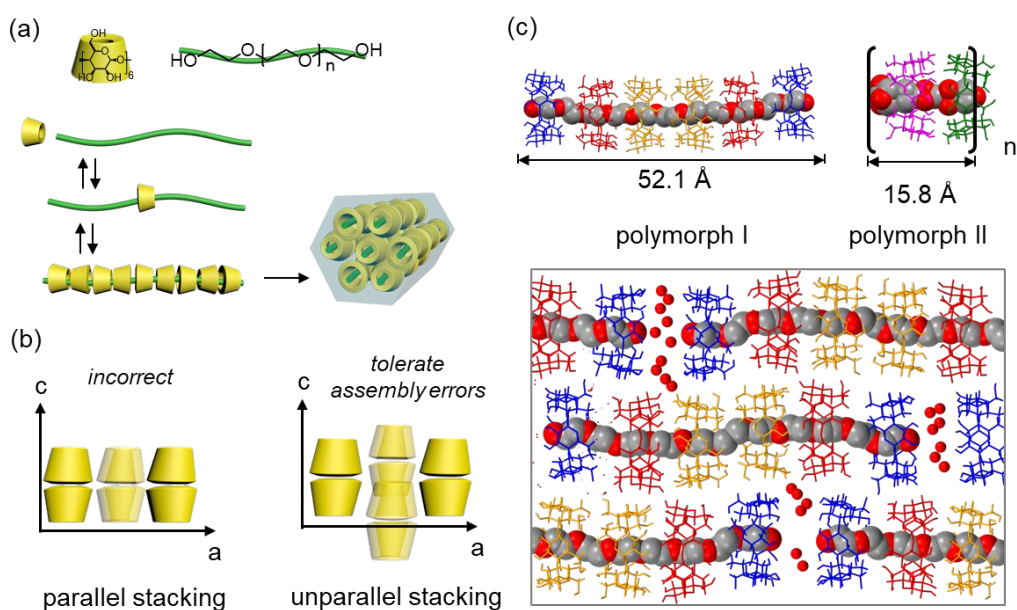
Fig. 9 (a) Schematic illustration of the formation of polypseudorotaxanes, which involves multi-step ring threading and crystallization. (b) The incorrect parallel stacking of $PEG_{600}/n(\alpha$-CD$)$ polypseudorotaxanes (*left*) and the corrected unparallel stacking (*right*). (c) Single crystal structures of two $PEG_{600}/n(\alpha$-CD$)$ polypseudorotaxane polymorphs. Water molecules bridge the polypseudorotaxanes and fill the voids. Reproduced with permission from reference 144. Copyright 2021 Elsevier.

When a PEG (4 kDa) is mixed with α-CD, the formed hydrogel undergoes phase separation upon vigorous shearing or shaking.[145] Ito *et al.* isolated highly crystalline polypseudorotaxane nanosheets with

thicknesses ranging from 14.6 to 33.8 nm.[140] The thicknesses of these nanosheets are well-correlated with the PEG contour lengths (Fig. 10a). When the axle is changed from a linear to a 4-arm PEG (1.25 kDa per arm), nanoplates with a thickness of 10.0 nm were also observed (Fig. 10b). These results suggest the close packing of linear and star polypseudorotaxanes as hexagonal crystalline domains are thermodynamically favored.[140] When linear PEGs with longer chain lengths are mixed with α-CD, hydrogels rather than crystalline nanoplates are formed. In 1994, Harada *et al*. reported the formation of stable polypseudorotaxane hydrogels by mixing α-CDs with long-chain PEGs ($M_n \geq 20$ kDa).[145] In their proposed model, segments of α-CDs are crystallized to form supramolecularly crosslinked networks (Fig. 10c). The elastic moduli of PEG$_{8k}$/α-CD and PEG$_{20k}$/α-CD polypseudorotaxane hydrogels were measured by Li *et al*. later,[146] as G′ of 200 Pa and 2×10^4 Pa, respectively (Fig. 10d). Time-dependent rheological sweeps showed that PEG$_{8k}$/α-CD and PEG$_{20k}$/α-CD polypseudorotaxane hydrogels slowly recovered to their original moduli (Fig. 10d), making them difficult for DIW. Cooper-White *et al*. investigated the rheological properties of hydrogels formed by Pluronic F68 and α-CD (Fig. 10e).[147] When F68 (10 wt%) was mixed with α-CD (10 wt%), a stable hydrogel with an elastic modulus of 4×10^5 Pa was formed, as shown in the angular frequency sweep (Fig. 10e). However, this gel took more than 20 minutes to recover in the time-dependent rheological studies. Zhang *et al*. introduced PEG-grafted heparin with α-CD to form strong polypseudorotaxane hydrogels (Fig. 10f).[148] PEG$_{5k}$-heparin was synthesized by coupling mPEG$_{5k}$-NH$_2$ with heparin sodium salt ($M_w = 6$–15 kDa) with a grafting ratio of 10%. In the presence of α-CD, a stable hydrogel with an elastic modulus of 2×10^4 Pa was obtained (Fig. 10f). This hydrogel showed good shear thinning feature, but the self-healing was not fast enough for DIW as suggested by the step-strain sweep.
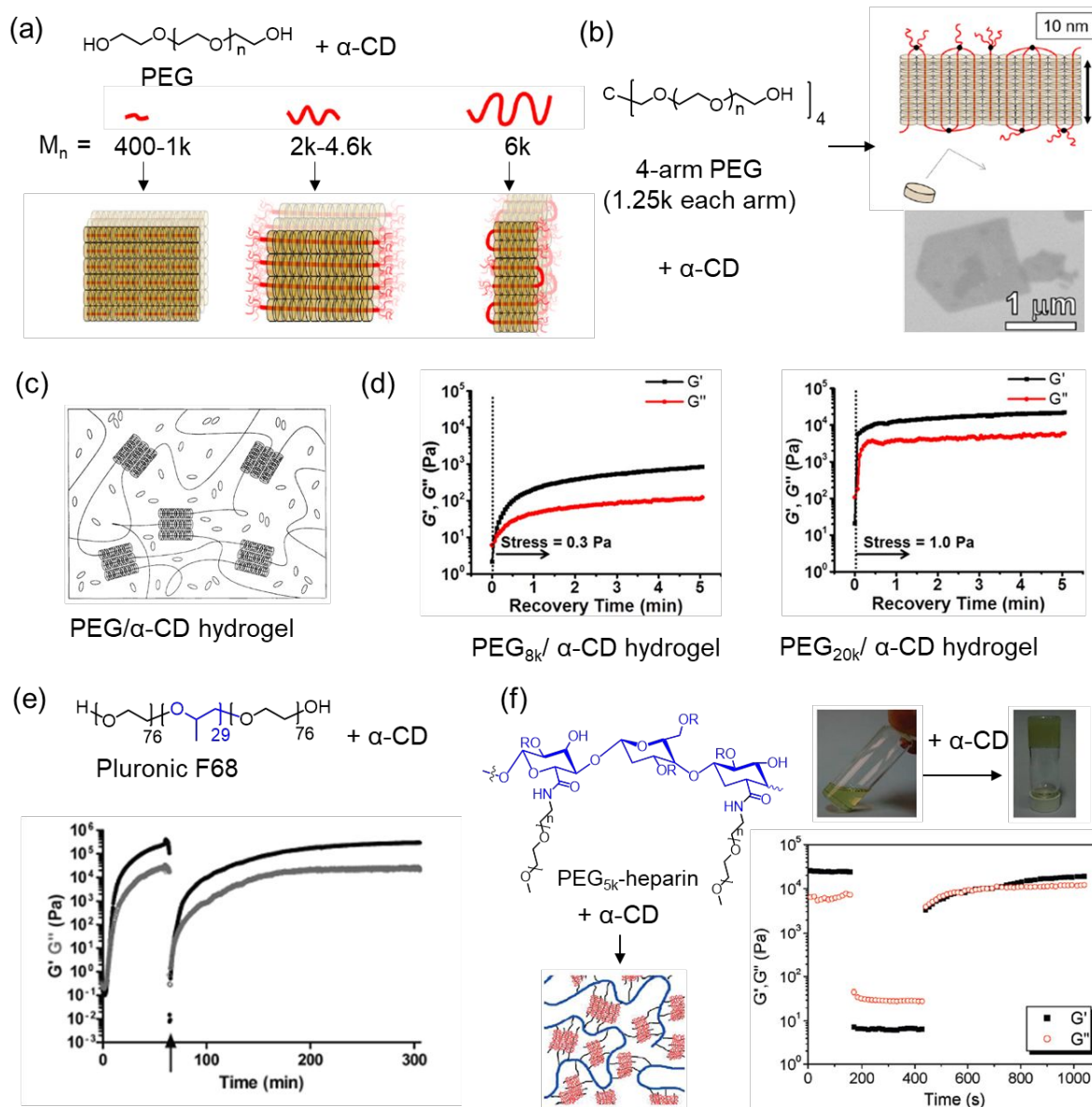
Fig. 10. (a-b) Schematic illustrations of the formation of polypseudorotaxane nanoplates using (a) linear PEGs and (b) a 4-arm PEG. The SEM image of the polypseudorotaxane nanoplates is shown on the right. Reproduced with permission from reference 140. Copyright 2019 American Chemical Society. (c) Proposed gelation mechanism of polypseudorotaxane hydrogels formed by linear PEGs and α-CDs. Reproduced with permission from reference 145. Copyright 1994 Springer Nature. (d) Time-dependent self-healing sweeps of PEG$_{8k}$/α-CD and PEG$_{20k}$/α-CD hydrogels. Reproduced with permission from reference 146. Copyright 2020 American Chemical Society. (e) Time-dependent self-healing sweeps of a polypseudorotaxane hydrogel formed by Pluronic F68 and α-CD. Reproduced with permission from reference 149. Copyright 2013 American Chemical Society. (f) A polypseudorotaxane hydrogel formed by

PEG$_{5k}$-heparin and its step-strain sweep. Reproduced with permission from reference 148. Copyright 2010 American Chemical Society.

Many α-CD-based polypseudorotaxane hydrogels,[150] which use high-molecular-weight PEG,[151, 152] PEG block copolymers,[153, 154] and branched/star PEG polymers[155, 156] as the axles, show high elastic moduli of G′ > 10^4 Pa and they are suitable for extrusion. More often than not, they are not great for DIW due to their limited self-healing capability shown in the step-strain sweeps. In Section 4.4, we will discuss the strategies for designing 3D-printable polypseudorotaxane hydrogels.

4. Supramolecularly designed DIW inks

### 4.1 DIW inks designed based on hydrogen-bonding interactions

Hydrogen bonds are prevalently used to build supramolecular assemblies. Natural polymers such as DNA,[157] proteins,[158] [157]and polysaccharides[159] with rich carbonyl, amide, and hydroxyl groups form hydrogels via the hydrogen-bonded networks. Some of these hydrogels formed by alginate, chitosan, carrageenan, gelatin, and xanthan, are extrudable at suitable concentrations,[160] which are potential candidates for DIW. To optimize the rheological properties for DIW, these natural polymers are chemically modified to introduce additional supramolecular and/or chemical crosslinking moieties. For example, when methacrylate sodium alginate (MA-SA) was mixed with a 2-(dimethylamino)-ethyl-methacrylate comonomer and a photoinitiator, an extrudable ink was formulated with an elastic modulus of ~200 Pa after photo-crosslinking the methacrylate groups.[161] The extruded structures were reinforced by Ca^{2+} and chitosan subsequently, demonstrating the feasibility of utilizing hydrogen bonding networks for DIW ink design.

Synthetic polymers like PVA also feature abundant hydroxyl groups for hydrogen-bonding.[162] Wang and Cai *et al.* reported the preparation of 3D-printable hydrogels (Fig. 11a) using PVA (10 wt %) and κ-carrageenan (κ-CA) (1–4 wt%),[163] in which inter-polymer hydrogen bonds are formed between the hydroxyl groups of PVA and sulfonate groups of κ-CA. The hydrogel exhibited good shear-thinning and self-healing properties for DIW (step-strain sweep, Fig. 11a). Multilayer complex structures such as quadrangular pyramids, dendritic tubes, and hydrogel letters were 3D-printed with adjustable linewidths (220–850 μm). Interestingly, PVA micro-crystallizes after freeze-thaw cycles, forming nano-crystalline domains.[164] Hence, these 3D-printed samples were mechanically strengthened after several freeze–thaw treatments. Under a similar principle, Wang *et al.* 3D-printed hydrogen-bond crosslinked PVA/chitosan hydrogels and reinforced the 3D-printed materials through freeze–thaw cycles (Fig. 11b).[165] The PVA/chitosan ink was prepared by mixing PVA (12.5 wt%) and chitosan (12.9 wt%) to allow for hydrogen bonding between PVA and chitosan. Notably, the hydrogel exhibited high yield stress at 3.8 kPa and an elastic modulus G′ of 5

kPa (Fig. 11b). After DIW, the freeze-thaw processed samples were soaked in sodium citrate solutions to form a secondary electrostatically linked network. After this treatment, the tensile strength, stretchability, Young's modulus, and work-to-rupture of the hydrogel reached 12.7 MPa, 300%, 14 MPa, 22 MJ/m^3, respectively.
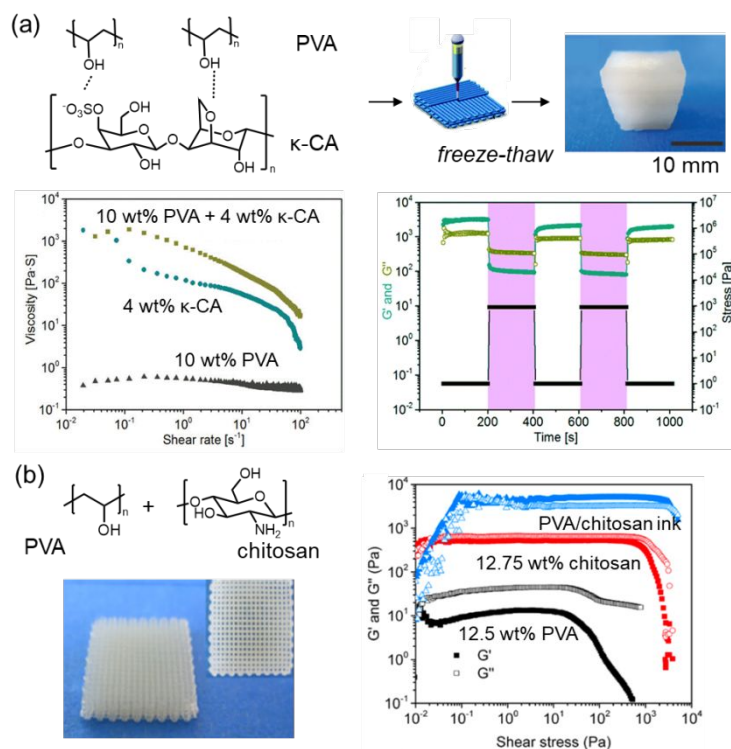
Fig. 11 (a) PVA/κ-CA hydrogels designed for DIW and their post-printing freeze-thaw treatments. Shear-rate and step-strain sweeps of the hydrogels are shown below. Reproduced with permission from reference 163. Copyright 2019 Royal Society of Chemistry. (b) PVA/chitosan hydrogels used for DIW and their shear stress sweeps. The 3D-printed samples were reinforced by freeze-thaw and sodium citrate treatments. Reproduced with permission from reference 165. Copyright 2020 American Chemical Society.
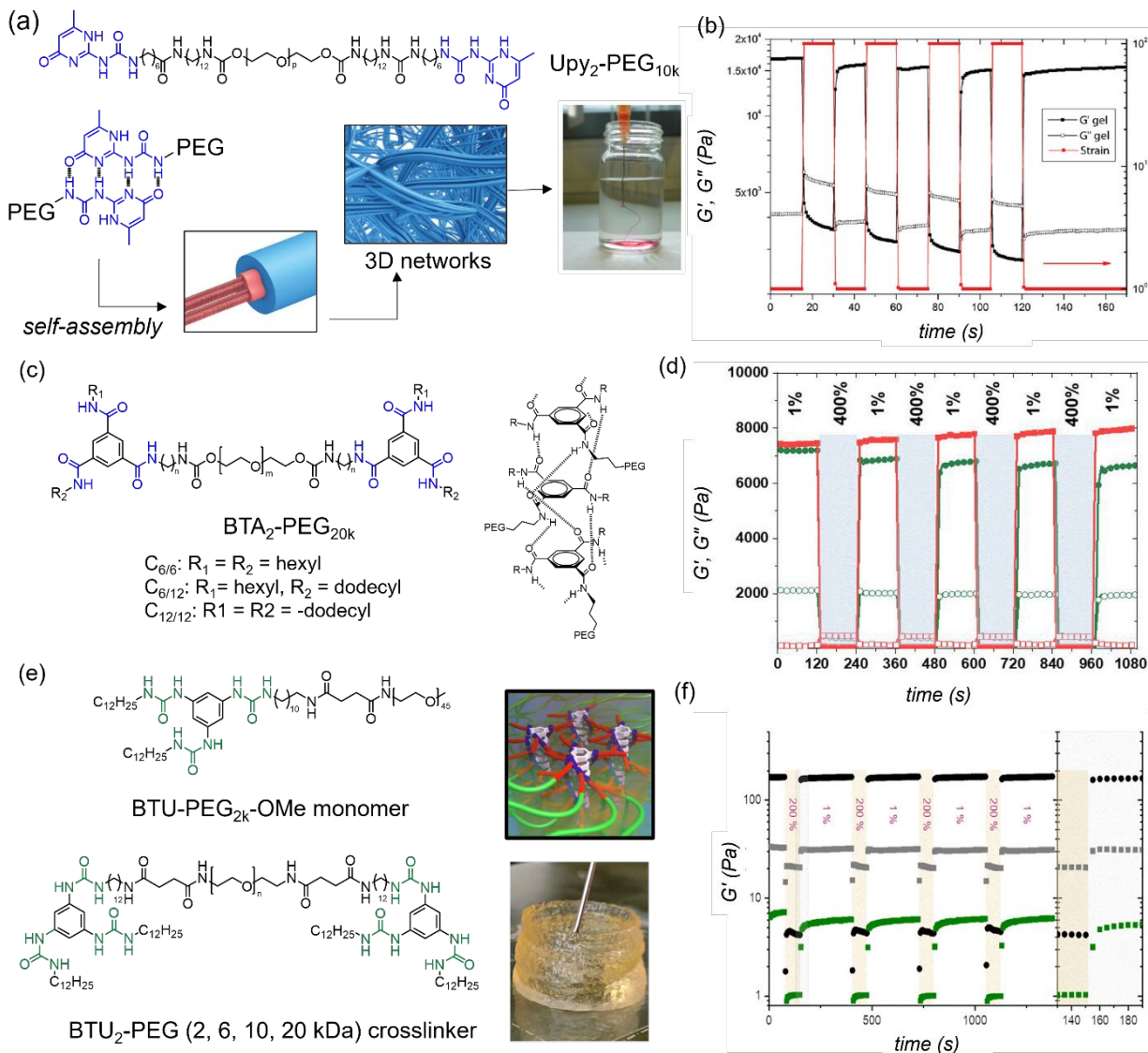
Fig. 12. (a) An extrudable hydrogel formed by self-assembled UPy$_2$-PEG$_{20k}$ via complementary hydrogen bonding interactions. (b) The step-strain sweeps of the Upy$_2$-PEG$_{20k}$ hydrogel. Reproduced with permission from reference 74. Copyright 2018 John Wiley & Sons, Inc. (c) BTA(C$_{6/6}$, C$_{6/12}$, C$_{12/12}$)-PEG$_{20k}$ with different lengths of side arms self-assembled into 1D supramolecular polymers. (d) The step-strain sweeps of BTA(C$_{6/6}$, C$_{6/12}$, C$_{12/12}$)-PEG$_{20k}$ hydrogels. Reproduced with permission from reference 166. Copyright 2022 American Chemical Society. (e) BTU-PEG$_{2k}$-OMe monomer and BTU$_2$-PEG (2, 6, 10, 20 kDa) crosslinkers self-assembled into 3D-printable hydrogels. (f) The step-strain sweeps of the hydrogels before and after the addition of the crosslinkers. Reproduced with permission from reference 167. Copyright 2022 American Chemical Society.

Synthetic polymers with multivalent hydrogen bonds also assemble to form viscoelastic gels for DIW. In an aqueous solution, Upy_2-PEG_{10k} self-assembled into 1D supramolecular polymers (Fig. 12a), and these supramolecular polymers further aggregated to form a crosslinked network.[74] At a concentration of 10 wt%, Upy_2-PEG_{10k} self-assembled into a strong hydrogel with an elastic modulus of 10^4 Pa. In the step-strain sweep, the hydrogel showed promising self-healing properties but required some extra time (2–3 s) for the network to recover fully (Fig. 12b). The hydrogel was extruded from a syringe needle into a neutral PBS solution to give fine filaments, showing pH-switchable sol-gel transitions, despite the fact that the hydrogel was not examined for DIW. Besides Upy motifs, benzene-1,3,5-tricarboxamide (BTA) derivatives with long alkyl arms have been extensively investigated to form supramolecular polymers.[168-172] When PEG arms are introduced to BTAs, water-soluble supramolecular polymers are formed via hydrogen bonding and hydrophobic effects.[173, 174] Meijer *et al*. synthesized telechelic PEGs (20 kDa) with BTA end groups of different alkyl arms.[175] They discovered that longer alkyl arms on BTA favor supramolecular polymerization. At a concentration of 10 wt%, BTA_2-PEG_{20k} self-assembled in water to form a supramolecular hydrogel with strong frequency-dependent moduli. Baker *et al*. optimized the system and synthesized three BTA-PEG derivatives (Fig. 12c).[166] At a concentration of 10 w/v%, $BTA(C_{6/12})_2$-PEG_{20k} and $BTA(C_{12/12})_2$-PEG_{20k} formed stable hydrogels with an elastic moduli of ~10^4 Pa. Step-strain sweeps (Fig. 12d) showed that the $BTA(C_{6/6})_2$-PEG_{20k} and $BTA(C_{6/12})_2$-PEG_{20k} hydrogels possess good self-healing properties, making them promising for DIW. At the same time, Brendel *et al*. synthesized a benzene trisurea (BTU)-based supramolecular monomer and a crosslinker (Fig. 12e) to construct supramolecularly crosslinked hydrogel.[167] BTU-PEG_{2k}-OMe monomers self-assembled to form a weak hydrogel with an elastic modulus of ~10 Pa. In the presence of the BTU_2-PEG crosslinker ([monomer]/[crosslinker] = 100), a supramolecularly crosslinked hydrogel was formed (G' ~100 Pa). This hydrogel showed fast self-healing property and it was successfully 3D-printed via DIW into a hollow cylinder (Fig. 12e).

DNAs are also used for the construction of hydrogen-bonded hydrogels, such as artificial extracellular matrices.[176] Liu and Shu *et al*. developed free-form 3D-printable DNA-based hydrogels (Fig. 13).[98] In this work, polypeptide–DNA hydrogels were prepared by mixing a polypeptide–DNA conjugate with a double-stranded DNA (Fig. 13). The double-stranded DNA acted as a supramolecular crosslinker to form complementary hydrogen bonds with the grafted DNA on the polypeptide–DNA conjugate. A supramolecular hydrogel was formed within one second at 5 wt% of the polypeptide–DNA conjugate and the double-stranded DNA. The frequency sweep of the hydrogel showed G′/G″ ≈ 10. The yield strain reached 30% in the strain sweep, suggesting that a large deformation is required to extensively break the hydrogen-bonded network. Co-extruding microdroplets of polypeptide–DNA conjugate and double-stranded DNA solutions allowed for the rapid gelation and successful 3D-printing of self-supportive architectures (20 layers) within a few minutes. Living cells were added to the ink solutions and 3D-printed

as cell-laden hydrogels, achieving good 3D-printability and cell viability at the same time. Further introducing protease into the hydrogel led to the degradation of polypeptide backbone and the collapse of the hydrogel networks.

Very recently, three-arm synthetic polypeptides-polymer conjugates with hydrogen-bonded β-sheets have been introduced for DIW.[177] In this design, hydrophobic poly(tyrosine) or poly(valine) have been introduced to form anti-parallel β-sheets, which serve as supramolecular crosslinkers for the network. The polypeptides-polymer conjugate hydrogels showed good shear-thinning and self-healing rheological properties, which were 3D-printed and photo-crosslinked as bio-compatible scaffolds to house bacteria. Under a very similar principle, Hartgerink *et al.* reported a nanofibrous hydrogel comprised of multidomain peptides with good viscoelastic properties for DIW.[178] The 3D-printed peptide hydrogels demonstrated their bio-computability for cell culturing.
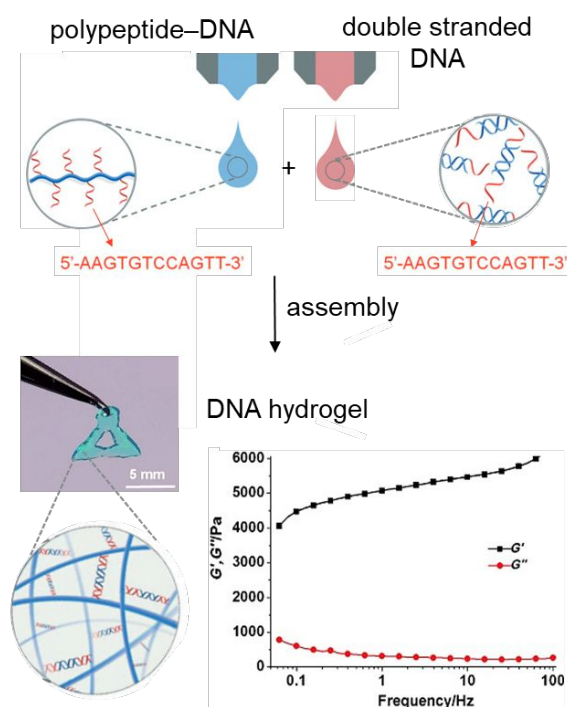
Fig. 13. DNA-based hydrogels formed by mixing solutions of polypeptide-DNA and double-stranded DNA. Samples were 3D-printed by co-extruding microdroplet of these solutions. The frequency sweep is shown at the bottom. Reproduced with permission from reference 98. Copyright 2015 John Wiley & Sons, Inc.

4.2 DIW inks designed based on host-guest interactions

Host-guest complexes such as β-CD/adamantyl (Ad) complexes ($K_a = 10^3–10^5$ M^{-1})[119] have been widely used to construct linear and crosslinked supramolecular polymers.[118, 179-181] Groll et al. proposed in a review[20] to introduce a variety of host-guest binding motifs to construct DIW-compatible hydrogels. Employing host-guest complexes to facilitate shear-thinning and self-healing properties to DIW inks seems straightforward. However, only limited successful examples have been reported so far, despite the disruption and reformation of host-guest complexes is highly reversible and kinetically fast. In these reported examples, host-guest-based gels usually possess good shear-thinning features, but only a few of them demonstrated fast self-healing and excellent self-supporting. Among these notable examples,[59, 75, 182] a secondary covalent or supramolecular network is introduced to the ink for successful DIW. Nonetheless, these host-guest-based DIW inks made them particularly attractive for biomedical applications.
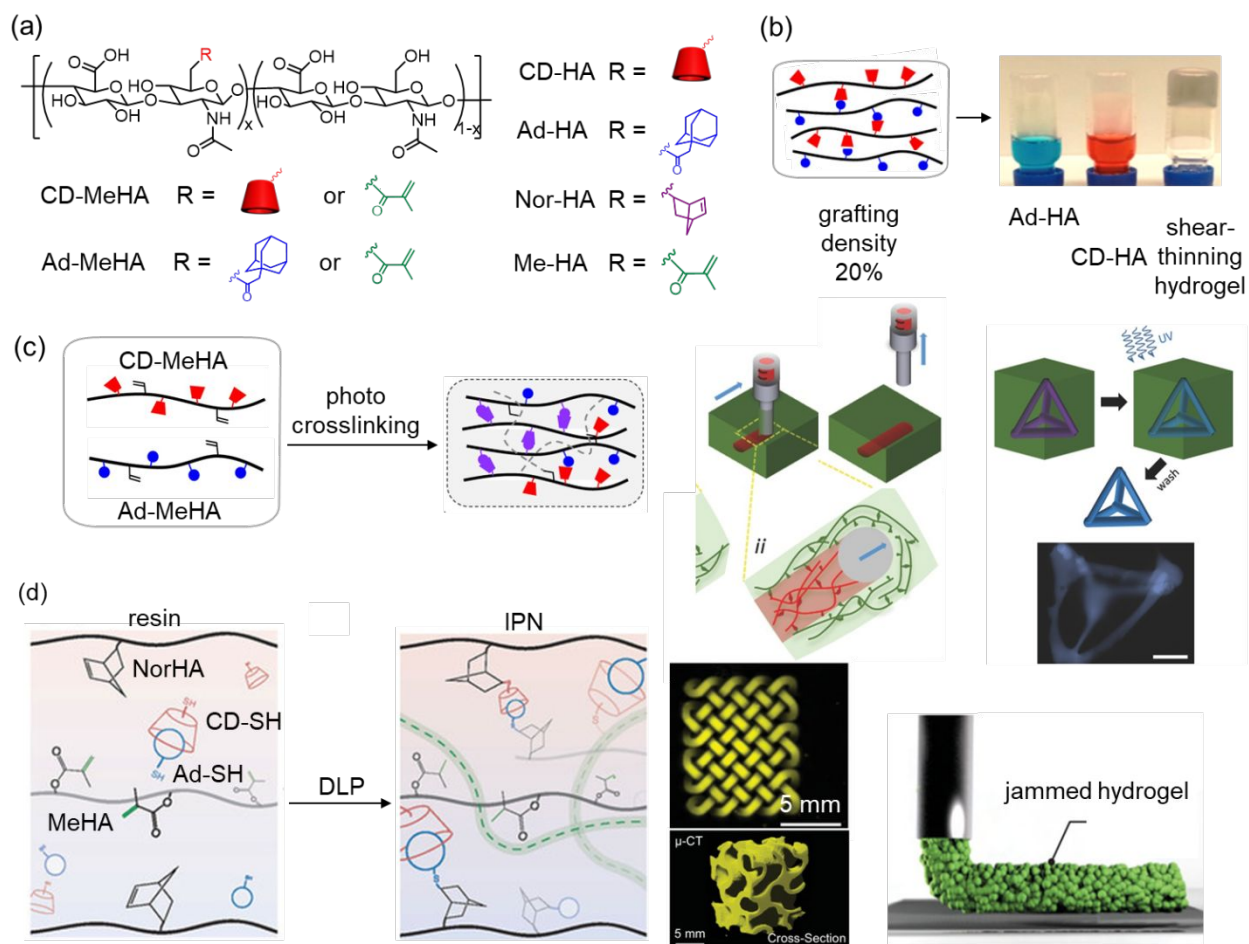
**Fig. 14.** (a) Modified HA derivatives used to construct hydrogels with host-guest networks. (b) Shear-thinning hydrogels formed by mixing CD-HA (red) with Ad-HA (blue). Reproduced with permission from reference 149. Copyright 2013 American Chemical Society. (c) 3D-printable HA hydrogels formed by methacrylate-modified CD-HA and Ad-HA, followed by photo-crosslinking. An ink gel (red colored) was

printed into a support gel (green colored), and 3D-printed self-supporting hydrogels were formed after photo-crosslinking and removal of the support. The confocal fluorescent image of the 3D-printed hydrogel was shown at the bottom. Reproduced with permission from reference 75 Copyright 2015 John Wiley & Sons, Inc. (d) DLP fabrication of IPN hydrogels consisting of a covalently crosslinked HA network and a supramolecularly crosslinked host-guest network. The host-guest network was formed by Nor-HA, CD-SH, and Ad-SH. Fluorescent images of the 3D-printed knotted mesh and gyroid structures are shown at the bottom. A jammed hydrogel DIW was performed using crosslinked IPN microgels as the ink. Reproduced with permission from reference 48. Copyright 2022 John Wiley & Sons, Inc.

An early example of β-CD/Ad complexation-enabled gelation was reported by Burdick *et al.* (Fig. 14a-b).[149] In this work, a series of β-CD and Ad grafted hyaluronic acid (HA) with different grafting densities were synthesized (M_n = 74 kDa, DP ~186). The grafting density of β-CD is 20%, and the grafting density of Ad groups varied between 20% and 50%. Upon mixing these two HA derivatives in 1:1 CD to Ad ratio, a stable hydrogel (5 wt%) was obtained with an elastic modulus G' of ~10^3 Pa. At a concentration of 7.5 wt%, the host-guest hydrogel showed good shear-thinning and rapid self-healing. However, this hydrogel was only extrudable because the loss modulus was close to the elastic modulus (G''/G' ~1). The high loss modulus in this hydrogel was attributed to the fast binding-site exchange between β-CD-HA and Ad-HA. To address this problem, CD-HA and Ad-HA with higher grafting densities (25% or 40%) were synthesized (Fig. 14a).[75] When CD-HA and Ad-HA polymers were mixed at 1:1 ratio, supramolecular hydrogels (3−7.5 w/v%) were formed at variable CD/Ad grafting densities (25%, 40%) through host-guest complexation. Step-strain rheological studies demonstrated that both hydrogels showed good self-healing properties upon repeated shearing. Different from conventional DIW, an interesting gel-in-gel printing was developed (Fig. 14c). They employed the hydrogel formed by 25% grafted CD-HA and Ad-HA at 5 w/v% as the 'ink' gel, and the hydrogel formed by 40% grafted CD-HA and Ad-HA at 4 w/v% as the 'support' gel. By printing the ink hydrogel into the support hydrogel, complicated architectures were obtained in the supported gel. This gel-in-gel printing design overcame traditional obstacles of DIW, such as 3D-printing large overhanging structures using ultra-soft 3D-printing inks. Subsequently, methacrylate groups were introduced to the host-guest polymers, and 3D-printed architectures were photo-crosslinked (Fig. 14c). After removing the supporting gel, 3D-printed hollow architectures and free-standing monoliths were obtained. To visualize the DIW process, a fluorescent tag was attached to the Ad-HA macromonomers. This tagged hydrogel also allowed for *in vivo* monitoring of the hydrogel degradation and the release of biomolecules.[59]

The host-guest-based supramolecular polymers are not only compatible with DIW designs, but also suitable for constructing interpenetrated polymer networks (IPNs)[183-186] for vat-polymerization-based 3D-

printing. Recently, Burdick *et al.* reported a DLP printing of interpenetrated host-guest networks at a low polymer concentration (5 wt%, Fig. 14e).[48] In this design, CD-Ad complexes were prepared by mixing adamantane thiol (Ad-SH) and β-CD thiol (CD-SH) stoichiometrically. This host-guest complex reacts with norbornyl-modified HA (Nor-HA) to form a host-guest crosslinked network. Partially methacrylated HA (MeHA) was mixed with a photoinitiator to form the secondary covalent network. Since these two networks were simultaneously formed by light-irradiated radical reactions, an one-pot photopolymerization afforded an interpenetrating network with good DLP processability. Complex architectures such as snowflakes, knotted mesh, and gyroids were printed at high speeds. Notably, the 3D-printed IPN hydrogels exhibited variable mechanical properties (stretchability, Young's modulus, and work of fracture) by tuning the proportions of MeHA to host-guest crosslinked networks. Interestingly, IPN hydrogel microparticles were synthesized using a microfluidic droplet method. These granular hydrogels were 3D-printed into jammed hydrogel monoliths via conventional DIW (Fig. 14e). These results highlight the interchangeable supramolecular designs and practices for DIW and vat-polymerization-based 3D printing.
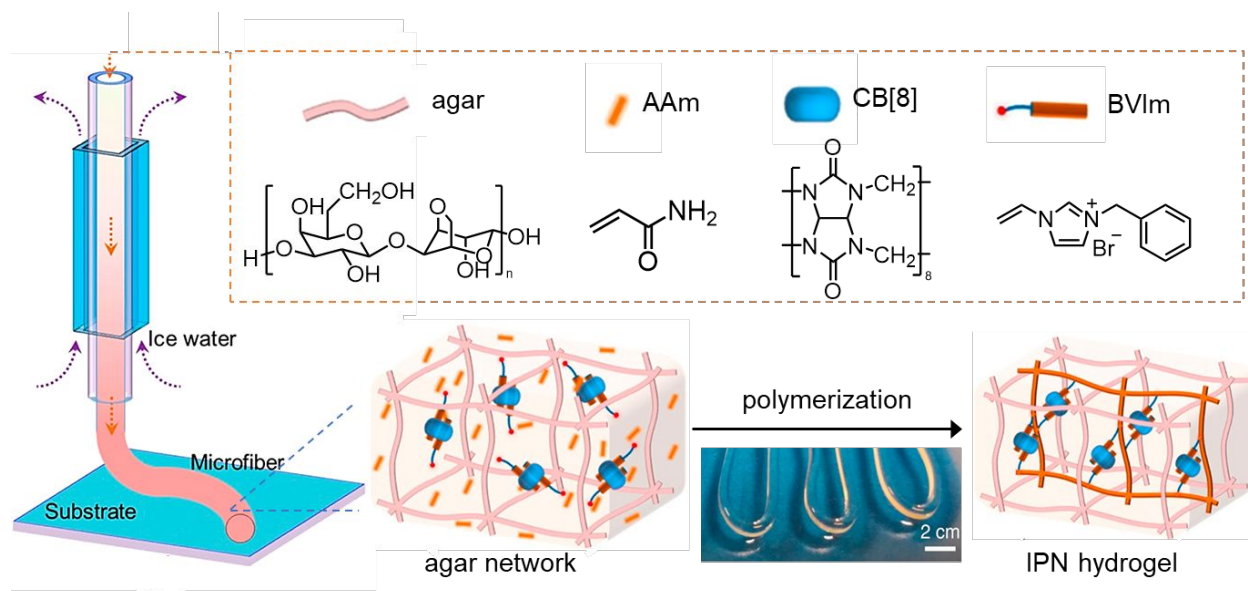
Fig. 15. Illustration for the fabrication of IPN hydrogel microfibers through host-guest complexation and microfluidic manufacturing. A hot agar solution with CB[8], AAm, and BVIm flowed through a cold-water jacked microfluidic channel. The extruded microfibers were photo-polymerized subsequently. Reprinted with permission from reference 182. Copyright 2020 American Chemical Society.

CB[8]-based inclusion complexes have also been introduced for IPN design to reinforce the fabricated hydrogels.[182, 187] As shown Fig. 15, IPN hydrogel microfibers comprised of a supramolecularly crosslinked agar network and an interpenetrated CB[8]-based polyacrylamide (PAAm) network were obtained. Experimentally, a hot aqueous solution of agar, acrylamide (AAm), CB[8], and 1-benzyl-3-

vinylimidazolium bromide (BVIm) was injected into a water-cooled microfluidic channel. The rapid cooling enabled the gelation of agar. UV-induced radical co-polymerization of AAm and BVIm in the presence of CB[8] formed the second supramolecularly crosslinked network. The continuous flowing of the hot solution through the water-cooled channel afforded meter-long, tough, and highly stretchable hydrogel microfibers (Fig. 15). Since this microfluidic device is similar to a DIW extrusion system (using a temperature-controlled printing head), we expect this supramolecular design is readily convertible to DIW.

4.3 DIW inks designed based on metal-ligand and electrostatic interactions

Compared to other supramolecular interactions, metal-ligand coordinations are generally stronger and more directional.[188] When metal ions are added to solutions of ligand-grafted polymers, the formed coordination complexes act as supramolecular crosslinkers.[189] Notably, the stability and reversibility of the coordination complexes could be adjusted by varying the metal ions, ligands, concentrations and ratios of metal/ligand, and pH/temperature of the environment.[190] For example, histidine-rich decapeptide/Zn^{2+} complexes have been used to build a coordination network in tough IPN hydrogels.[191] At different Zn^{2+} to histidine ratios, the coordination complexes adopted linear or tetrahedral geometries with different binding affinities. In particular, a tandem-multiple ligand binding showed strong binding ($K_{a1} \sim 3 \times 10^4$ M^{-1}, $K_{a2} \sim 9 \times 10^6$ M^{-1}), which endowed the IPN hydrogel with good energy dissipation capability, compressibility, and fast recovery. On the other hand, self-healing polymers have also been constructed via metal-ligand coordinations due to their inherent reversibility.[192]
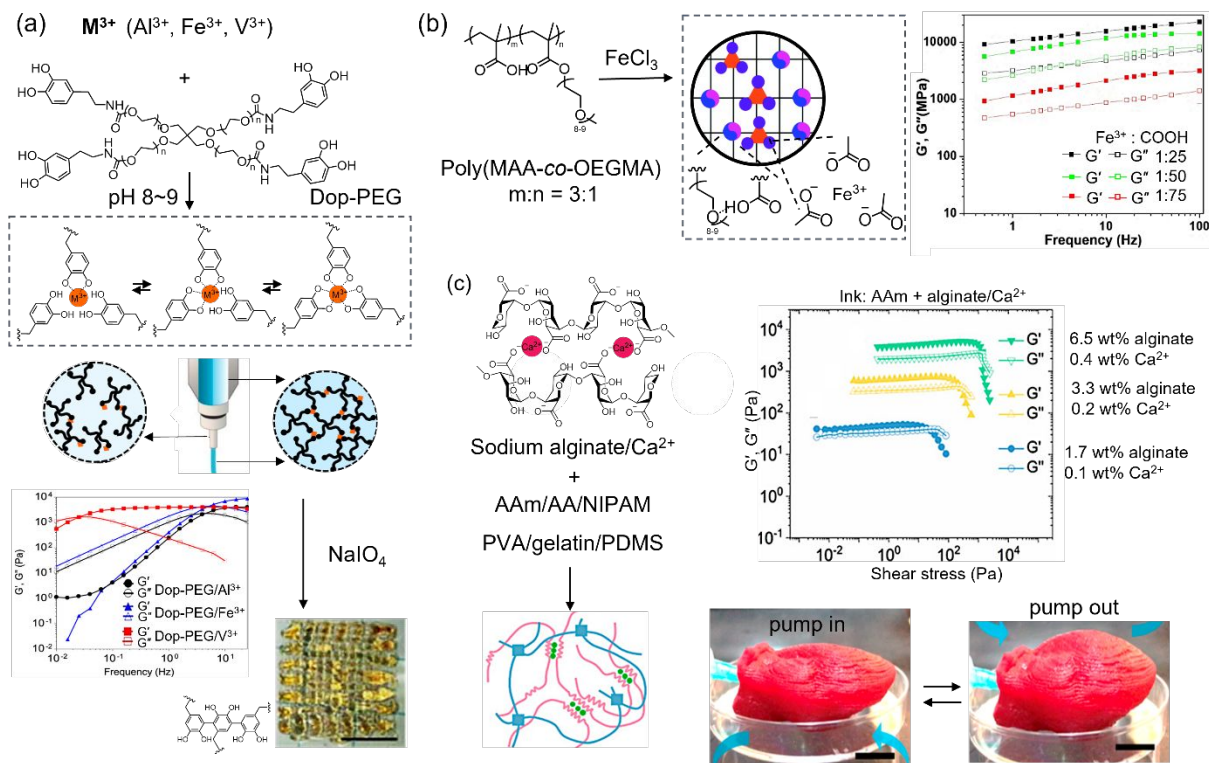
Fig. 16. (a) Illustrations of inks formed by mixing Dop-PEG and metal ions (Al^{3+}, Fe^{3+}, and V^{3+}). The dynamic metal-ligand coordination and angular frequency sweep are illustrated below. During DIW, the ink was further reinforced by $NaIO_4$ oxidation, forming an additional covalently crosslinked network Reproduced with permission from reference 76. Copyright 2020 IOP Publishing Ltd. (b) DIW inks formed by carboxylic/Fe^{3+} coordination and hydrogen bonding using poly(MAA-*co*-OEGMA). The angular frequency sweeps of the inks are shown on the right. Reproduced with permission from reference 193. Copyright 2021 Royal Society of Chemistry (c) Aglinate/Ca^{2+} hydrogels with AAm, AA, NIPAM monomers or PVA, gelatin, PDMS polymers were 3D-printed. Inks with monomers were photo-crosslinked in the next step. Rheology data of the AAm/alginate/Ca^{2+} hydrogel was shown here. A 3D-printed PVA-alginate/Ca^{2+} artificial heart beating upon pneumatic pumping Reproduced with permission from reference 194. Copyright 2019 American Chemical Society.

   Catechol coordinates with various metal ions, forming different coordination geometries.[195] In nature, marine mussels took advantage of the triscatechol/Fe^{3+} complex (K_a ~10^{40} M^{-1}) in their byssal threads to adhere firmly on various surfaces.[196] Introducing catechol/metal complexes to form metal-ligand crosslinked hydrogels have been demonstrated with good self-healing properties.[190] For instance, Campo and Włodarczyk *et al.* reported a series of catechol-metal-based DIW-compatible inks comprised of dopamine-functionalized PEG (Dop-PEG, 5 w/v%) and trivalent metal ions (M^{3+}: V^{3+}, Fe^{3+}, and Al^{3+}, Fig. 16a).[76] Dop-PEG/M^{3+} networks were formed by mixing the Dop-PEG and M^{3+} in acidic solutions and then

increasing the pH to 8.6–8.9. Since the pK_a of catechol are 9.25 and 13.0,[197] despite the Dop:M^{3+} ratio being fixed at 3:1, a mixture of mono-, bis-, and tris-coordinated crosslinkages were formed, and they were interconverting (Fig. 16a).[198] Rheological studies showed that all Dop-PEG/M^{3+} hydrogels were shear-thinning for extrusion, but the loss moduli G″ are larger than elastic moduli G′ at low frequencies in the angular frequency sweep (Fig. 16a). These studies suggest that these hydrogels are not self-supportive over a long period; hence only low-profile lattices were 3D-printed. Sodium periodate was added to each printed layer before printing the next layer to oxidize the catechol end groups to polyquinones. The oxidative condensation of Dop-PEG formed a covalently crosslinked network, thus reinforcing the 3D-printed structure.

Connal *et al.* employed poly(MAA-*co*-OEGMA)/Fe^{3+} coordination complexes for DIW ink design (Fig. 16b).[193] Copolymerizing MAA and OEGMA at a 3:1 molar ratio afforded poly(MAA-co-OEGMA), which self-assembled as a hydrogen-bonding crosslinked network. Next, $FeCl_3$ was added to poly(MAA-*co*-OEGMA) to form an additional low crosslinking-density coordination network. The dual-crosslinked hydrogels with different Fe^{3+}-to-COOH ratios (1: 75 to 1: 5) showed significantly higher elastic moduli G′ and loss moduli G″ than the hydrogen-bonded network. The elastic moduli G′ were higher than loss moduli G″ over the whole frequency range for the dual-crosslinked hydrogels. The hydrogel with a 1:75 Fe^{3+}:COOH molar ratio possesses high toughness (13 MJ·m^{-3}) and stretchability (180%) with good self-healing features. Therefore, it was selected to build humidity-sensitive actuators. A flower was printed as a demonstration to show humidity-driven shape transformations (Fig. 16b), where reversible bending motions were observed by changing the relative humidity.

The sodium alginate/Ca^{2+} complex represents another commonly used coordination complex for hydrogel formation.[199] In these hydrogels, the divalent Ca^{2+} cations bind to multiple guluronic acids of sodium alginate, forming the well-known "egg-box" crosslinkages.[200] Ho *et al.* reported the construction of DIW inks comprised of sodium alginate and $CaCl_2$ supramolecular network and a series of polymer precursors (Fig. 16c).[194] Sodium alginate/Ca^{2+} complex solutions were mixed with monomers (AAm, AA, NIPAM) or polymer precursors (PVA, gelatin, PDMS). After adding sodium alginate (6.5 wt%) and $CaCl_2$ (0.4 wt%) to a non-viscous AAm solution (η = 1.5 mPa·s), the viscosity of the ink reached ~1.6×10^4 Pa·s at a low shear rate (0.01 s^{-1}) and decreased to ~50 Pa·s at a high shear rate (50 s^{-1}). The elastic moduli G′ reached 4650 Pa and are constantly higher than G″ (Fig. 16c). After photo-polymerization, a secondary covalent network was formed in the 3D-printed samples, which exhibited the typical mechanical features of IPN gels. Consequently, soft robots were fabricated with different functions, e.g., a PVA-based robotic heart with beating-transporting motions (Fig. 16c).

Electrostatic interactions between polycations and polyanions have also been explored to design 3D-printable supramolecular networks, facilitating shearing-thinning and self-healing features. However, when oppositely charged polyelectrolytes are mixed, the solubility of the complex drops significantly,[201] rendering problems such as inhomogeneity and complex sol-gel transitions. For example, the rapid assembly of two polyelectrolytes at the interface hinders the extensive diffusion of these polyelectrolytes, resulting in a high crosslinking density at the interface but low crosslinking density inside of the ink.[202] Hence, limited successful examples have been reported so far.

Electrostatically crosslinked 3D-printing inks have been synthesized using natural polymers (e.g., gelatin and sodium alginate) or synthetic polymers (e.g., polyacrylic acid). For example, Li *et al.* reported an alternating DIW of two oppositely charged ionic hydrogels by binding hydrogels layer-by-layer (Fig. 17a).[160] A group of polymers, including cationic chitosan, anionic sodium alginate, xanthan, κ-CA, zwitterionic gelatin, and GelMA, underwent gelation in buffer solutions. These cationic, anionic, and zwitterionic hydrogels showed shear-thinning behavior under a wide range of shear rates ($0.5-500$ s^{-1}) and thixotropic properties under high shear rates (100 s^{-1}). Zwitterionic GelMA hydrogel (10 wt%) and anionic κ-CA hydrogel (2 wt%) were printed alternately as 20-layered grids with good structural integrities (Fig. 17a). Cao and Zhen *et al.* reported a polyionic ink comprised of a cationic chitosan and an anionic sodium alginate (Fig. 17b).[77] In a sodium alginate solution (10 w/v%), chitosan (0–1.2 *equiv.* to alginate) was dissolved at pH < 4, forming electrostatically crosslinked hydrogels. During DIW, an HCl solution (0.5 M) was sprayed onto each layer of the extruded inks to protonate the chitosan to induce fast and uniform electrostatic crosslinking. Accordingly, the inks became viscous with shear-thinning characteristics, and the viscosity reached 3600 Pa·s at a 0.01 s^{-1} shear rate and quickly decreased to below 10 Pa·s at a 100 s^{-1} shear rate. The HCl-treated chitosan/alginate constructs showed good compressibility ($\varepsilon > 90\%$) and high toughness (> 100 kJ/m^3) due to the strong electrostatic interactions.
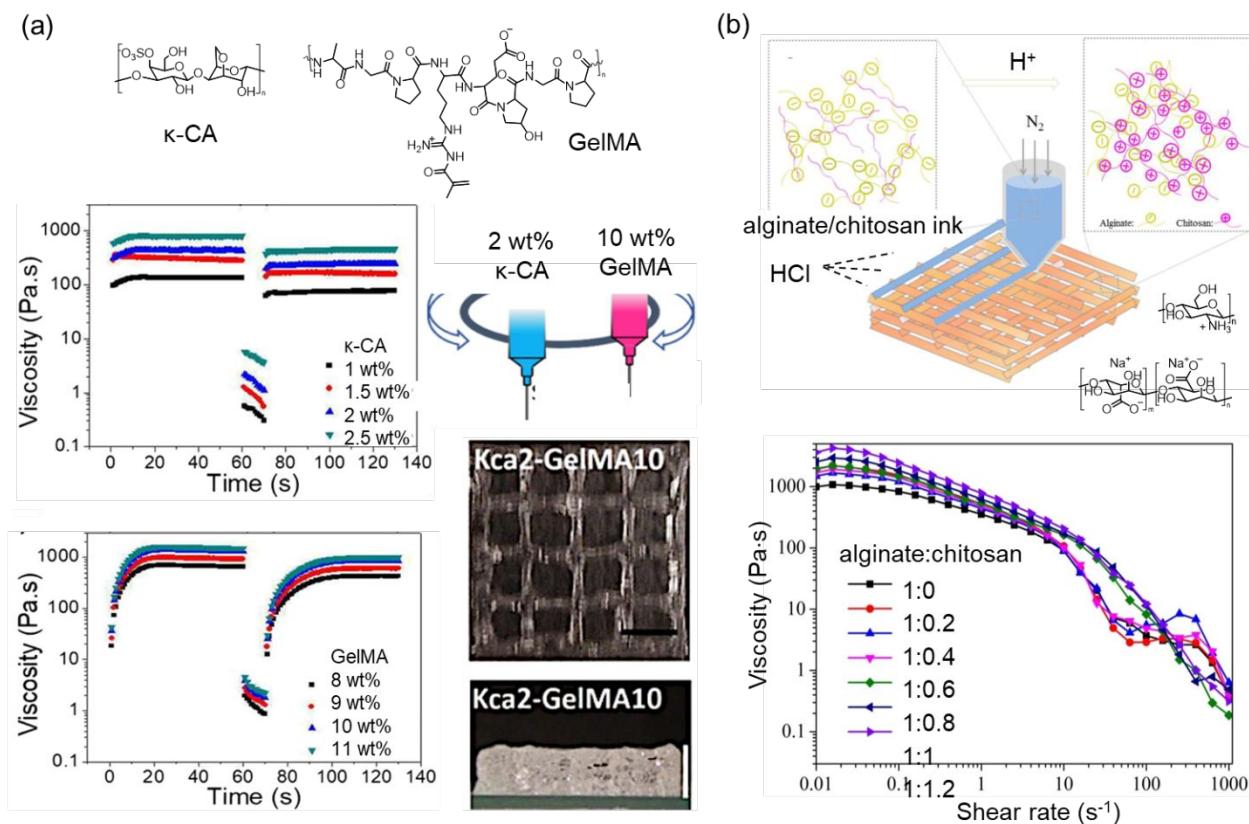
Fig. 17 (a) Chemical structures and step-strain sweeps of the zwitterionic GelMA and anionic κ-CA hydrogels. The image of a 3D-printed κ-CA/GelMA heterogeneous lattice was shown on the right. Reproduced with permission from reference 160. Copyright 2018 American Chemical Society. (b) Illustration of DIW of alginate/chitosan inks with HCl sprayed after the deposition of each layer. The shear rate sweeps of the inks at various alginate/chitosan ratios without the HCl treatment were shown on the right. Reproduced with permission from reference 77. Copyright 2018 MDPI.

4.4 DIW inks designed based on micro-crystallization

As discussed in section 3, PEG (M_n > 20 kDa) and α-CD form extrudable polypseudorotaxane hydrogels, but they have limited self-healing properties for DIW. From a molecular design perspective, the limited self-healing ability of polypseudorotaxane hydrogels comes from the slow re-crystallization of the disrupted crystalline domains after the removal of shear forces. Increasing the density of the crystalline domains by threading more α-CDs onto the polymer axle in the hydrogel is one possible approach to improve the self-healing property of polypseudorotaxane hydrogels. Hence, we chose Pluronic F127 triblock copolymer as the axle to test the feasibility (Fig. 18a).[78] In an aqueous solution of F127 (5 wt%), α-CDs thread on the PEG blocks, leaving the PPG block uncovered, forming viscoelastic hydrogels at various α-CD concentrations. The rheological properties of these hydrogels were investigated at different α-CD-to-F127

ratios (Fig. 18b). At 10 wt% α-CD, a hydrogel with G' ~10^3 Pa was obtained, but the elastic moduli of the hydrogel dropped to 20 Pa after one step-strain cycle (Fig. 18b, *left*). At 15 wt% α-CD, the elastic moduli of the hydrogel reached 10^4 Pa. In the step-strain sweep, the elastic moduli G' of the hydrogel was reduced to 10^3 Pa after the first step-strain cycle, and it was further weakened under multiple step-strain cycles (Fig. 18b, *middle*). It is worth noting that α-CD reached saturation at 15 wt% at room temperature, and most investigations on α-CD-based polypseudorotaxane hydrogels did not seek higher α-CD concentrations for gelation. To thread more α-CDs onto F127, we prepared a 20 wt% α-CD solution at 60 °C, since the solubility of α-CD is significantly higher at this temperature. After mixing F127 and α-CD at 60 °C followed by natural cooling, a stronger polypseudorotaxane hydrogel was formed with an elastic modulus G' of 4 × 10^4 Pa. This hydrogel showed outstanding self-healing properties in the step-strain investigations (Fig. 18b, *right*). The significantly improved self-healing property of the polypseudorotaxane hydrogels at higher α-CD concentrations confirmed that increasing the crystalline domain density effectively promotes the rheological properties for DIW.
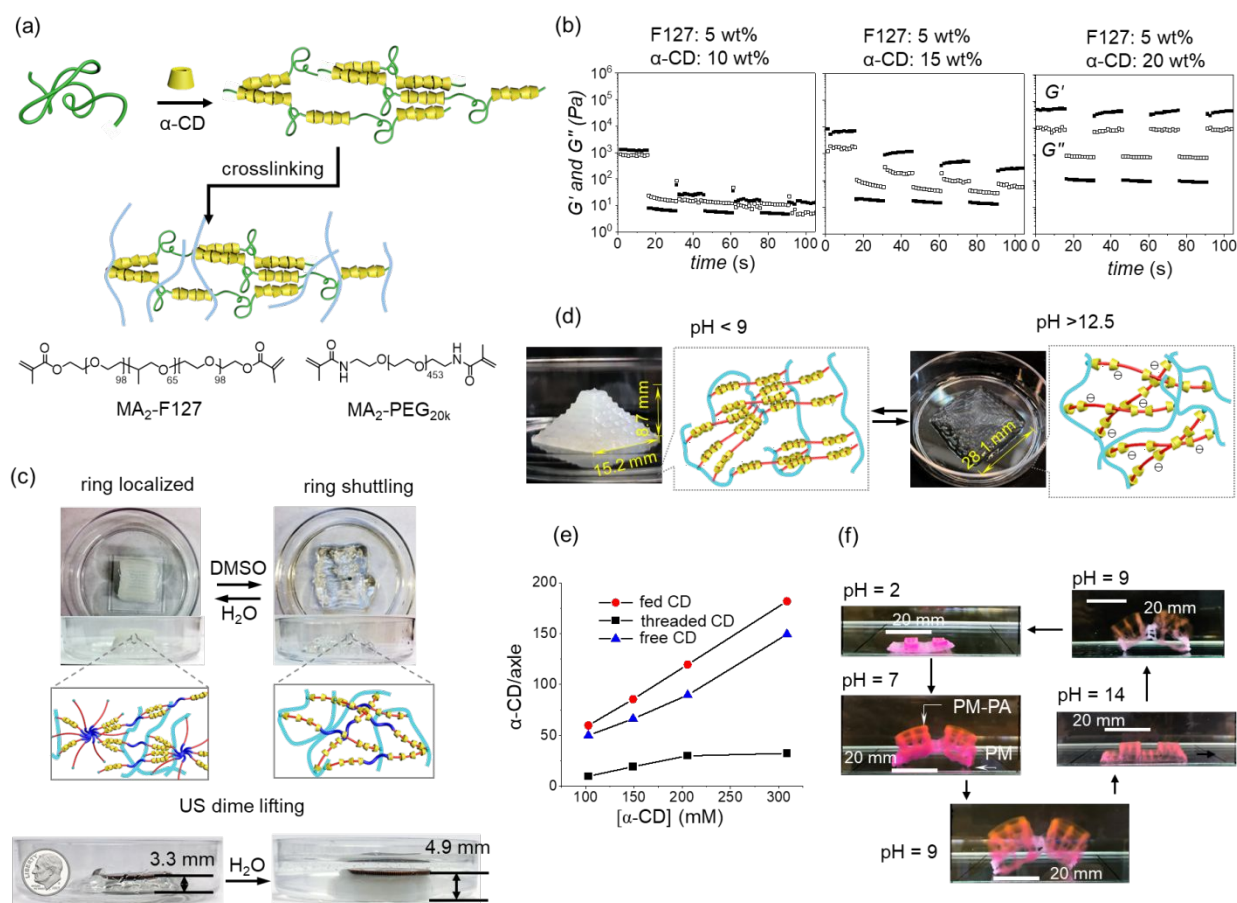

Fig. 18. (a) Schematic illustration of the formation of 3D-printable polypseudorotaxane hydrogels using α-CD with Pluronic polymers and long-chain PEGs. (b) Step-strain sweeps of polypseudorotaxane hydrogels

with different amounts of F127 and α-CD. (c) 3D-printed PMs underwent DMSO/H_2O-induced shape morphing. The threaded α-CDs were switched between crystalline and random shuttling states. A PM lattice lifted a US dime after the DMSO-to-H_2O exchange. (b-c) reproduced with permission from reference 78. Copyright 2017 John Wiley & Sons, Inc. (d) 3D-printed PMs underwent pH-induced shape morphing. (e) Numbers of mechanically interlocked α-CDs in PMs obtained at different fed α-CD concentrations. (f) A pH-responsive worm-mimic fabricated by PM and PM/PAA showed multi-stage shape morphing. (d-f) reproduced with permission from reference 203. Copyright 2018 The Royal Society of Chemistry.

The polypseudorotaxane hydrogel with 20 wt% of α-CD was 3D-printed as woodpile lattices (Fig. 18c).[78] When telechelic MA_2-F127 was used, crosslinked polyrotaxane monoliths (PMs) were generated after post-printing photo-polymerization (Fig. 18c). In these PMs, α-CDs were mechanically interlocked by the crosslinked F127 network. They crystallized as micro-crystalline domains, being static along the F127 axle. When these micro-crystalline domains are disrupted, α-CDs are freed to shuttle randomly along the F127 axle. For example, the micro-crystalline domains were gradually dismantled when a PM lattice was immersed in DMSO. The elastic modulus of the PM was reduced, and the 3D-printed lattice collapsed into a soft puddle (Fig. 18c). Re-establishing the hydrogen bonding interactions between α-CDs allows for rapid re-crystallization, thereby regenerating the micro-crystalline domains. In water, the deformed DMSO-gel recovered its shape within two minutes. The disruption and crystallization of α-CD crystalline domains are visible as the PM changed from opaque to transparent and returned to opaque during these reversible processes (Fig. 18c). The chemical energy of the reformation of α-CD crystalline domains in PM was transferred to perform useful work, lifting a US dime against gravity (2.268 g, more than 20-time as the dry gel's weight, Fig. 18c, *bottom*).

We later noticed that the hydrophobic PPO block in F127 is not required for the formation of 3D-printable polypseudorotaxane hydrogels, and high molecular-weight PEGs with α-CDs also form viscoelastic hydrogels for DIW.[203] When α-CD (20 wt%) was mixed with PEG_{20k} (5 wt%), a viscoelastic hydrogel formed. In this hydrogel, α-CDs segregated on the PEG axle and crystallized to form crystalline domains, and the unthreaded PEG acted as amorphous chains to connect the crystalline domains (Fig. 18a). The polypseudorotaxane hydrogel showed similar rheological features to those formed by F127 and α-CD. After photo-polymerizing the methylacrylamide end groups of MA_2-PEG_{20k} and removing the free α-CDs, a PM pyramid was obtained (Fig. 18d). By comparing the amounts of fed α-CD in the hydrogel formation to the mechanically interlocked α-CD in the PM, we noticed that a large amount of free α-CD was critical for the formation of a 3D-printable hydrogel (Fig. 18e). An excess of free α-CD allowed for the threading of more α-CDs onto the PEG axle, thereby promoting viscoelasticity for DIW. When a PM was immersed into a NaOH solution, the hydroxyl groups of α-CD were deprotonated (pK_a = 12.3 and 13.5)[204] and the crystalline

domains were dismantled. As shown in Fig. 18d, a 3D-printed pyramid was deformed into a transparent hydrogel at pH 14. Reducing the pH to below 9 allowed for a rapid shape recovery of the PM. When the pH-responsive PM was integrated with polyacrylic acid (pK_a = 4.5) through multi-material 3D printing, a worm-mimic showed multi-stage shape morphing at different pHs (Fig. 18f).
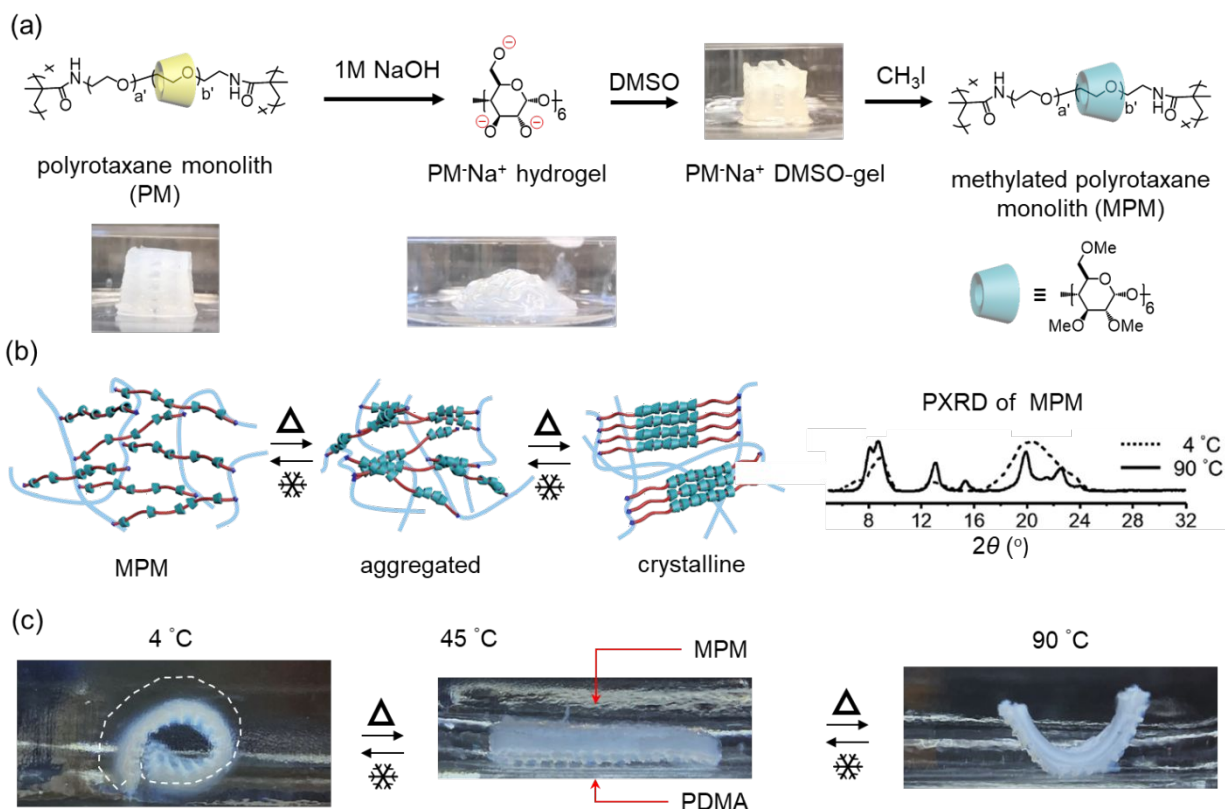
Fig. 19. (a) Post-printing methylation of PM. (b) Illustration of a two-stage thermal-induced aggregation of MPM. A crystalline phase was observed at 90 °C in the WAXS analysis. (c) Thermal-induced shape morphing of a bilayer monolith. Its top layer consists of MPM, and its bottom layer consists of a crosslinked PDMA. Reproduced with permission from reference 205. Copyright 2020 The Royal Society of Chemistry.

We also demonstrated post-printing methylation of α-CDs of 3D-printed PM (Fig. 19a).[205] To control the degree of methylation, the α-CDs must be deprotonated while the PM is maintained in a swelled state. When t-BuOK deprotonation was carried out in DMSO, the deprotonated α-CDs aggregated and de-swelled the PM, preventing further diffusion of t-BuOK for additional deprotonation. When NaOH deprotonated PMs in water, the hydrogel remained swelled for controlled deprotonation (Fig. 19a). In the MPM, methylated α-CDs shuttle freely along the PEG axles since the α-CD-α-CD hydrogen bonding interactions have been diminished (Fig. 19b). From 4 °C to 25 °C, these methylated α-CDs aggregate as supramolecular crosslinkages, strengthening the network macroscopically (Fig. 19b). This lower critical solution

temperature (LCST) is consistent with other methylated α-CDs and polyrotaxanes.[206-208] Interestingly, we discovered a new crystalline phase when the MPM was heated to 70 ℃ (Fig. 19b). Unlike amorphous methylated-α-CD aggregates, the MPM showed a clear long-range order in the WAXS analysis (Fig. 19b). When the MPM is integrated with a conventional poly(dimethylacrylamide) (PDMA) hydrogel through multi-material 3D printing, the 3D-printed bilayer showed a two-stage shape curving in water at 4, 40, and 90 ℃, respectively (Fig. 19c). The two-stage shape-morphing was attributed to the two-stage methylated-α-CD aggregation and crystallization, highlighting the molecular-motion induced macroscale shape-changes.

Different from long-chain PEGs, medium molecular weight PEGs (2–5 kDa) form meta-stable hydrogels with α-CD (Fig. 20a), which gradually precipitate as crystallites. Kinetically, α-CDs rapidly thread onto the PEG axle and then the formed polypseudorotaxanes slowly crystallize as precipitates. When a large hydrophobic end group (e.g., Ad-, d = 6.6 Å) is installed onto the PEGs, the formation kinetics of the polypseudorotaxanes is changed (Fig. 20a).[144] α-CDs are attracted to the Ad- group to form side-on inclusion complexes. Hence, they need to translocate the entire length of an Ad-PEG to reach the Ad- group. The extended translocation distance decelerates the threading and translocation of α-CDs, thereby slowing down the formation of polypseudorotaxanes. As a result, blocks of α-CDs are segregated on the PEG axles, which crystallize to form kinetically trapped hydrogels (Fig. 20a). Instead of using bulky Ad- groups, installing two Nor- end groups (d = 4.7 Å) as 'speed bumps' also enabled the kinetic trapping of polypseudorotaxane hydrogels (Fig. 20b).

The kinetically trapped polypseudorotaxane hydrogels showed drastically different viscoelasticity to those formed by bare PEG and α-CDs (Fig. 20c).[144] Ad-PEG$_{5k}$/α-CD polypseudorotaxane hydrogels possess much higher elastic moduli G' than those of PEG$_{5k}$-OH/α-CD hydrogels. The crystalline network densities and micro-crystal domain sizes were tuned by varying the fed EG/α-CD ratios. In contrast, a minimum variation of elastic moduli was observed in HO-PEG$_{5k}$/α-CD hydrogels at different EG/α-CD ratios. Kinetically trapped Ad-PEG$_{5k}$/α-CD hydrogels exhibited good self-healing properties for DIW, but HO-PEG$_{5k}$/α-CD hydrogels were not 3D-printable (Fig. 20c).
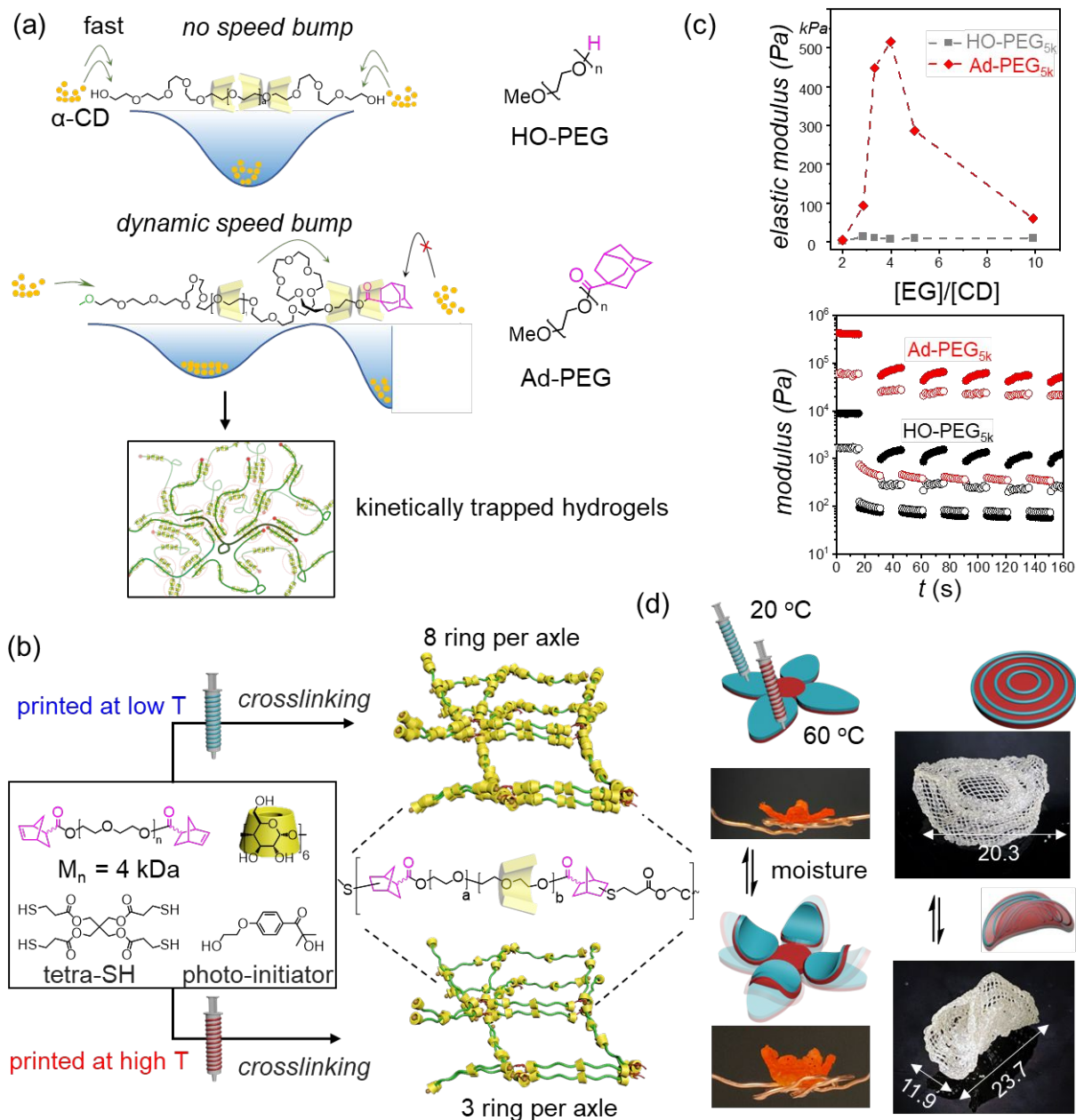
Fig. 20. (a) Kinetically trapping polypseudorotaxane networks using Ad-PEG and α-CD. (b) Angular frequency and step-strain sweeps of polypseudorotaxane hydrogels formed at different EG/α-CD ratios. (c) Kinetically trapping polypseudorotaxane networks at room temperature and 60 ℃. PMs with different numbers of threaded α-CDs were formed after photo-crosslinking. (d) Fabrication of heterogenous moisture actuators using one ink printed at different temperatures. Shape morphing occurred when the actuators were exposed to moisture. Reproduced with permission from reference 144. Copyright 2021 Elsevier.

The kinetic trapping method enables simultaneous access to multiple PMs using a single polypseudorotaxane ink (Fig. 20b). In a DIW ink formed by Nor_2-PEG_{4k} and α-CDs, two kinetically trapped polypseudorotaxane hydrogels with different numbers of threaded α-CDs on the PEG axle were formed at 25 °C and 60 °C. When this ink was 3D-printed through two temperature-controlled nozzles at room temperature and 60 °C, heterogeneous constructs with different polypseudorotaxanes were fabricated. After photo-crosslinking, the heterogeneous construct consisting of two PMs was formed. These PMs have identical covalently crosslinked PEG networks but different numbers of threaded α-CDs (Fig. 20b). When the heterogenous PM constructs were exposed to moisture, they morphed into designed shapes due to their different ability to swell (Fig. 20d). The PM with more threaded α-CDs swelled less, due to the denser micro-crystalline α-CD domains formed in the hydrogel.

Instead of using sterically demanding end groups on medium-chain PEGs, the kinetic trapping synthesis of 3D-printable hydrogels is expanded to short-chain PEGs (M_n = 950 Da).[209] As a result, a series of PEG_{950}-grafted copolymers (P1-P10, M_n = 6.5–24.0 kDa, Fig. 21a). with different degrees of polymerization (DP) and grafting densities were synthesized via reversible addition-fragmentation chain-transfer polymerization. Copolymers P1 and P2 with low DPs (41, 60, M_n = 6.5, 9.4 kDa) formed crystalline precipitates in the presence of α-CD (Fig. 21a). In contrast, copolymers with higher DPs (P5-P10) formed viscoelastic hydrogels, because the folding of the copolymer backbone acts as the kinetic barrier to slow down the crystallization of the side-chain polypseudorotaxanes. Therefore, less-ordered crystalline domains were kinetically trapped in these 3D-printable hydrogels. The decreased sizes of crystalline domains were evident in SAXS studies (Fig. 21b).

P5 (PEG grafting density 5%) and P6 (PEG grafting density = 27%) showed exceptional 3D printability with α-CD and were synthetically modified with methacrylate into P5-MA and P6-MA (Fig. 21b). The P5-MA/α-CD and P6-MA/α-CD hydrogel were photo-crosslinked after DIW, affording crosslinked polymers CP5 and CP6. The previously threaded α-CDs on the PEG side chains of CP5 and CP6 were dethreaded after a DMSO washing. When 3D-printed CP5 and CP6 were immersed into α-CD solutions, the re-threading of α-CD and reformation of micro-crystalline domains triggered an elastic-to-plastic transformation as shown in the tensile tests (Fig. 21c). CP5 and CP6 showed two orders of magnitude enhancement in their elastic moduli (Fig. 21 c). We further introduced a slide-ring crosslinker[210-212] to synthesize a highly stretchable CP10, which demonstrated multi-stage shape morphing at different concentrations of α-CDs (Fig. 21d). Since CP6 and CP10 showed drastically different mechanical properties at the same concentration of the α-CD solution, we sought to design a sea cucumber mimic through multi-material 3D-printing (Fig. 21e). In this sea cucumber mimic, papillae and skin were made of CP6 and CP10, respectively. In the absence of α-CD, the soft monolith deformed to mimic sea cucumbers'

soft bodies. In a 50 mM α-CD solution, the papillae drastically increased its rigidity, but the skin remained flexible. In a 150 mM α-CD solution, the monolith was reinforced into a rigid construct, mimicking the state that sea cucumbers defend against predators.
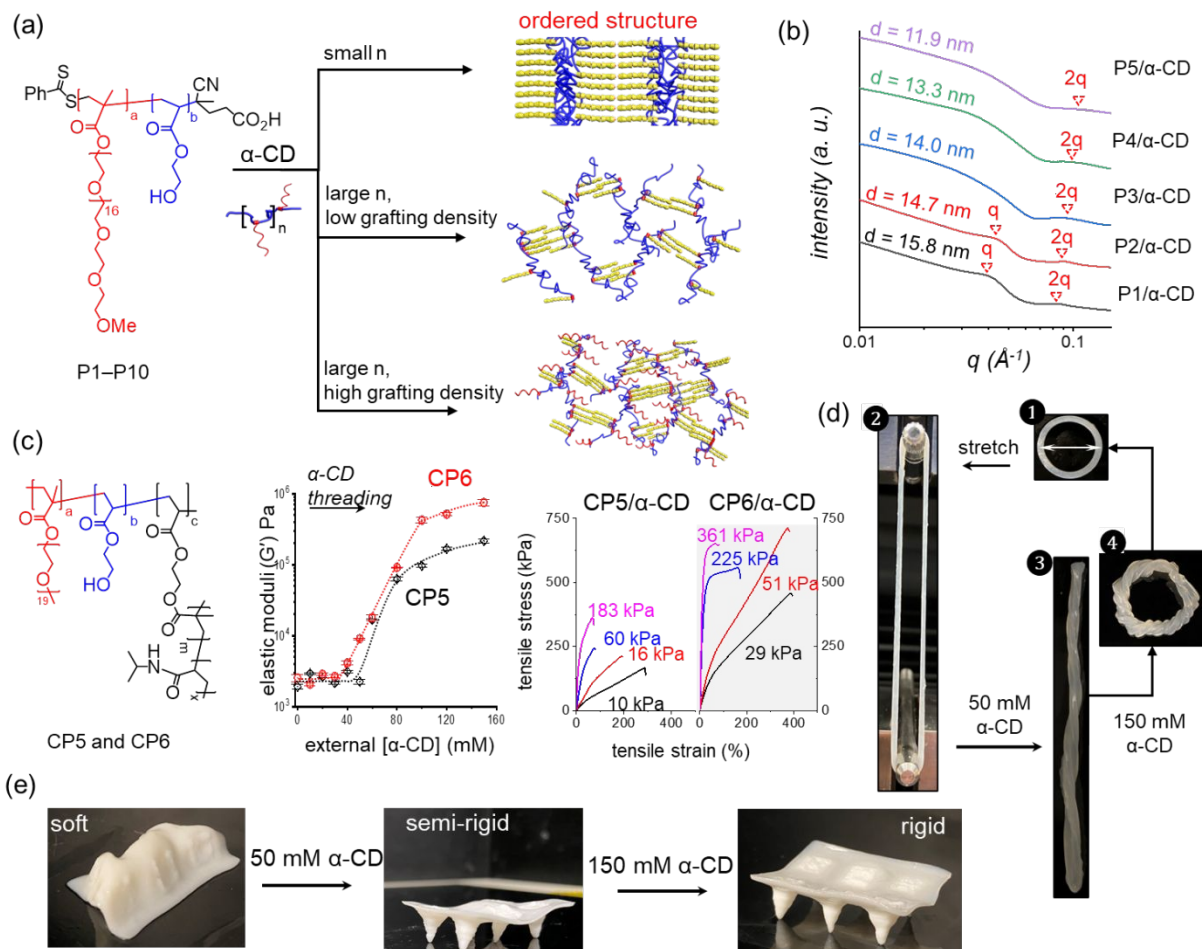
Fig. 21. (a) PEG-grafted copolymer P1–P10 used to form kinetically trapped hydrogels with α-CDs. (b) SAXS profiles of the P1–P5/α-CD polypseudorotaxane hydrogels. (c) Crosslinked side-chain polymer networks CP5 and CP6, and their tunable mechanical properties at different concentrations of α-CD. The elastic moduli change of CP5 and CP6 using rheometer and their tensile strain-stress profiles are shown. (d) Multi-stage shape morphing of CP10. (e) A sea cucumber mimic comprised of rigid papillae and soft skin fabricated with CP6 and CP10. The mimic undergoes a gradual modulus change upon α-CD threading. Reproduced with permission from reference 209. Copyright 2021 John Wiley & Sons, Inc.

4.5 DIW inks designed based on non-specific supramolecular interactions

Block copolymers with dissimilar blocks self-assemble in solution as spherical micelles, worm-like micelles, and vesicles at the nanometer scale and cubic, hexagonal, lamellar, and bi-continuous mesophases

at the sub-micrometer scale.[213-217] These nano-to-meso scale assemblies are spatially arranged to form viscoelastic gels for DIW. A typical example is Pluronic F127, in which the PPO block aggregates above the critical micelle concentration (CMC, 0.2 mM) to form spherical micelles with sizes ranging from 8 to 16 nm.[218, 219] Above 20 wt%, F127 self-assembled into DIW-compatible hydrogels.[220-222] SAXS and small-angle neutron scattering (SANS) showed that 2D hexagonally packed layers of micelles are vertically stacked in a face-centered cubic or hexagonal packing mode (Fig. 18a).[223-226] SANS reveals that micelles glide along the direction of the shear force.[225] Once the shear force is removed, the original micro lattice is reformed. The elastic modulus of the F127 hydrogel is measured as $\sim 5 \times 10^5$ Pa (1 rad/s).[225] The F127-gel is also temperature sensitive, showing a gel-sol transition below the critical micelle temperature (CMT). [227] The thermal reversibility of F127-gel enables its use as a templating ink in DIW, which can be removed at a lower temperature.[221, 227, 228]
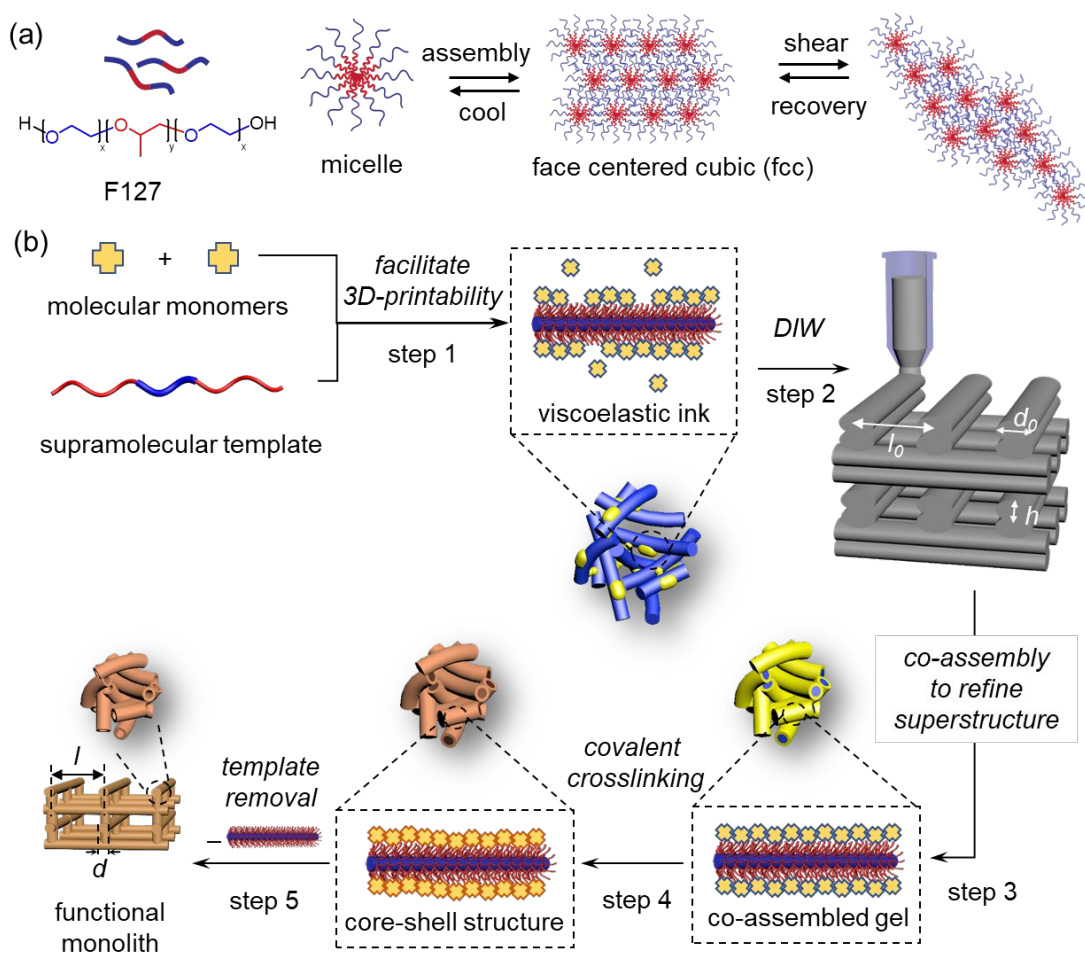
Fig. 22 (a) Illustrations of the self-assembly of a Pluronic F127 gel and its shear-thinning behavior. Reproduced with permission from reference 25. Copyright 2019 John Wiley & Sons, Inc. (b) Illustrations

of the hierarchical co-assembly enhanced direct-ink-writing. Reproduced with permission from reference 229. Copyright 2018 John Wiley & Sons, Inc.

The amphiphilic nature of F127 hydrogels also allows for the incorporation of a variety of guest molecules for controlled release.[230, 231] Recently, we developed an F127/small molecule co-assembly approach to construct functional DIW inks (Fig. 18b).[229] In this design, F127 micellar gel is a polymer template for the co-assembly and a rheological template for DIW. Co-assembled gels comprised of reactive molecules and F127 were 3D-printed into different architectures. Finally, the 3D-printed samples undergo a post-printing assembly and crosslinking to form 3D-printed monoliths with ordered molecular features.
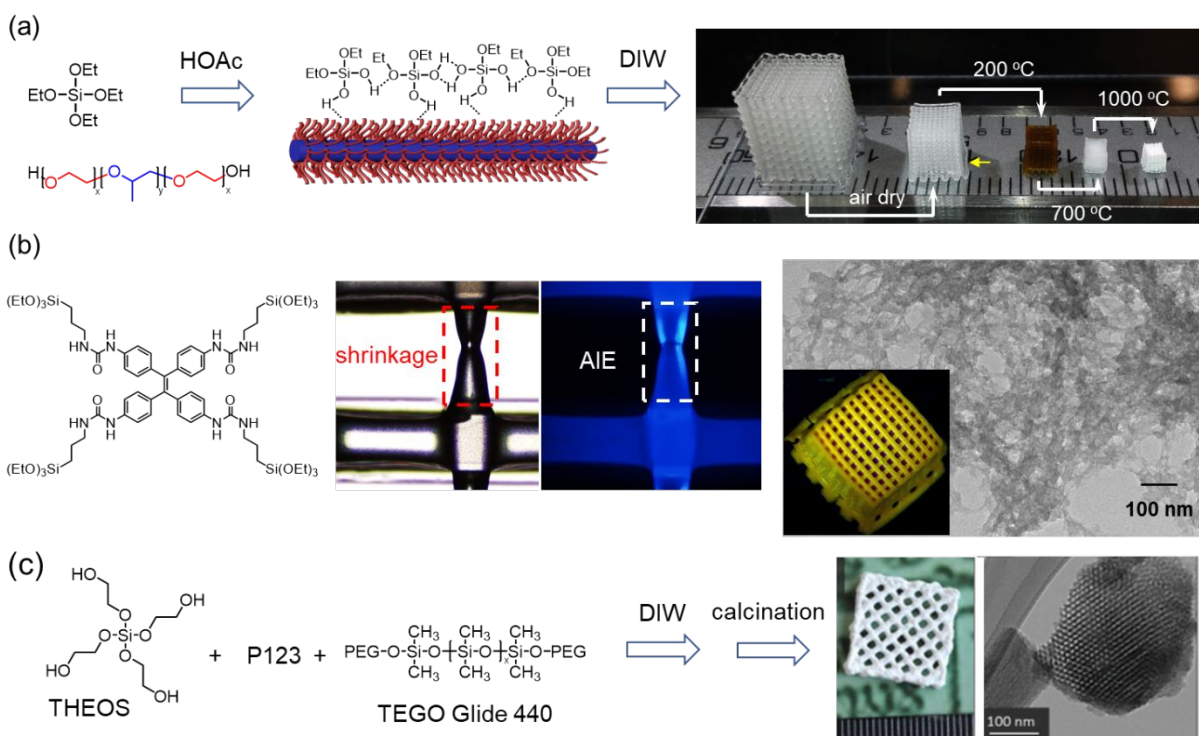
Fig. 23. (a) Fabrication of 3D-printed mesoporous silica monoliths enabled by hierarchical co-assembly of TEOS and F127. (b) Aggregation-induced-emission of a TPE-based siloxane tracker during the evaporation-induced co-assembly. This TPE-based siloxane also formed 3D-printed porous materials through the hierarchical co-assembly enabled DIW. Reproduced with permission from reference 229. Copyright 2018 John Wiley & Sons, Inc. (c) A 3D-printed mesoporous silica monolith formed by THEOS, P123, and TEOG Glide 440. Optical and TEM images of the 3D-printed lattice are shown on the right. Reproduced with permission from reference 232. Copyright 2018 John Wiley & Sons, Inc.

We demonstrated the feasibility of the design using tetraethyl orthosilicate (TEOS) as the reactive molecule (Fig. 23a).[229] TEOS and F127 have been shown to co-assemble for the synthesis of mesoporous

silica.[233] Different from conventional mesoporous silica synthesis,[233-236] where the polycondensation is carried out in a reaction vessel, the polycondensation of TEOS in a 3D-printed monolith needs to be controlled to retain the macroscale architecture. We noticed that during the polycondensation, the generated ethanol severely reduced the stability of the macroscopic structure. Therefore, only a small amount of acetic acid was introduced to the F127/TEOS ink to limit the polycondensation rate. After DIW, the monolith was placed in a humidity-controlled chamber to slowly evaporate water and EtOH, matching the rates of evaporation and polycondensation. Next, the dried monolith was gradually heated to 200 ℃, 700 ℃, and 1000 ℃. Above 300 ℃, the monolith underwent extensive polycondensation and F127 decomposed completely. SEM and TEM analysis showed that samples calcinated at 600 ℃ showed typical mesoporous structures (5 nm pore) with a BET surface area of 304 m^2/g.
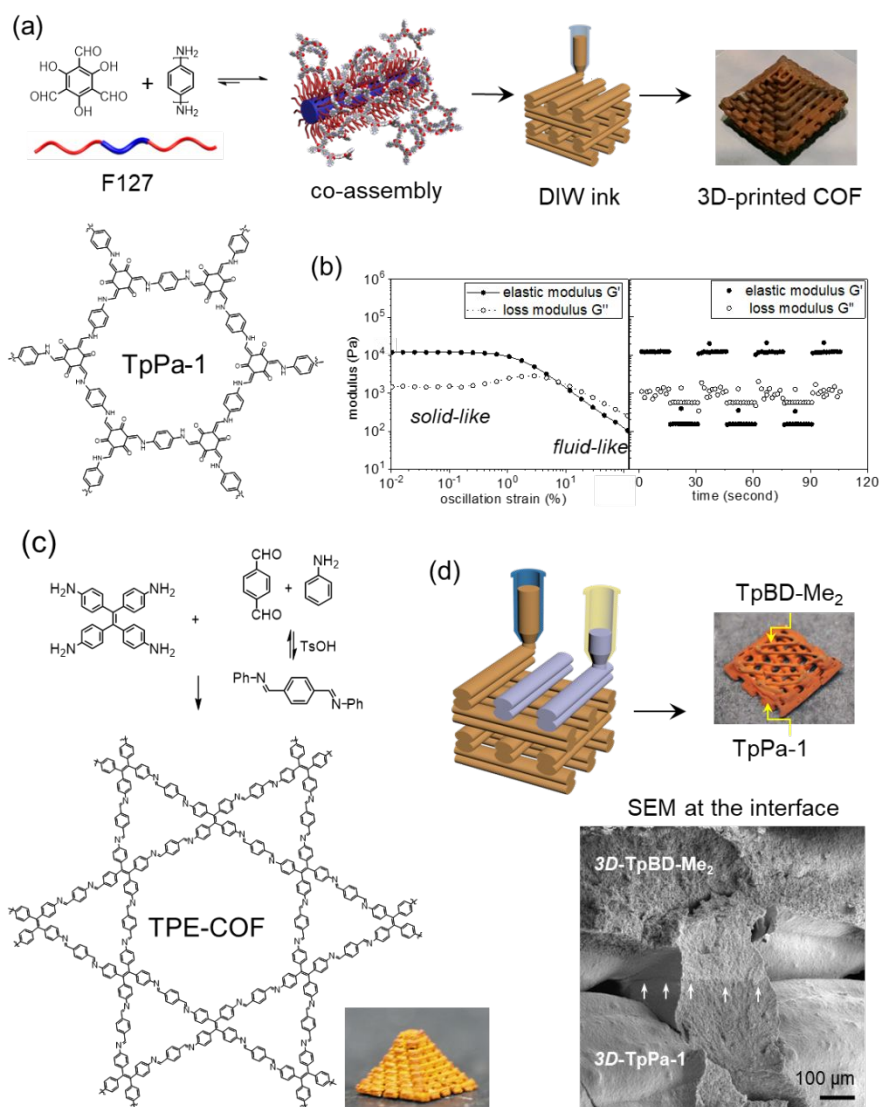
Fig. 24. (a) The hierarchical co-assembly enabled DIW for the fabrication of 3D-printed β-ketoenamine COF TpPa-1. (b) The strain sweep and step-strain sweep of TpPa-1/F127 co-assembled gel. (c) Fabrication of a 3D-printed TPE-COF pyramid through the transamination method. (d) Dual-COF DIW and 3D-printed dual COF monolith comprised of TpPa-1 and TpBD-Me$_2$. A SEM image was recorded at the interface of the two COFs. Reproduced with permission from reference 93. Copyright 2019 American Chemical Society.

To offer molecular insights into the hierarchical co-assembly, a tetraphenylethylene (TPE)-based siloxane tracker was added to the hydrogel as a dopant.[229] Upon evaporation, the linewidth of the 3D-printed monolith shrunk, and localized fluorescence enhancement was observed due to aggregation-induced emission.[237, 238] The localized fluorescent emission change provided molecular evidence of controlled post-printing assembly in a 3D-printed monolith. This TPE-based siloxane was also used to construct 3D-printed porous organosilicate. Mixing this molecule with F127 formed a viscoelastic ink for DIW. The 3D-printed monolith underwent similar post-printing processes to afford a mesoporous organosilicate monolith with 5-20 nm pores and a BET-surface area of 177 m^2/g.

Hüsing *et al*. fabricated porous silica using Pluronic P123 and tetrakis(2-hydroxyethyl)orthosilicate (THEOS) (Fig. 23c).[232] A triblock copolymer TEGO Glide 440 (PEG-PDMS-PEG, 0.8 wt%) was added as a rheological additive to P123 and THEOS to form viscoelastic hydrogels for DIW. The 3D-printed monolith was aged in a sealed chamber at 40 °C for 7 days to allow for extensive polycondensation. Then, P123 and TEGO Glide 440 were removed by organic solvent extraction. As a result, a 3D-printed mesoporous silica monolith was obtained with ordered cylindrical mesopores with a BET surface area of 678 m^2/g (Fig. 23c).

The hierarchical co-assembly enhanced DIW also applies to other reactive molecules, such as amines and aldehydes. As such, we expanded this method to construct 3D-printed imine and β-ketoenamine COFs TpPa-1 and TpBD-Me$_2$.[93] In a mixture of F127, amine, and aldehyde (Fig. 24a), the extension of the imine polycondensation needs to be limited to allow the formation of viscoelastic hydrogels for DIW. 1,3,5-Triformylphloroglucinol (*Tp*), *p*-phenylenediamine (*Pa*), *p*-toluenesulfonic acid (TsOH), and Pluronic F127 were mixed for the construction of a β-ketoenamine TpPa-1 COF. The 3D-printable ink showed similar viscoelastic properties to the F127-only hydrogels with a measured elastic modulus of 1.2×10^4 Pa, possessing rapid self-healing property in the step-strain sweep (Fig. 24b). Large amounts of TsOH and water limited the imine condensation during the hydrogel formation and DIW processes. After 3D-printing, the sample underwent controlled evaporation followed by heating, during which the imine condensation proceeded extensively and an amorphous-to-crystalline imine network transformation occurred.[239] 3D-printed TpPa-1 monolith was obtained after removing the F127 template via solvent extractions with acetone. TpPa-1 was annealed in dioxane/mesitylene/acetic acid mixture at 150 °C for 72 hours to further

enhance the crystallinity. The annealed 3D-printed monolith showed a similar powder X-ray diffraction (PXRD) profile and BET surface area of 587 m^2/g to those polycrystalline TpPa-1 powders synthesized conventionally.[240, 241] If the reactive molecules polymerize rapidly, the polymerization must be further retarded during the ink formation. For example, tetrakis(4-aminophenyl)ethene and terephthalaldehyde polymerized rapidly in the F127-templated gel, affording yellow precipitates. Hence, aniline was introduced to react with terephthalaldehyde to form an imine intermediate, which slowly reacted with tetrakis(4-aminophenyl)ethene through trans-imination (Fig. 21c). The trans-imination allowed for the formation of a 3D-printable ink, and this TPE-COF was successfully fabricated with a BET surface area of 1373 m^2/g. When two COF precursor inks were employed for multi-materials 3D printing (Fig. 24d), heterogeneous dual-COF monoliths were fabricated. SEM studies at the COF-COF interface revealed that two COFs were bound together tightly via the cross-imination at the interface (Fig. 24d).
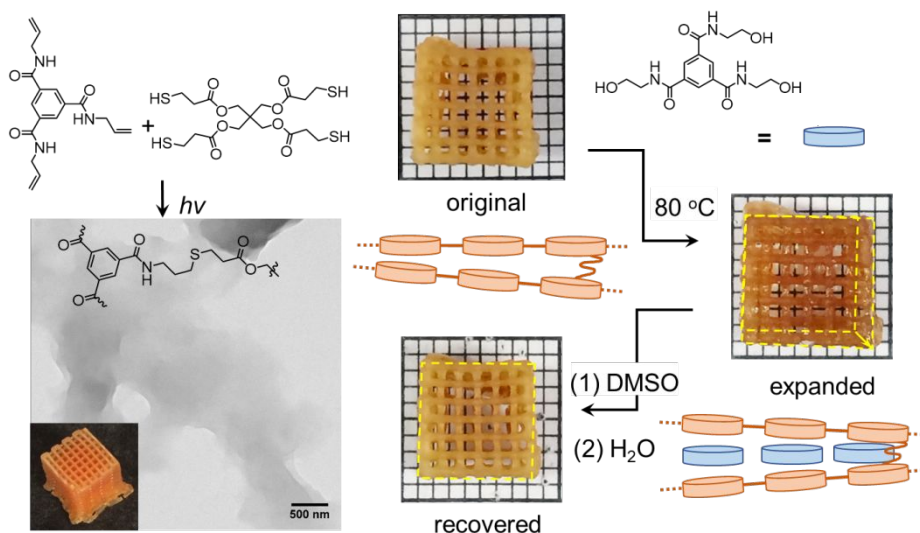
Fig. 25 Construction of a crosslinked BTA network through co-assembly and thiol-ene crosslinking. A water-soluble trihydroxyethyl-BTA was supramolecularly inserted into the crosslinked BTA monolith, inducing a macroscopic size expansion. Reproduced with permission from reference 229. Copyright 2018 John Wiley & Sons, Inc.

Compared to the previously discussed approaches, the hierarchical co-assembly approach allows for the incorporation of reactive small molecules that are otherwise difficult to satisfy the rheological prerequisites of DIW. For example, the design of 3D-printable BTA-based supramolecular polymers (section 4.1) requires water-soluble PEG arms and hydrophobic alkyl arms installed on the BTA. In contrast, co-assembling BTA-based molecules with the F127 template to form 3D-printable inks simplifies the supramolecular design. We synthesized a triallyl-BTA (Fig. 25), and mixed it with a tetra-thiol crosslinker, a photoinitiator, and the F127 template in water to form a viscoelastic hydrogel.[229] The hydrogel possessed

similar viscoelastic properties as pure F127 gels due to the co-assembly, with an elastic modulus of 2×10^4 Pa and rapid self-healing properties. The hydrogel was 3D-printed into a woodpile cube and photo-crosslinked via a thiol-ene reaction. After ethanol extraction to remove the F127 template, a BTA-based monolith was obtained. When a trihydroxyethyl-BTA was introduced to the BTA monolith in water, it was inserted between the crosslinked BTA moieties and expanded the hydrogel macroscopically (156% volume expansion). Removing this trihydroxyethyl-BTAs from the 3D-printed monolith allowed for recovery to the original state (Fig. 25). It is worth noting that since the crosslinking density of the BTA monolith is much higher than those discussed in section 4.1, the BTA monolith obtained via the co-assembly method only allowed for the insertion of 1–2 trihydroxyethyl-BTA rather than the supramolecular copolymerization. Future designs of BTA-based 3D-printable monolith can combine the benefits of both approaches.
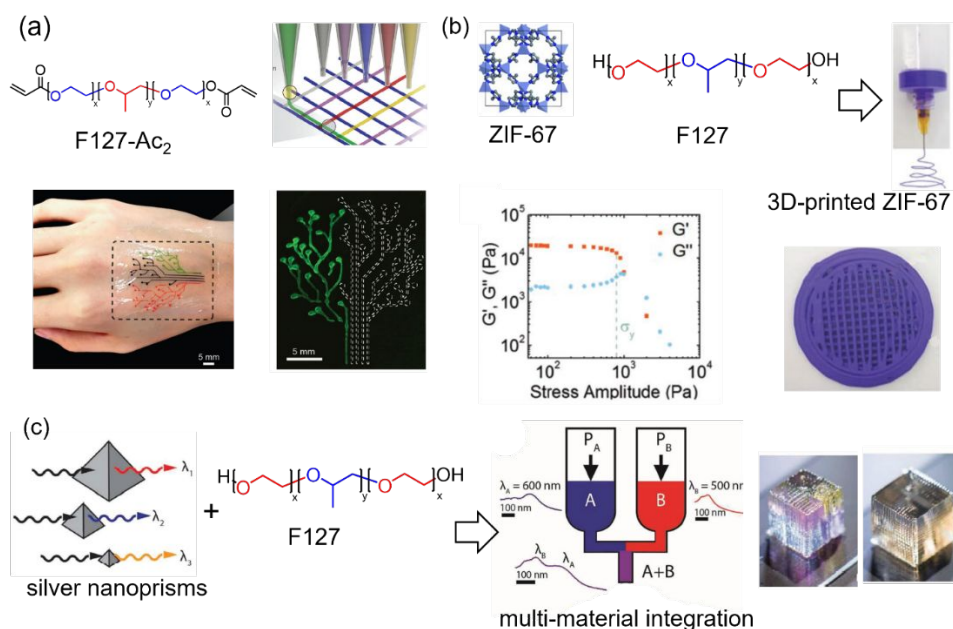
Fig. 26. (a) Integration of living bacterial cells with F127-Ac$_2$ gels. A living tattoo was fabricated, emitting fluorescent signals upon chemical stimuli. Reproduced with permission from reference 222. Copyright 2018 John Wiley & Sons, Inc. (b) Preparation of a 3D-printable MOF hydrogel by mixing ZIF-67 with F127. The strain sweep of the hydrogels and the 3D printed ZIF-67 with porous structures are shown at the bottom. Reproduced with permission from reference 242. Copyright 2019 John Wiley & Sons, Inc. (c) Fabrication of plasmonic constructs comprised of silver nanoprisms and F127. Constructs with discrete and gradient materials were printed using multi-material extruders. Reproduced with permission from reference 88. Copyright 2017 John Wiley & Sons, Inc.

When the F127 hydrogel was only used as a rheological template, it enabled 3D-printing of a variety of functional materials. For example, Zhao *et al*. presented a method to fabricate living responsive materials

by introducing bacterial cells, chemicals and nutrients into the F127 micellar hydrogels (F127-Ac$_2$, Fig. 26a).[222] The F127 hydrogels at concentrations of 20–35 wt% are 3D-printable, and the samples were photo-crosslinked after DIW to form robust covalent networks. As such, a living tattoo was fabricated by integrating bacterial cells into a covalently crosslinked network (Fig. 26b). When the tattoo was exposed to rhamnose, *β*-D-1-thiogalactopyranoside, and *N*-acyl-homoserine lactone, the corresponding regions of the living tattoo emitted different colors of fluorescence as the bacterial cells expressed green fluorescence protein (Fig. 26b). Wang *et al*. reported 3D-printing of MOF-derived carbon frameworks as Li/O$_2$ battery cathode materials (Fig. 26c).[242] A Co-based MOF (ZIF-67) and F127 were mixed to form a viscoelastic hydrogel, which was printed into lattices (Fig. 26c). Calcination of the printed monolith at 800 °C in N$_2$ removed the F127 template and converted the ZIF-67 to a microporous carbon with embedded Co nanoparticles (Fig. 26c). The carbon material demonstrated good electric conductivity with the redox active Co nanoparticles, affording the 3D-printed Li/O$_2$ batteries good performance. Johnson and Liu *et al*. fabricated a series of plasmonic constructs by introducing silver nanoprisms (AgNPs) into the F127 hydrogel (Fig. 26d).[88] AgNPs and F127 are bound via non-specific supramolecular interactions, and the optical properties of F127/AgNPs hydrogels remained the same compared to their solution states. Using a mixing-and-printing extruder, heterogenous 3D-printed constructs comprising up to eight inks were fabricated (Fig. 26d).

Bottlebrush copolymers also self-assemble into mesoscale cubic or hexagonal lattices.[243, 244] Recently, Chabinyc and Bates *et al.* provided an example of using a bottlebrush copolymer poly(PDMS)-*stat*-poly(PEO) for DIW to construct ultra-soft and solvent-free elastomers.[245] The bottlebrush copolymers poly(PDMS)-*stat*-poly(PEO) were synthesized by copolymerizing Nor-PEO and Nor-PDMS via ring-opening metathesis polymerization[246, 247] (Fig. 27a). The statistical bottlebrush copolymer self-assembled into a body-centered cubic (BCC) phase in a solvent-free condition as indicated by SAXS. The self-assembly is driven by the phase separation of the polar PEO and non-polar PDMS segments. The step-strain measurements indicated the copolymer had suitable shear thinning and fast self-healing properties for DIW, with an elastic modulus of ~10^5 Pa (Fig. 27a). When the copolymer is mixed with a telechelic benzophenone-PDMS crosslinker, 3D-printed elastomers were obtained, exhibiting ultra-soft mechanical properties (Young's moduli: 32, 7.7 kPa) and excellent recovery during cyclic loading-unloading measurements. These mechanical properties of the elastomer are attributed to the reversible structural transition between the BCC and disordered micelles phases. The 3D-printed samples showed similar mechanical properties when they were stretched and released (Fig. 27a).

Diao *et al.* incorporated photonic crystals into 2D-patterned structures using bottlebrush block copolymers and the setup of a DIW.[248] A Bottlebrush block copolymer poly(PDMS)-*b*-poly(PLA) was

synthesized via ring-opening metathesis polymerization using Nor-PDMS and Nor-PLA macromonomers (Fig. 27b). When the PDMS-*b*-PLA was dissolved in THF, the concentrated polymer solution was ready for patterning. The photonic properties of the block copolymer were successfully transduced into the printed patterns uniformly in a controlled and highly tunable manner. Both the printing speed (15 – 480 mm/min) and temperature (25 – 70 °C) determined the structural colors of the patterns by changing the d-spacings of the lamellar mesophases, where redshifts were observed when the patterns were printed at a lower speed or higher temperatures. Although 3D-printed architectures are not shown here, we envision that evaporation-controlled block copolymer self-assembly and DIW deposition could be integrated in the near future.
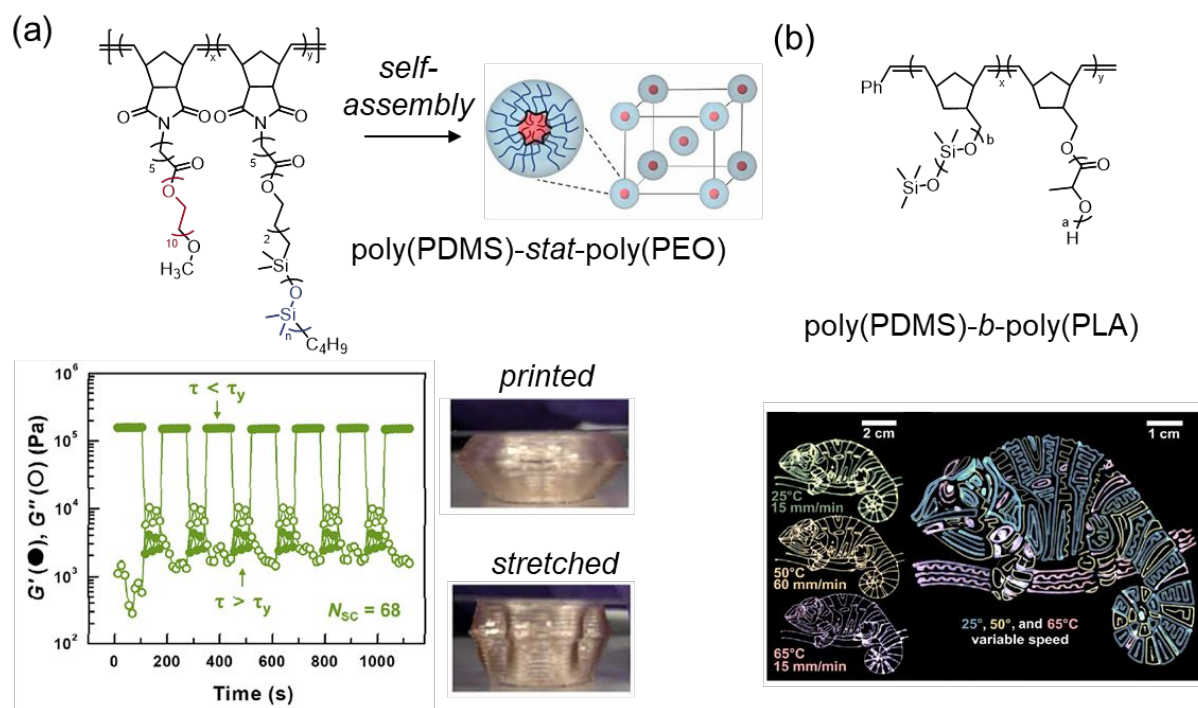
Fig. 27. (a) Bottlebrush statistical copolymer poly(PDMS)-*stat*-poly(PEO) self-assembled into BCC spheres, which enabled solvent-free DIW. Step-strain sweep of the copolymer and 3D-printed samples are shown on the right. Reproduced with permission from reference 245. Copyright 2020 American Association for the Advancement of Science. (b) Extrusion and evaporation of a bottlebrush block copolymer poly(PDMS)-*b*-poly(PLA) to generate 2D patterns with structural colors. Reproduced with permission from reference 248. Copyright 2020 American Association for the Advancement of Science.

5. Summary and outlook

The past two decades have witnessed tremendous advancements in soft materials 3D printing. In earlier days, the development of 3D printers and the associated materials were largely independent. Recently, materials development has started to show a significant impact on the development of 3D printers, as 3D

printing materials with tailored chemical features inspire new designs of the corresponding 3D printers, e.g., fast SLA/DLP printing.[249] Furthermore, the development of viscoelastic inks for DIW has started to unleash the potential of this fabrication tool, such as bioinks for biomedical uses.[73, 250] The fundamental understanding of supramolecular interactions in viscoelastic inks have greatly accelerated the materials development for DIW. For example, particle-based rheological modifiers were often needed in the early designs of DIW inks,[30, 251, 252] but they were gradually phased out due to more sophisticated design to enable the ink's innate viscoelasticity. Supramolecularly designed inks for DIW started to attract more awareness in chemistry, materials science, and engineering communities due to their highly dynamic and reversible features.[20, 69] 3D-printed soft materials with self-healing properties,[59, 166, 167, 192] enhanced mechanical strengths,[163, 193, 194] multiple-stimuli responsiveness,[74, 78, 144, 193] and complex shape-morphing capabilities[203, 205, 209] have been demonstrated and discussed in this review. These exciting features come from the functional motifs that are hydrogen bonded,[253] host-guest bound,[118] metal-ligand coordinated,[131] or assembled via van der Waals forces.[220, 254, 255] While this review mainly focuses on the development of self-supporting viscoelastic inks for DIW, it must be noted that extrudable inks could also be converted to self-standing constructs through post-printing or in-printing treatments. Notable examples include ink-in-bath printings[60, 220, 221, 256, 257] and *in-situ* photopolymerizations.[258-260] However, they often require adjustments to the DIW printers.[258] The supramolecular design principles discussed in this review are also transferable to other 3D printing systems, such as SLA, DLP, CLIP, and CAL.[13-18, 26]

Currently, only a small fraction of supramolecular binding entities has been successfully introduced for DIW, leaving an extensive library of supramolecular systems under-utilized. For example, the extrudable supramolecular networks discussed in Section 3 could be tailored for DIW after some chemical modifications. Notable examples include crown-ether/ammonium-based polymers,[115, 130, 261] cucurbituril-based host-guest polymers,[122] polymers with self-complementary hydrogen bonding motifs,[74, 112] and supramolecular systems that are connected via halogen bonds[262-266] and chalcogen bonds.[267, 268] Introducing high-affinity binding motifs to the construction of DIW inks is another promising strategy,[269] allowing for the formation of 3D-printable inks at lower concentrations. The multivalency and positive cooperativity[83] in supramolecular binding are also helpful in the DIW ink designs. Multivalent interactions[85] afford much higher overall binding affinities, which could be further strengthened by positive cooperativity.[84-87] At bulk, the inks will possess higher elastic moduli and more effective self-healing property for successful DIW. Furthermore, the development of DIW inks will be benefited by establishing clear structure-property relationships between the binding motifs at the molecular level and their viscoelastic properties at bulk. For example, the on-off kinetics of supramolecular binding motifs can significantly impact the self-healing rate in the step-strain sweeps.[99]

While supramolecular interactions facilitate the self-healing properties in the materials,[270, 271] these materials are usually soft. Introducing another interpenetrated covalent network effectively addresses this problem, and this approach has been demonstrated in this review.[48] Future advancements could benefit from developing more orthogonal supramolecular and covalent crosslinking methods and introducing high-performance polymers to the supramolecularly crosslinked networks. For example, DIW inks with micro-crystalline domains are opaque, which limits the light penetration depths for effective photo-crosslinking. The covalent networks currently mostly constitute acrylate-based polymers, but their mechanical performance is often limited. Another benefit of introducing supramolecular binding motifs to DIW inks is that the binding association/dissociation dissipates energy, which enhances the toughness of the materials.[272, 273] Depending on the on-off binding rates, large or small mechanical hysteresis are observed during the loading/unloading experiments.[272, 273] Opportunities will arise when sophisticated supramolecular designs are introduced to the DIW inks to enhance the toughness of the material or reduce the loading/unloading hysteresis. Slide-ring gels[210-212, 274-277] and other mechanically interlocked systems,[278, 279] such as polycatenanes,[280] are particularly attractive in this aspect.

During DIW, shear-thinned inks may have inhomogeneous materials distributions at flow. Introducing dynamic covalent chemistry could mitigate this problem for the construction of isotropic constructs. On the other hand, the complex flow opens up exciting opportunities to produce meta-stable materials that are out of equilibrium. For example, the integration of microfluidic designs and kinetically trapped supramolecular systems is expected to enable more soft robotic designs beyond the capability of liquid-crystalline materials-based DIW constructs.[61, 281-283]

Since DIW is particularly powerful at integrating multiple materials, the binding between two materials at the interface is also critical.[49] Delamination often occurs when there is insufficient binding at the interface of different materials. In addition, undesired diffusions between two inks also need to be mitigated. Hence, supramolecularly designed solutions are particularly welcome to address these problems.

The development of computational simulations and designs for DIW is also crucial.[284-288] Current structural simulations of 3D-printing designs are primarily based on the assumption of linear elasticity of the printed materials.[289] However, most DIW inks are viscoelastic. Hence, the current simulation and design need to go beyond elastic voxels to account for the viscoelastic properties.

Compared to vat-polymerization-based 3D printing, DIW fabrication at the large-scale remains a significant bottleneck. Moreover, DIW inks often show large variations when printed at different speeds using different extrusion pressures or shear forces. Hence, many 3D-printing demonstrations discussed in this review are small laboratory-scale productions, and constructs are optimized individually with

significant human interventions. Automation and in-line monitoring systems[290-292] with advanced machine learning algorithms are crucial to mitigate printing defects within each printed construct. From a material design perspective, producing consistent 3D-printed constructs requires more defect-tolerated supramolecular designs. We envision the integration of supramolecular designs with the advancement of automatic and inline-correcting DIW will greatly shorten the timeline from materials to products. Lastly, reducing energy footprint and establishing a sustainable life cycle for DIW materials is critical for the development of a sustainable society. The incorporation of supramolecular designs is particularly attractive since these materials can be recycled or repaired easily.

Conflicts of Interest

There are no conflicts to declare.

Acknowledgment

Author profiles
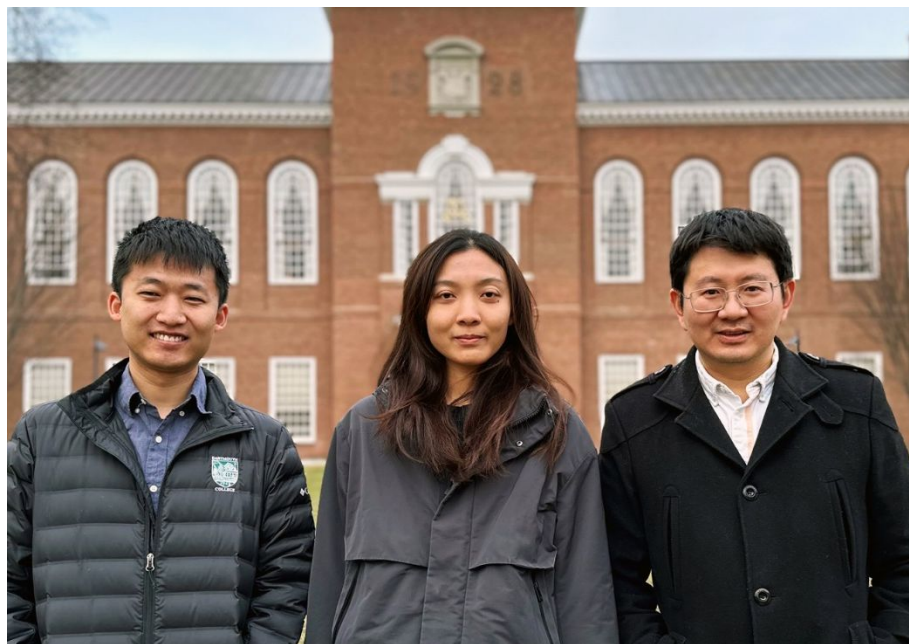
Left to right: Miao Tang, Zhuoran Zhong, and Chenfeng Ke

Miao Tang is a Ph.D. student in the Department of Chemistry at Dartmouth College under the supervision of Professor Chenfeng Ke. He received his B.S. degree in materials chemistry from Yuanpei College, Peking University, in 2017. His research focuses on designing 3D-printable hydrogels using supramolecular principles.

Zhuoran Zhong is a Ph.D. student in the Department of Chemistry at Dartmouth College. She obtained her B.E. in Macromolecular Science and Engineering at Fudan University in 2020. She began her graduate work with Professor Chenfeng Ke at Dartmouth College in 2020. Her research interest focuses on designing supramolecular materials and smart hydrogels for 3D printing.

Chenfeng Ke is an Associate Professor in the Department of Chemistry at Dartmouth College. He obtained his B.S. and Ph.D. from the College of Chemistry, Nankai University, in 2004 and 2009, respectively. He worked with Prof. Anthony Davis at the University of Bristol (2009–2011, Newton fellow, Royal Society), and Sir Fraser Stoddart at Northwestern University (2011–2015), before taking the current faculty position at Dartmouth College (2015 to present). His research focuses on developing smart supramolecular materials for 3D printing and crystalline porous materials for energy and environmental-related applications. He co-initiated and co-chaired the first Gordon Research Conference on Additive Manufacturing of Soft Materials in 2022.

Table 1. A summary of DIW inks designed based on supramolecular interactions

supramolecular interaction	composition	network architecture	G' (Pa)	nozzle size or line width (μm)	application	reference
hydrogen bonding	PVA, κ-CA	dual-H-bond crosslinked	10^3–10^4	220–850	cell proliferation	163
	PVA, chitosan		10^3–10^4	500	shape morphing	165
	Upy$_2$-PEG$_{10k}$	H-bond polymer crosslinked via aggregation	10^4	n.d.[a]	drug delivery for heart disease treatment	74
	BTA$_2$-PEG$_{20k}$	H-bond crosslinked	10^3–10^4	n.d.	cytocompatibility	166
	BTU-PEG$_{2k}$-OMe BTU$_2$-PEG		10^2–10^3	n.d.	n.d.	167
	polypeptide-DNA double-stranded DNA	DNA-crosslinked	10^3–10^4	500	cell adhesion	98
	polypeptide star copolymers	β-sheets	10^4–10^6	600	bacterial composite	177
	multidomain peptides	β-sheets fibrilization	10^3–10^4	310-500	cell culturing	178
host-guest interaction	CD-MeHA Ad-MeHA	H-G and covalently crosslinked	10^4	100	*in vivo* degradation and biomolecule release	75
	MeHA NorHA + CD-SH		n.d. (DLP)	100	cell adhesion	48
	Agar, P(AAm-co-BVIm) + CB[8]	H-bond and H-G crosslinked	n.d. (microfluidics)	700	fabrication of microfibers	182
metal-ligand coordination	Dop-PEG Al^{3+}/ Fe^{3+} / V^{3+}	coordination crosslinked	10^3–10^4	260	cell proliferation	76
	poly(MAA-*co*-OEGMA) Fe^{3+}	H-bond and coordination crosslinked	10^3–10^4	300	humidity-sensitive actuators	193
	Alginate + Ca^{2+}, crosslinked PAAm	coordination and covalently crosslinked	10^3–10^4	n.d.	soft robots	194
electrostatic	GelMA κ-CA	electrostatically crosslinked	10^2–10^3	250	cell adhesion	160

interaction	alginate protonated chitosan		n.d.	n.d.	cell adhesion	77
micro-crystallization	MA$_2$-F127 α-CD	crystallized polypseudorotaxane network	10^4–10^5	400	solvent-induced actuator	78
	MA$_2$-PEG$_{20k}$ α-CD		10^5–10^6	400	pH-induced actuator	203
	MA$_2$-PEG$_{20k}$ methylated α-CD [b]		10^5–10^6 10^2–$10^{3\,b}$	400	thermal-induced actuator	205
	Norb$_2$-PEG$_{4k}$ α-CD		10^5–10^6	400	humidity-induced actuator	144
	P(PEG-co-HEA) α-CD		10^4–10^5	400	biomimicry	209
co-assembly	F127 TEOS and its derivatives	micellar network	10^4–10^5	25–200	mesoporous silica	229
	P123 + THEOS TEGO Glide 440		n.d.	800	mesoporous silica	232
	F127 amine + aldehyde		$2×10^4$	400	micro-and mesoporous COFs	93
	F127 triallyl-BTA		10^4–10^5	200	supramolecular insertion	229
	F127-Ac$_2$ bacterial cells		$2×10^4$	30–200	living sensing tattoo	222
	F127, ZIF-67		$2×10^4$	200–400	Li-O$_2$ battery	242
	F127 silver nanoplates		n.d.	200	plasmonic constructs	88
hierarchical assembly	PDMS-*stat*-PEO	phase-separation	10^4–10^5	152–410	soft elastomer	245
	PDMS-*b*-PLA		n.d.	100	structural color patterning	248

[a] n.d. stands for 'not described'. [b] Examples synthesized after post-printing methylation. The rheology data was recorded on the methylated samples.

Page 49

Notes and references

1. R. L. Truby and J. A. Lewis, *Nature*, 2016, **540**, 371–378

2. S. C. Ligon, R. Liska, J. Stampfl, M. Gurr and R. Mülhaupt, *Chem. Rev.*, 2017, **117**, 10212–10290

3. E. MacDonald and R. Wicker, *Science*, 2016, **353**, aaf2093

4. T. J. Wallin, J. Pikul and R. F. Shepherd, *Nat. Rev. Mater.*, 2018, **3**, 84–100

5. A. Carlson, A. M. Bowen, Y. Huang, R. G. Nuzzo and J. A. Rogers, *Adv. Mater.*, 2012, **24**, 5284–5318

6. Z. Chen, Z. Li, J. Li, C. Liu, C. Lao, Y. Fu, C. Liu, Y. Li, P. Wang and Y. He, *J. Eur. Ceram. Soc.*, 2019, **39**, 661–687

7. A. K. Au, W. Huynh, L. F. Horowitz and A. Folch, *Angew. Chem. Int. Ed.*, 2016, **55**, 3862–3881

8. D. L. Taylor and M. in het Panhuis, *Adv. Mater.*, 2016, **28**, 9060–9093

9. Y. S. Rim, S.-H. Bae, H. Chen, N. De Marco and Y. Yang, *Adv. Mater.*, 2016, **28**, 4415–4440

10. D. Chimene, R. Kaunas and A. K. Gaharwar, *Adv. Mater.*, 2020, **32**, 1902026

11. B. Brenken, E. Barocio, A. Favaloro, V. Kunc and R. B. Pipes, *Addit. Manuf.*, 2018, **21**, 1–16

12. V. Dhinakaran, K. P. Manoj Kumar, P. M. Bupathi Ram, M. Ravichandran and M. Vinayagamoorthy, *Mater. Today Proc.*, 2020, **27**, 752–756

13. J. Z. Manapat, Q. Chen, P. Ye and R. C. Advincula, *Macromol. Mater. Eng.*, 2017, **302**, 1600553

14. Z. Zhao, X. Tian and X. Song, *J. Mater. Chem. C.*, 2020, **8**, 13896–13917

15. X. Xia, C. M. Spadaccini and J. R. Greer, *Nat. Rev. Mater.*, 2022, **7**, 683–701

16. B. E. Kelly, I. Bhattacharya, H. Heidari, M. Shusteff, C. M. Spadaccini and H. K. Taylor, *Science*, 2019, **363**, 1075–1079

17. J. T. Toombs, M. Luitz, C. C. Cook, S. Jenne, C. C. Li, B. E. Rapp, F. Kotz-Helmer and H. K. Taylor, *Science*, 2022, **376**, 308–312

18. M. Regehly, Y. Garmshausen, M. Reuter, N. F. König, E. Israel, D. P. Kelly, C.-Y. Chou, K. Koch, B. Asfari and S. Hecht, *Nature*, 2020, **588**, 620–624

19. J. A. Lewis, *Adv. Funct. Mater.*, 2006, **16**, 2193–2204

20. T. Jungst, W. Smolan, K. Schacht, T. Scheibel and J. Groll, *Chem. Rev.*, 2016, **116**, 1496–1539

21. Y. Dong, S. Wang, Y. Ke, L. Ding, X. Zeng, S. Magdassi and Y. Long, *Adv. Mater. Technol.*, 2020, **5**, 2000034

22. J.-Y. Lee, J. An and C. K. Chua, *Appl. Mater. Today*, 2017, **7**, 120–133

23. M. Champeau, D. A. Heinze, T. N. Viana, E. R. de Souza, A. C. Chinellato and S. Titotto, *Adv. Funct. Mater.*, 2020, **30**, 1910606

24. R. D. Farahani, M. Dubé and D. Therriault, *Adv. Mater.*, 2016, **28**, 5794–5821

25. L. Li, Q. Lin, M. Tang, A. J. E. Duncan and C. Ke, *Chem. Eur. J.*, 2019, **25**, 10768–10781

26. J. R. Tumbleston, D. Shirvanyants, N. Ermoshkin, R. Januszewicz, A. R. Johnson, D. Kelly, K. Chen, R. Pinschmidt, J. P. Rolland, A. Ermoshkin, E. T. Samulski and J. M. DeSimone, *Science*, 2015, **347**, 1349–1352

27. K. P. Cortés-Guzmán, A. R. Parikh, M. L. Sparacin, A. K. Remy, L. Adegoke, C. Chitrakar, M. Ecker, W. E. Voit and R. A. Smaldone, *ACS Sustain. Chem. Eng.*, 2022, **10**, 13091–13099

28. A. Durand-Silva, K. P. Cortés-Guzmán, R. M. Johnson, S. D. Perera, S. D. Diwakara and R. A. Smaldone, *ACS Macro Lett.*, 2021, **10**, 486–491

29. Q. Shi, K. Yu, X. Kuang, X. Mu, C. K. Dunn, M. L. Dunn, T. Wang and H. J. Qi, *Mater. Horiz.*, 2017, **4**, 598–607

30. A. Sydney Gladman, E. A. Matsumoto, R. G. Nuzzo, L. Mahadevan and J. A. Lewis, *Nat. Mater.*, 2016, **15**, 413–418

31. F. Puza and K. Lienkamp, *Adv. Funct. Mater.*, 2022, **32**, 2205345

32. S. Hong, D. Sycks, H. F. Chan, S. Lin, G. P. Lopez, F. Guilak, K. W. Leong and X. Zhao, *Adv. Mater.*, 2015, **27**, 4035–4040

33. S. V. Murphy and A. Atala, *Nat. Biotechnol.*, 2014, **32**, 773–785

34. Y. S. Zhang, G. Haghiashtiani, T. Hübscher, D. J. Kelly, J. M. Lee, M. Lutolf, M. C. McAlpine, W. Y. Yeong, M. Zenobi-Wong and J. Malda, *Nat. Rev. Dis. Primer*, 2021, **1**, 75

35. A. Lambert, S. Valiulis and Q. Cheng, *ACS Sens.*, 2018, **3**, 2475–2491

36. Z. Jiang, B. Diggle, M. L. Tan, J. Viktorova, C. W. Bennett and L. A. Connal, *Adv. Sci.*, 2020, **7**, 2001379

37. B. Narupai and A. Nelson, *ACS Macro Lett.*, 2020, **9**, 627–638

38. G. A. Appuhamillage, N. Chartrain, V. Meenakshisundaram, K. D. Feller, C. B. Williams and T. E. Long, *Ind. Eng. Chem. Res.*, 2019, **58**, 15109–15118

39. C. A. Murphy, K. S. Lim and T. B. F. Woodfield, *Adv. Mater.*, 2022, **34**, 2107759

40. W. Li, L. S. Mille, J. A. Robledo, T. Uribe, V. Huerta and Y. S. Zhang, *Adv. Healthc. Mater.*, 2020, **9**, 2000156

41. K. L. Sampson, B. Deore, A. Go, M. A. Nayak, A. Orth, M. Gallerneault, P. R. L. Malenfant and C. Paquet, *ACS Appl. Polym. Mater.*, 2021, **3**, 4304–4324

42. C. Xu, B. Quinn, L. L. Lebel, D. Therriault and G. L'Espérance, *ACS Appl. Mater. Interfaces*, 2019, **11**, 8499–8506

43. S. B. Walker and J. A. Lewis, *J. Am. Chem. Soc.*, 2012, **134**, 1419-1421

44. G. M. Gratson, M. Xu and J. A. Lewis, *Nature*, 2004, **428**, 386–386

45. K. Sun, T.-S. Wei, B. Y. Ahn, J. Y. Seo, S. J. Dillon and J. A. Lewis, *Adv. Mater.*, 2013, **25**, 4539–4543

46. L. J. Tan, W. Zhu and K. Zhou, *Adv. Funct. Mater.*, 2020, **30**, 2003062

47. C. Yu, J. Schimelman, P. Wang, K. L. Miller, X. Ma, S. You, J. Guan, B. Sun, W. Zhu and S. Chen, *Chem. Rev.*, 2020, **120**, 10695–10743

48. A. P. Dhand, M. D. Davidson, J. H. Galarraga, T. H. Qazi, R. C. Locke, R. L. Mauck and J. A. Burdick, *Adv. Mater.*, 2022, **34**, 2202261

49. D. Han and H. Lee, *Curr. Opin. Chem. Eng.*, 2020, **28**, 158–166

50. B. Narupai, P. T. Smith and A. Nelson, *Adv. Funct. Mater.*, 2021, **31**, 2011012

51. M. A. Skylar-Scott, J. Mueller, C. W. Visser and J. A. Lewis, *Nature*, 2019, **575**, 330–335

52. P. J. Smith and A. Morrin, *J. Mater. Chem.*, 2012, **22**, 10965–10970

53. S. C. Millik, A. M. Dostie, D. G. Karis, P. T. Smith, M. McKenna, N. Chan, C. D. Curtis, E. Nance, A. B. Theberge and A. Nelson, *Biofabrication*, 2019, **11**, 045009

54. M. Habibi, S. Foroughi, V. Karamzadeh and M. Packirisamy, *Nat. Commun.*, 2022, **13**, 1800

55. C. B. Arrington, M. Hegde, V. Meenakshisundaram, J. M. Dennis, C. B. Williams and T. E. Long, *ACS Appl. Mater.*, 2021, **13**, 48061–48070

56. Y. Kim, H. Yuk, R. Zhao, S. A. Chester and X. Zhao, *Nature*, 2018, **558**, 274–279

57. T. J. Hinton, Q. Jallerat, R. N. Palchesko, J. H. Park, M. S. Grodzicki, H.-J. Shue, M. H. Ramadan, A. R. Hudson and A. W. Feinberg, *Sci. Adv.*, 2015, **1**, e1500758

58. A. Lee, A. R. Hudson, D. J. Shiwarski, J. W. Tashman, T. J. Hinton, S. Yerneni, J. M. Bliley, P. G. Campbell and A. W. Feinberg, *Science*, 2019, **365**, 482–487

59. C. Loebel, C. B. Rodell, M. H. Chen and J. A. Burdick, *Nat. Protoc.*, 2017, **12**, 1521–1541

60. J. Forth, X. Liu, J. Hasnain, A. Toor, K. Miszta, S. Shi, P. L. Geissler, T. Emrick, B. A. Helms and T. P. Russell, *Adv. Mater.*, 2018, **30**, 1707603

61. A. Kotikian, R. L. Truby, J. W. Boley, T. J. White and J. A. Lewis, *Adv. Mater.*, 2018, **30**, 1706164

62. M. Cheng, Y. Jiang, W. Yao, Y. Yuan, R. Deivanayagam, T. Foroozan, Z. Huang, B. Song, R. Rojaee, T. Shokuhfar, Y. Pan, J. Lu and R. Shahbazian-Yassar, *Adv. Mater.*, 2018, **30**, 1800615

63. I. D. Robertson, M. Yourdkhani, P. J. Centellas, J. E. Aw, D. G. Ivanoff, E. Goli, E. M. Lloyd, L. M. Dean, N. R. Sottos, P. H. Geubelle, J. S. Moore and S. R. White, *Nature*, 2018, **557**, 223–227

64. T. G. McKenzie, F. Karimi, M. Ashokkumar and G. G. Qiao, *Chem. Eur. J.*, 2019, **25**, 5372–5388

65. A. G. Athanassiadis, Z. Ma, N. Moreno-Gomez, K. Melde, E. Choi, R. Goyal and P. Fischer, *Chem. Rev.*, 2022, **122**, 5165–5208

66. J. Li, C. Nagamani and J. S. Moore, *Acc. Chem. Res.*, 2015, **48**, 2181–2190

67. G. I. Peterson, M. B. Larsen, M. A. Ganter, D. W. Storti and A. J. Boydston, *ACS Appl. Mater.*, 2015, **7**, 577–583

68. M. A. Ghanem, A. Basu, R. Behrou, N. Boechler, A. J. Boydston, S. L. Craig, Y. Lin, B. E. Lynde, A. Nelson, H. Shen and D. W. Storti, *Nat. Rev. Mater.*, 2021, **6**, 84–98

69. A. M. Pekkanen, R. J. Mondschein, C. B. Williams and T. E. Long, *Biomacromolecules*, 2017, **18**, 2669–2687

70. J. A. Lewis, *Curr. Opin. Solid State Mater. Sci.*, 2002, **6**, 245-250

71. C. Zhu, A. J. Pascall, N. Dudukovic, M. A. Worsley, J. D. Kuntz, E. B. Duoss and C. M. Spadaccini, *Annu. Rev. Chem. Biomol. Eng.*, 2019, **10**, 17-42

72. M. Zeng and Y. Zhang, *J. Mater. Chem. A*, 2019, **7**, 23301-23336

73. V. G. Muir and J. A. Burdick, *Chem. Rev.*, 2021, **121**, 10908-10949

74. M. M. C. Bastings, S. Koudstaal, R. E. Kieltyka, Y. Nakano, A. C. H. Pape, D. A. M. Feyen, F. J. van Slochteren, P. A. Doevendans, J. P. G. Sluijter, E. W. Meijer, S. A. J. Chamuleau and P. Y. W. Dankers, *Adv. Healthc. Mater.*, 2014, **3**, 70–78

75. C. B. Highley, C. B. Rodell and J. A. Burdick, *Adv. Mater.*, 2015, **27**, 5075–5079

76. M. K. Włodarczyk-Biegun, J. I. Paez, M. Villiou, J. Feng and A. del Campo, *Biofabrication*, 2020, **12**, 035009

77. Q. Liu, Q. Li, S. Xu, Q. Zheng and X. Cao, *Polymers*, 2018, **10**, 664

78. Q. Lin, X. Hou and C. Ke, *Angew. Chem. Int. Ed.*, 2017, **56**, 4452–4457

79. P. Thordarson, *Chem. Soc. Rev.*, 2011, **40**, 1305–1323

80. J. H. Jordan, H. S. Ashbaugh, J. T. Mague and B. C. Gibb, *J. Am. Chem. Soc.*, 2021, **143**, 18605–18616

81. M. D. Pluth and K. N. Raymond, *Chem. Soc. Rev.*, 2007, **36**, 161–171

82. Y. Liu, Z. Wang and X. Zhang, *Chem. Soc. Rev.*, 2012, **41**, 5922–5932

83. C. A. Hunter and H. L. Anderson, *Angew. Chem. Int. Ed.*, 2009, **48**, 7488–7499

84. L. K. S. v. Krbek, C. A. Schalley and P. Thordarson, *Chem. Soc. Rev.*, 2017, **46**, 2622–2637

85. J. D. Badjić, A. Nelson, S. J. Cantrill, W. B. Turnbull and J. F. Stoddart, *Acc. Chem. Res.*, 2005, **38**, 723–732

86. M. E. Belowich, C. Valente, R. A. Smaldone, D. C. Friedman, J. Thiel, L. Cronin and J. F. Stoddart, *J. Am. Chem. Soc.*, 2012, **134**, 5243–5261

87. A.-J. Avestro, M. E. Belowich and J. Fraser Stoddart, *Chem. Soc. Rev.*, 2012, **41**, 5881–5895

88. A. P. Haring, A. U. Khan, G. Liu and B. N. Johnson, *Adv. Opt. Mater.*, 2017, **5**, 1700367

89. V. A. Bobrin, K. Lee, J. Zhang, N. Corrigan and C. Boyer, *Adv. Mater.*, 2022, **34**, 2107643

90. C. M. Portela, B. W. Edwards, D. Veysset, Y. Sun, K. A. Nelson, D. M. Kochmann and J. R. Greer, *Nat. Mater.*, 2021, **20**, 1491–1497

91. G. J. H. Lim, Y. Wu, B. B. Shah, J. J. Koh, C. K. Liu, D. Zhao, A. K. Cheetham, J. Wang and J. Ding, *ACS Mater. Lett.*, 2019, **1**, 147–153

92. D. Petta, D. W. Grijpma, M. Alini, D. Eglin and M. D'Este, *ACS Biomater. Sci. Eng.*, 2018, **4**, 3088–3098

93. M. Zhang, L. Li, Q. Lin, M. Tang, Y. Wu and C. Ke, *J. Am. Chem. Soc.*, 2019, **141**, 5154–5158

94. C. S. O'Bryan, T. Bhattacharjee, S. Hart, C. P. Kabb, K. D. Schulze, I. Chilakala, B. S. Sumerlin, W. G. Sawyer and T. E. Angelini, *Sci. Adv.*, 2017, **3**, e1602800

95. D. T. N. Chen, Q. Wen, P. A. Janmey, J. C. Crocker and A. G. Yodh, *Annu. Rev. Condens. Matter Phys.*, 2010, **1**, 301–322

96. R. S. Lenk, *Polymer Rheology*, Springer Science & Business Media, 2012.

97. W. Y. Shih, W.-H. Shih and I. A. Aksay, *J. Am. Chem. Soc.*, 1999, **82**, 616–624

98. C. Li, A. Faulkner-Jones, A. R. Dun, J. Jin, P. Chen, Y. Xing, Z. Yang, Z. Li, W. Shu, D. Liu and R. R. Duncan, *Angew. Chem. Int. Ed.*, 2015, **54**, 3957–3961

99. M. K. Sing, J. Ramírez and B. D. Olsen, *J. Chem. Phys.*, 2017, **147**, 194902

100. M. J. Webber and M. W. Tibbitt, *Nat. Rev. Mater.*, 2022, **7**, 541–556

101. M. Guvendiren, H. D. Lu and J. A. Burdick, *Soft Matter*, 2012, **8**, 260–272

102. D. Y. Wu, S. Meure and D. Solomon, *Prog. Polym. Sci.*, 2008, **33**, 479–522

103. M. Burnworth, L. Tang, J. R. Kumpfer, A. J. Duncan, F. L. Beyer, G. L. Fiore, S. J. Rowan and C. Weder, *Nature*, 2011, **472**, 334–337

104. A. Campanella, D. Döhler and W. H. Binder, *Macromol. Rapid Commun.*, 2018, **39**, 1700739

105. T. Aida, E. W. Meijer and S. I. Stupp, *Science*, 2012, **335**, 813–817

106. X. Ma and H. Tian, *Acc. Chem. Res.*, 2014, **47**, 1971–1981

107. E. A. Appel, R. A. Forster, M. J. Rowland and O. A. Scherman, *Biomaterials*, 2014, **35**, 9897–9903

108. Z. Yu, J. Liu, C. S. Y. Tan, O. A. Scherman and C. Abell, *Angew. Chem. Int. Ed.*, 2018, **57**, 3079–3083

109. M. Yokoya, S. Kimura and M. Yamanaka, *Chem. Eur. J.*, 2021, **27**, 5601–5614

110. J. Zheng, R. Fan, H. Wu, H. Yao, Y. Yan, J. Liu, L. Ran, Z. Sun, L. Yi, L. Dang, P. Gan, P. Zheng, T. Yang, Y. Zhang, T. Tang and Y. Wang, *Nat. Commun.*, 2019, **10**, 1604

111. D. A. Stone, L. Hsu and S. I. Stupp, *Soft Matter*, 2009, **5**, 1990–1993

112. P. Y. W. Dankers, M. C. Harmsen, L. A. Brouwer, M. J. A. Van Luyn and E. W. Meijer, *Nat. Mater.*, 2005, **4**, 568–574

113. L. Lu, W. Zhou, Z. Chen, Y. Hu, Y. Yang, G. Zhang and Z. Yang, *Gels*, 2022, **8**, 244

114. S. Dong, Y. Luo, X. Yan, B. Zheng, X. Ding, Y. Yu, Z. Ma, Q. Zhao and F. Huang, *Angew. Chem. Int. Ed.*, 2011, **50**, 1905–1909

115. L. Wang, L. Cheng, G. Li, K. Liu, Z. Zhang, P. Li, S. Dong, W. Yu, F. Huang and X. Yan, *J. Am. Chem. Soc.*, 2020, **142**, 2051–2058

116. M. Nakahata, Y. Takashima, H. Yamaguchi and A. Harada, *Nat. Commun.*, 2011, **2**, 511

117. E. A. Appel, X. J. Loh, S. T. Jones, F. Biedermann, C. A. Dreiss and O. A. Scherman, *J. Am. Chem. Soc.*, 2012, **134**, 11767–11773

118. D. Xia, P. Wang, X. Ji, N. M. Khashab, J. L. Sessler and F. Huang, *Chem. Rev.*, 2020, **120**, 6070–6123

119. M. V. Rekharsky and Y. Inoue, *Chem. Rev.*, 1998, **98**, 1875–1918

120. A. Harada, Y. Takashima and M. Nakahata, *Acc. Chem. Res.*, 2014, **47**, 2128–2140

121. J. W. Lee, S. Samal, N. Selvapalam, H.-J. Kim and K. Kim, *Acc. Chem. Res.*, 2003, **36**, 621–630

122. S. J. Barrow, S. Kasera, M. J. Rowland, J. del Barrio and O. A. Scherman, *Chem. Rev.*, 2015, **115**, 12320–12406

123. M. d. Pozo, P. Hernández, L. Hernández and C. Quintana, *J. Mater. Chem.*, 2011, **21**, 13657–13663

124. F. Biedermann, M. Vendruscolo, O. A. Scherman, A. De Simone and W. M. Nau, *J. Am. Chem. Soc.*, 2013, **135**, 14879–14888

125. Y. Liu, H. Yang, Z. Wang and X. Zhang, *Chem. Asian J.*, 2013, **8**, 1626–1632

126. M. J. Rowland, E. A. Appel, R. J. Coulston and O. A. Scherman, *J. Mater. Chem. B*, 2013, **1**, 2904–2910

127. Y. Zhu, Q. Luo, H. Zhang, Q. Cai, X. Li, Z. Shen and W. Zhu, *Biomater. Sci.*, 2020, **8**, 1394–1404

128. A. V. Zhukhovitskiy, M. Zhong, E. G. Keeler, V. K. Michaelis, J. E. P. Sun, M. J. A. Hore, D. J. Pochan, R. G. Griffin, A. P. Willard and J. A. Johnson, *Nat. Chem.*, 2016, **8**, 33–41

129. N. Wanasingha, P. Dorishetty, N. K. Dutta and N. R. Choudhury, *Gels*, 2021, **7**, 148

130. P. Wei, X. Yan and F. Huang, *Chem. Soc. Rev.*, 2015, **44**, 815–832

131. A. Y. Tam and V. W. Yam, *Chem. Soc. Rev.*, 2013, **42**, 1540–1567

132. D. Y. Yoon and P. J. Flory, *Polymer*, 1977, **18**, 509–513

133. H. A. Maddah, *J. Polym. Sci.*, 2016, **6**, 1–11

134. Q. Fang and M. A. Hanna, *Ind. Crops Prod.*, 1999, **10**, 47–53

135. R. L. N. Hailes, A. M. Oliver, J. Gwyther, G. R. Whittell and I. Manners, *Chem. Soc. Rev.*, 2016, **45**, 5358–5407

136. L. MacFarlane, C. Zhao, J. Cai, H. Qiu and I. Manners, *Chem. Sci.*, 2021, **12**, 4661–4682

137. J. Cai, C. Li, N. Kong, Y. Lu, G. Lin, X. Wang, Y. Yao, I. Manners and H. Qiu, *Science*, 2019, **366**, 1095–1098

138. Y. Wu, D. U. Shah, C. Liu, Z. Yu, J. Liu, X. Ren, M. J. Rowland, C. Abell, M. H. Ramage and O. A. Scherman, *Proc. Natl. Acad. Sci. U.S.A.*, 2017, **114**, 8163–8168

139. A. Harada, J. Li and M. Kamachi, *Nature*, 1992, **356**, 325–327

140. S. Uenuma, R. Maeda, H. Yokoyama and K. Ito, *Macromolecules*, 2019, **52**, 3881–3887

141. Y. Okumura, K. Ito and R. Hayakawa, *Polym. Adv. Technol.*, 2000, **11**, 815–819

142. C. C. Rusa, T. A. Bullions, J. Fox, F. E. Porbeni, X. Wang and A. E. Tonelli, *Langmuir*, 2002, **18**, 10016–10023

143. I. N. Topchieva, A. E. Tonelli, I. G. Panova, E. V. Matuchina, F. A. Kalashnikov, V. I. Gerasimov, C. C. Rusa, M. Rusa and M. A. Hunt, *Langmuir*, 2004, **20**, 9036–9043

144. Q. Lin, L. Li, M. Tang, S. Uenuma, J. Samanta, S. Li, X. Jiang, L. Zou, K. Ito and C. Ke, *Chem*, 2021, **7**, 2442–2459

145. J. Li, A. Harada and M. Kamachi, *Polym. J.*, 1994, **26**, 1019–1026

146. X. Song, Z. Zhang, J. Zhu, Y. Wen, F. Zhao, L. Lei, N. Phan-Thien, B. C. Khoo and J. Li, *Biomacromolecules*, 2020, **21**, 1516–1527

147. C. Pradal, K. S. Jack, L. Grøndahl and J. J. Cooper-White, *Biomacromolecules*, 2013, **14**, 3780–3792

148. D. Ma, K. Tu and L.-M. Zhang, *Biomacromolecules*, 2010, **11**, 2204–2212

149. C. B. Rodell, A. L. Kaminski and J. A. Burdick, *Biomacromolecules*, 2013, **14**, 4125–4134

150. K. L. Liu, Z. Zhang and J. Li, *Soft Matter*, 2011, **7**, 11290–11297

151. J. Li, X. Ni and K. W. Leong, *J. Biomed. Mater. Res.*, 2003, **65A**, 196–202

152. H. Kuang, H. He, Z. Zhang, Y. Qi, Z. Xie, X. Jing and Y. Huang, *J. Mater. Chem. B*, 2014, **2**, 659–667

153. S. Payyappilly, S. Dhara and S. Chattopadhyay, *J. Biomed. Mater. Res. A*, 2014, **102**, 1500–1509

154. S.-P. Zhao, L.-M. Zhang, D. Ma, C. Yang and L. Yan, *J. Phys. Chem. B*, 2006, **110**, 16503–16507

155. J. Wang, G. S. Williamson and H. Yang, *Colloids Surf. B*, 2018, **165**, 144–149

156. N. A. Nakeeb, Z. Kochovski, T. Li, Y. Zhang, Y. Lu and B. V. K. J. Schmidt, *RSC Adv.*, 2019, **9**, 4993–5001

157. Y. H. Roh, R. C. Ruiz, S. Peng, J. B. Lee and D. Luo, *Chem. Soc. Rev.*, 2011, **40**, 5730–5744

158. X. Hu, P. Cebe, A. S. Weiss, F. Omenetto and D. L. Kaplan, *Mater. Today*, 2012, **15**, 208–215

159. J. Nie, B. Pei, Z. Wang and Q. Hu, *Carbohydr. Polym.*, 2019, **205**, 225–235

160. H. Li, Y. J. Tan, S. Liu and L. Li, *ACS Appl. Mater. Interfaces*, 2018, **10**, 11164–11174

161. P. Cao, L. Tao, J. Gong, T. Wang, Q. Wang, J. Ju and Y. Zhang, *ACS Appl. Polym. Mater.*, 2021, **3**, 6167–6175

162. Y. Tamai, H. Tanaka and K. Nakanishi, *Macromolecules*, 1996, **29**, 6750–6760

163. P. Jiang, C. Yan, Y. Guo, X. Zhang, M. Cai, X. Jia, X. Wang and F. Zhou, *Biomater. Sci.*, 2019, **7**, 1805–1814

164. J. Liu, S. Lin, X. Liu, Z. Qin, Y. Yang, J. Zang and X. Zhao, *Nat. Commun.*, 2020, **11**, 1071

165. P. Jiang, P. Lin, C. Yang, H. Qin, X. Wang and F. Zhou, *Chem. Mater.*, 2020, **32**, 9983–9995

166. S. Hafeez, H. W. Ooi, D. Suylen, H. Duimel, T. M. Hackeng, C. van Blitterswijk and M. B. Baker, *J. Am. Chem. Soc.*, 2022, **144**, 4057–4070

167. F. V. Gruschwitz, F. Hausig, P. Schüler, J. Kimmig, S. Hoeppener, D. Pretzel, U. S. Schubert, S. Catrouillet and J. C. Brendel, *Chem. Mater.*, 2022, **34**, 2206–2217

168. L. Brunsveld, A. P. H. J. Schenning, M. A. C. Broeren, H. M. Janssen, J. A. J. M. Vekemans and E. W. Meijer, *Chem. Lett.*, 2000, **29**, 292–293

169. M. M. J. Smulders, A. P. H. J. Schenning and E. W. Meijer, *J. Am. Chem. Soc.*, 2008, **130**, 606–611

170. S. Cantekin, T. F. A. D. Greef and A. R. A. Palmans, *Chem. Soc. Rev.*, 2012, **41**, 6125–6137

171. A. Desmarchelier, B. G. Alvarenga, X. Caumes, L. Dubreucq, C. Trouffland, M. Tessier, N. Vanthuyne, J. Idé, T. Maistriaux, D. Beljonne, P. Brocorens, R. Lazzaroni, M. Raynal and L. Bouteiller, *Soft Matter*, 2016, **12**, 7824–7838

172. S. Cantekin, D. W. R. Balkenende, M. M. J. Smulders, A. R. A. Palmans and E. W. Meijer, *Nat. Chem.*, 2011, **3**, 42–46

173. L. Albertazzi, F. J. Martinez-Veracoechea, C. M. A. Leenders, I. K. Voets, D. Frenkel and E. W. Meijer, *Proc. Natl. Acad. Sci. U.S.A.*, 2013, **110**, 12203–12208

174. L. Albertazzi, D. V. D. Zwaag, C. M. A. Leenders, R. Fitzner, R. W. V. D. Hofstad and E. W. Meijer, *Science*, 2014, **344**, 491–495

175. C. M. A. Leenders, T. Mes, M. B. Baker, M. M. E. Koenigs, P. Besenius, A. R. A. Palmans and E. W. Meijer, *Mater. Horiz.*, 2014, **1**, 116–120

176. A. Singh and D. Bhatia, In *Methods in Cell Biology*, ed. A. K. Shukla, Academic Press, 2022, **169**, 323–346

177. R. D. Murphy, R. V. Garcia, S. J. Oh, T. J. Wood, K. D. Jo, J. Read de Alaniz, E. Perkins and C. J. Hawker, *Adv. Mater.*, 2022, 2207542

178. A. C. Farsheed, A. J. Thomas, B. H. Pogostin and J. D. Hartgerink, *Adv. Mater.*, 2023, 2210378

179. G. Wenz, B.-H. Han and A. Müller, *Chem. Rev.*, 2006, **106**, 782–817

180. T. F. A. De Greef, M. M. J. Smulders, M. Wolffs, A. P. H. J. Schenning, R. P. Sijbesma and E. W. Meijer, *Chem. Rev.*, 2009, **109**, 5687–5754

181. S. Dong, B. Zheng, F. Wang and F. Huang, *Acc. Chem. Res.*, 2014, **47**, 1982–1994

182. Z.-J. Meng, J. Liu, Z. Yu, H. Zhou, X. Deng, C. Abell and O. A. Scherman, *ACS Appl. Mater. Interfaces*, 2020, **12**, 17929–17935

183. J. P. Gong, Y. Katsuyama, T. Kurokawa and Y. Osada, *Adv. Mater.*, 2003, **15**, 1155–1158

184. M. A. Haque, T. Kurokawa and J. P. Gong, *Polymer*, 2012, **53**, 1805–1822

185. P. Matricardi, C. Di Meo, T. Coviello, W. E. Hennink and F. Alhaique, *Adv. Drug Deliv. Rev.*, 2013, **65**, 1172–1187

186. E. S. Dragan, *Chem. Eng. J.*, 2014, **243**, 572–590

187. Z. Huang, X. Chen, S. J. K. O'Neill, G. Wu, D. J. Whitaker, J. Li, J. A. McCune and O. A. Scherman, *Nat. Mater.*, 2022, **21**, 103–109

188. S. Datta, M. L. Saha and P. J. Stang, *Acc. Chem. Res.*, 2018, **51**, 2047–2063

189. A. GhavamiNejad, N. Ashammakhi, X. Y. Wu and A. Khademhosseini, *Small*, 2020, **16**, 2002931

190. N. Holten-Andersen, M. J. Harrington, H. Birkedal, B. P. Lee, P. B. Messersmith, K. Y. C. Lee and J. H. Waite, *Proc. Natl. Acad. Sci. U.S.A.*, 2011, **108**, 2651–2655

191. W. Sun, B. Xue, Q. Fan, R. Tao, C. Wang, X. Wang, Y. Li, M. Qin, W. Wang, B. Chen and Y. Cao, *Sci. Adv.*, 2020, **6**, eaaz9531

192. L. Shi, P. Ding, Y. Wang, Y. Zhang, D. Ossipov and J. Hilborn, *Macromol. Rapid Commun.*, 2019, **40**, 1800837

193. Z. Jiang, P. Shen, M. L. Tan, Q. Yan, J. Viktorova, C. Cementon, X. Peng, P. Xiao and L. A. Connal, *Mater. Adv.*, 2021, **2**, 5124–5134

194. Y. Cheng, K. H. Chan, X.-Q. Wang, T. Ding, T. Li, X. Lu and G. W. Ho, *ACS Nano*, 2019, **13**, 13176–13184

195. M. J. Sever and J. J. Wilker, *Dalton Trans.*, 2004, 1061–1072

196. M. J. Harrington, A. Masic, N. Holten-Andersen, J. H. Waite and P. Fratzl, *Science*, 2010, **328**, 216–220

197. N. Schweigert, A. J. Zehnder and R. I. Eggen, *Environ. Microbiol.*, 2001, **3**, 81–91

198. N. Holten-Andersen, A. Jaishankar, M. J. Harrington, D. E. Fullenkamp, G. DiMarco, L. He, G. H. McKinley, P. B. Messersmith and K. Y. C. Lee, *J. Mater. Chem. B.*, 2014, **2**, 2467–2472

199. K. Y. Lee and D. J. Mooney, *Prog. Polym. Sci.*, 2012, **37**, 106–126

200. I. Braccini and S. Pérez, *Biomacromolecules*, 2001, **2**, 1089–1096

201. R. M. Fuoss and H. Sadek, *Science*, 1949, **110**, 552–554

202. A. GhavamiNejad, N. Ashammakhi, X. Y. Wu and A. Khademhosseini, *Small*, 2020, **16**, 2002931

203. Q. Lin, L. Li, M. Tang, X. Hou and C. Ke, *J. Mater. Chem. C*, 2018, **6**, 11956–11960

204. K. A. Connors, *Chem. Rev.*, 1997, **97**, 1325–1358

205. Q. Lin, M. Tang and C. Ke, *Polym. Chem.*, 2020, **11**, 304–308

206. T. Karino, Y. Okumura, C. Zhao, M. Kidowaki, T. Kataoka, K. Ito and M. Shibayama, *Macromolecules*, 2006, **39**, 9435–9440

207. M. Kidowaki, C. Zhao, T. Kataoka and K. Ito, *Chem. Commun.*, 2006, 4102–4103.

208. K. Dikshit and C. J. Bruns, *Soft Matter*, 2021, **17**, 5248–5257

209. L. Li, Q. Lin, M. Tang, E. H. R. Tsai and C. Ke, *Angew. Chem., Int. Ed.*, 2021, **60**, 10186–10193

210. Y. Okumura and K. Ito, *Adv. Mater.*, 2001, **13**, 485–487

211. A. Bin Imran, K. Esaki, H. Gotoh, T. Seki, K. Ito, Y. Sakai and Y. Takeoka, *Nat. Commun.*, 2014, **5**, 5124

212. C. Liu, N. Morimoto, L. Jiang, S. Kawahara, T. Noritomi, H. Yokoyama, K. Mayumi and K. Ito, *Science*, 2021, **372**, 1078–1081

213. H.-A. Klok and S. Lecommandoux, *Adv. Mater.*, 2001, **13**, 1217–1229

214. Y. Mai and A. Eisenberg, *Chem. Soc. Rev.*, 2012, **41**, 5969–5985

215. H.-C. Kim, S.-M. Park and W. D. Hinsberg, *Chem. Rev.*, 2010, **110**, 146–177

216. H. Feng, X. Lu, W. Wang, N.-G. Kang and J. W. Mays, *Polymers*, 2017, **9**, 494

217. C. Cummins, R. Lundy, J. J. Walsh, V. Ponsinet, G. Fleury and M. A. Morris, *Nano Today*, 2020, **35**, 100936

218. D. Attwood, J. H. Collett and C. J. Tait, *Int. J. Pharm.*, 1985, **26**, 25–33

219. A. M. Pragatheeswaran and S. B. Chen, *Langmuir*, 2013, **29**, 9694–9701

220. C. J. Hansen, W. Wu, K. S. Toohey, N. R. Sottos, S. R. White and J. A. Lewis, *Adv. Mater.*, 2009, **21**, 4143–4147

221. W. Wu, A. DeConinck and J. A. Lewis, *Adv. Mater.*, 2011, **23**, H178–H183

222. X. Liu, H. Yuk, S. Lin, G. A. Parada, T.-C. Tang, E. Tham, C. de la Fuente-Nunez, T. K. Lu and X. Zhao, *Adv. Mater.*, 2018, **30**, 1704821

223. P. Holmqvist, P. Alexandridis and B. Lindman, *Macromolecules*, 1997, **30**, 6788–6797

224. P. Holmqvist, P. Alexandridis and B. Lindman, *J. Phys. Chem. B*, 1998, **102**, 1149–1158

225. J. Jiang, C. Burger, C. Li, J. Li, M. Y. Lin, R. H. Colby, M. H. Rafailovich and J. C. Sokolov, *Macromolecules*, 2007, **40**, 4016–4022

226. C. R. López-Barrón, N. J. Wagner and L. Porcar, *J. Rheol.*, 2015, **59**, 793–820

227. M. Bohorquez, C. Koch, T. Trygstad and N. Pandit, *J. Colloid Interface Sci.*, 1999, **216**, 34–40

228. J. P. K. Armstrong, M. Burke, B. M. Carter, S. A. Davis and A. W. Perriman, *Adv. Healthc. Mater.*, 2016, **5**, 1724–1730

229. L. Li, P. Zhang, Z. Zhang, Q. Lin, Y. Wu, A. Cheng, Y. Lin, C. M. Thompson, R. A. Smaldone and C. Ke, *Angew. Chem. Int. Ed.*, 2018, **57**, 5105–5109

230. A. Pitto-Barry and N. P. E. Barry, *Polym. Chem.*, 2014, **5**, 3291–3297

231. P. Zarrintaj, J. D. Ramsey, A. Samadi, Z. Atoufi, M. K. Yazdi, M. R. Ganjali, L. M. Amirabad, E. Zangene, M. Farokhi, K. Formela, M. R. Saeb, M. Mozafari and S. Thomas, *Acta Biomater.*, 2020, **110**, 37–67

232. F. Putz, S. Scherer, M. Ober, R. Morak, O. Paris and N. Hüsing, *Adv. Mater. Technol.*, 2018, **3**, 1800060

233. S.-H. Wu, C.-Y. Mou and H.-P. Lin, *Chem. Soc. Rev.*, 2013, **42**, 3862–3875

234. D. Zhao, J. Feng, Q. Huo, N. Melosh, G. H. Fredrickson, B. F. Chmelka and G. D. Stucky, *Science*, 1998, **279**, 548–552

235. S. Che, Z. Liu, T. Ohsuna, K. Sakamoto, O. Terasaki and T. Tatsumi, *Nature*, 2004, **429**, 281–284

236. F. Tang, L. Li and D. Chen, *Adv. Mater.*, 2012, **24**, 1504–1534

237. Y. Hong, J. W. Y. Lam and B. Zhong Tang, *Chem. Commun.*, 2009, 4332–4353

238. Y. Hong, J. W. Y. Lam and B. Zhong Tang, *Chem. Soc. Rev.*, 2011, **40**, 5361–5388

239. B. J. Smith, A. C. Overholts, N. Hwang and W. R. Dichtel, *Chem. Commun.*, 2016, **52**, 3690–3693

240. S. Kandambeth, A. Mallick, B. Lukose, M. V. Mane, T. Heine and R. Banerjee, *J. Am. Chem. Soc.*, 2012, **134**, 19524–19527

241. S. Karak, S. Kandambeth, B. P. Biswal, H. S. Sasmal, S. Kumar, P. Pachfule and R. Banerjee, *J. Am. Chem. Soc.*, 2017, **139**, 1856–1862

242. Z. Lyu, G. J. H. Lim, R. Guo, Z. Kou, T. Wang, C. Guan, J. Ding, W. Chen and J. Wang, *Adv. Funct. Mater.*, 2019, **29**, 1806658

243. K. Huang and J. Rzayev, *J. Am. Chem. Soc.*, 2009, **131**, 6880–6885

244. R. Verduzco, X. Li, S. L. Pesek and G. E. Stein, *Chem. Soc. Rev.*, 2015, **44**, 2405–2420

245. R. Xie, S. Mukherjee, A. E. Levi, V. G. Reynolds, H. Wang, M. L. Chabinyc and C. M. Bates, *Sci. Adv.*, 2020, **6**, eabc6900

246. S. T. Nguyen, L. K. Johnson, R. H. Grubbs and J. W. Ziller, *J. Am. Chem. Soc.*, 1992, **114**, 3974–3975

247. C. W. Bielawski and R. H. Grubbs, *Prog. Polym. Sci.*, 2007, **32**, 1–29

248. B. B. Patel, D. J. Walsh, D. H. Kim, J. Kwok, B. Lee, D. Guironnet and Y. Diao, *Sci. Adv.*, 2020, **6**, eaaz7202

249. D. A. Walker, J. L. Hedrick and C. A. Mirkin, *Science*, 2019, **366**, 360–364

250. J. L. Mann, A. C. Yu, G. Agmon and E. A. Appel, *Biomater. Sci.*, 2018, **6**, 10–37

251. B. G. Compton and J. A. Lewis, *Adv. Mater.*, 2014, **26**, 5930–5935

252. G. Liu, Y. Zhao, G. Wu and J. Lu, *Sci. Adv.*, 2018, **4**, eaat0641

253. P. Song and H. Wang, *Adv. Mater.*, 2020, **32**, 1901244

254. M. Zhang, A. Vora, W. Han, R. J. Wojtecki, H. Maune, A. B. A. Le, L. E. Thompson, G. M. McClelland, F. Ribet, A. C. Engler and A. Nelson, *Macromolecules*, 2015, **48**, 6482–6488

255. D. G. Karis, R. J. Ono, M. Zhang, A. Vora, D. Storti, M. A. Ganter and A. Nelson, *Polym. Chem.*, 2017, **8**, 4199–4206

256. A. McCormack, C. B. Highley, N. R. Leslie and F. P. W. Melchels, *Trends Biotechnol.*, 2020, **38**, 584–593

257. W. Hua, K. Mitchell, L. Raymond, B. Godina, D. Zhao, W. Zhou and Y. Jin, *ACS Biomater. Sci. Eng.*, 2021, **7**, 4736–4756

258. L. L. Lebel, B. Aissa, M. A. E. Khakani and D. Therriault, *Adv. Mater.*, 2010, **22**, 592–596

259. L. A. Hockaday, K. H. Kang, N. W. Colangelo, P. Y. C. Cheung, B. Duan, E. Malone, J. Wu, L. N. Girardi, L. J. Bonassar, H. Lipson, C. C. Chu and J. T. Butcher, *Biofabrication*, 2012, **4**, 035005

260. D. A. Rau, J. Herzberger, T. E. Long and C. B. Williams, *ACS Appl. Mater. Interfaces*, 2018, **10**, 34828–34833

261. D. Zhao, Z. Zhang, J. Zhao, K. Liu, Y. Liu, G. Li, X. Zhang, R. Bai, X. Yang and X. Yan, *Angew. Chem. Int. Ed.*, 2021, **60**, 16224–16229

262. L. Meazza, J. A. Foster, K. Fucke, P. Metrangolo, G. Resnati and J. W. Steed, *Nat. Chem.*, 2013, **5**, 42-47

263. G. Berger, J. Soubhye and F. Meyer, *Polym. Chem.*, 2015, **6**, 3559-3580

264. L. C. Gilday, S. W. Robinson, T. A. Barendt, M. J. Langton, B. R. Mullaney and P. D. Beer, *Chem. Rev.*, 2015, **115**, 7118-7195

265. P. Liu, Z. Li, B. Shi, J. Liu, H. Zhu and F. Huang, *Chem. Eur. J.*, 2018, **24**, 4264-4267

266. R. Kampes, S. Zechel, M. D. Hager and U. S. Schubert, *Chem. Sci.*, 2021, **12**, 9275-9286

267. R. Zeng, Z. Gong and Q. Yan, *J. Org. Chem.*, 2020, **85**, 8397-8404

268. N. Biot and D. Bonifazi, *Coord. Chem. Rev.*, 2020, **413**, 213243

269. S. Sarkar, P. Ballester, M. Spektor and E. A. Kataev, *Angew. Chem. Int. Ed.*, 2022, DOI: 10.1002/anie.202214705.

270. M. J. Webber, E. A. Appel, E. W. Meijer and R. Langer, *Nat. Mater.*, 2016, **15**, 13–26

271. D. B. Amabilino, D. K. Smith and J. W. Steed, *Chem. Soc. Rev.*, 2017, **46**, 2404–2420

272. T. L. Sun, T. Kurokawa, S. Kuroda, A. B. Ihsan, T. Akasaki, K. Sato, M. A. Haque, T. Nakajima and J. P. Gong, *Nat. Mater.*, 2013, **12**, 932–937

273. M. Hua, S. Wu, Y. Ma, Y. Zhao, Z. Chen, I. Frenkel, J. Strzalka, H. Zhou, X. Zhu and X. He, *Nature*, 2021, **590**, 594–599

274. S. Choi, T.-W. Kwon, A. Coskun and J. W. Choi, *Science*, 2017, **357**, 279–283

275. Y. Jiang, Z. Zhang, Y.-X. Wang, D. Li, C.-T. Coen, E. Hwaun, G. Chen, H.-C. Wu, D. Zhong, S. Niu, W. Wang, A. Saberi, J.-C. Lai, Y. Wu, Y. Wang, A. A. Trotsyuk, K. Y. Loh, C.-C. Shih, W. Xu, K. Liang, K. Zhang, Y. Bai, G. Gurusankar, W. Hu, W. Jia, Z. Cheng, R. H. Dauskardt, G. C. Gurtner, J. B.-H. Tok, K. Deisseroth, I. Soltesz and Z. Bao, *Science*, 2022, **375**, 1411–1417

276. Q. Lin and C. Ke, *Chem. Commun.*, 2022, **58**, 250–253

277. M. Tang and C. Ke, *Matter*, 2021, **4**, 2664–2665

278. L. Fang, M. A. Olson, D. Benítez, E. Tkatchouk, W. A. G. Iii and J. Fraser Stoddart, *Chem. Soc. Rev.*, 2010, **39**, 17–29

279. T. Takata, *Polym. J.*, 2006, **38**, 1–20

280. Q. Wu, P. M. Rauscher, X. Lang, R. J. Wojtecki, J. J. de Pablo, M. J. A. Hore and S. J. Rowan, *Science*, 2017, **358**, 1434–1439

281. A. Kotikian, J. M. Morales, A. Lu, J. Mueller, Z. S. Davidson, J. W. Boley and J. A. Lewis, *Adv. Mater.*, 2021, **33**, 2101814

282. X. Peng, S. Wu, X. Sun, L. Yue, S. M. Montgomery, F. Demoly, K. Zhou, R. R. Zhao and H. J. Qi, *Adv. Mater.*, 2022, **34**, 2204890

283. M. Zadan, D. K. Patel, A. P. Sabelhaus, J. Liao, A. Wertz, L. Yao and C. Majidi, *Adv. Mater.*, 2022, **34**, 2200857

284. M. P. Bendsoe and O. Sigmund, *Topology Optimization: Theory, Methods, and Applications*, Springer Science & Business Media, 2003

285. G. Kazakis, I. Kanellopoulos, S. Sotiropoulos and N. D. Lagaros, *Heliyon*, 2017, **3**, e00431

286. F. Sui, R. Guo, Z. Zhang, G. X. Gu and L. Lin, *ACS Mater. Lett.*, 2021, **3**, 1433–1439

287. Z. Zhang, Z. Zhang, F. Di Caprio and G. X. Gu, *Compos. Struct.*, 2022, **285**, 115233

288. A. E. Gongora, K. L. Snapp, R. Pang, T. M. Tiano, K. G. Reyes, E. Whiting, T. J. Lawton, E. F. Morgan and K. A. Brown, *Matter*, 2022, **5**, 2829–2846

289. J. Panetta, Q. Zhou, L. Malomo, N. Pietroni, P. Cignoni and D. Zorin, *ACM Trans. Graph.*, 2015, **34**, 135

290. E. Stach, B. DeCost, A. G. Kusne, J. Hattrick-Simpers, K. A. Brown, K. G. Reyes, J. Schrier, S. Billinge, T. Buonassisi, I. Foster, C. P. Gomes, J. M. Gregoire, A. Mehta, J. Montoya, E. Olivetti, C. Park, E. Rotenberg, S. K. Saikin, S. Smullin, V. Stanev and B. Maruyama, *Matter*, 2021, **4**, 2702–2726

291. A. E. Gongora, B. Xu, W. Perry, C. Okoye, P. Riley, K. G. Reyes, E. F. Morgan and K. A. Brown, *Sci. Adv.*, 2020, **6**, eaaz1708

292. Z. Jin, Z. Zhang and G. X. Gu, *Manuf. Lett.*, 2019, **22**, 11–15